NASA CONTRACTOR
REPORT

NASA CR-6

ON OPTIMUM TRANSFER BETWEEN
TWO TERMINAL POINTS FOR MINIMUM
INITIAL IMPULSE UNDER AN
ARBITRARY INITIAL VELOCITY VECTOR

by Fang Toh Sun

ON OPTIMUM TRANSFER BETWEEN TWO TERMINAL POINTS

FOR MINIMUM INITIAL IMPULSE UNDER AN

ARBITRARY INITIAL VELOCITY VECTOR

By Fang Toh Sun

ACKNOWLEDGMENT

TABLE OF CONTENTS

TABLE OF CONTENTS (Concluded)

LIST OF TABLES

LIST OF FIGURES

NOMENCLATURE

A	semi-transversal axis, constraining hyperbola
B	semi-conjugate axis, constraining hyperbola
C	center-to-focus distance, constraining hyperbola
C_1, C_2	parameters defined by Eqs. (38)
d	the perpendicular distance from the field center to the chord of the base triangle
e	eccentricity, constraining hyperbola
h	angular momentum per unit mass
I	an invariant of the orthogonality quartic (see Eq. (18))
J	an invariant of the orthogonality quartic (see Eq. (18))
K	Godal's compatibility constant $= \frac{\mu}{d} \tan \frac{\Psi}{2}$
M,N	orthogonal projections of a velocity vector on the local radial and chordal axes respectively
m, n	nondimensional form of M and N: M/V_{S1}, N/V_{S1}
n	distance ratio $\equiv r_2/r_1$
r	radial distance
V	velocity
V_S	circular speed $= \sqrt{\mu/r}$
ν	dimensionless velocity $\equiv V\, h/\mu$
x,y	displacement coordinates
X*,Y*	critical coordinates, given by Eqs. (33)
Δ	discriminant of the orthogonality quartic
ΔV	velocity increment

NOMENCLATURE (Continued)

$\Delta\nu$	dimensionless velocity increment $= \Delta V/V_{S1}$
ϵ	eccentricity
κ	dimensionless Godal's compatibility constant $\equiv K/V_{S1}$
μ	strength of the gravity field
ν	dimensionless velocity $\equiv V/V_{S1}$
$\bar{\nu}$	value ov ν satisfying Eq. (22)
ρ	distance of the optimum origin from the radical center, (T) in the hodograph plane
ρ'	distance of the optimum origin from the hodograph image of the initial terminal point Q_1
σ	included angle of the local radial and chordal axes (Fig. 1c)
Φ	the path angle with reference to the minimum energy direction
ϕ	the path angle with reference to the local horizontal
φ	the interior angle of the base triangle at the terminal point
ψ	the vertex angle of the base triangle (Fig. 1a)
Ψ	the range angle
ω	the inclination of the initial velocity vector to the plane of the base triangle
ω	a parametric angle, defined by Eq. (B-1), Appendix B

Subscripts

*	ortho-point, or orthogonal solution in Chapters 2,3; optimum condition elsewhere
**	absolute minimum solution
0	initial condition

NOMENCLATURE (Concluded)

1   initial terminal, unless otherwise indicated

2   final terminal, unless otherwise indicated

d   chord perpendicular

L   lower limit

U   upper limit

opt   optimum

c,R   chordal and radial pair of directions

r,θ   radial and transversal pair of directions

χ,ζ   outward directions of the interior and exterior angle bisectors
         of the base triangle respectively

p,n   in-plane and out-of-plane components

Superscripts

*   critical

ABSTRACT

The problem of minimizing the initial impulse required for the transfer between two terminal points in space under an arbitrarily prescribed initial velocity vector is analytically investigated. The chordal and radial components of the in-plane velocity are introduced, and a geometrical approach in the hodograph space is employed. In terms of these velocity coordinates Stark's optimum quartic equation is reformulated and critically examined for the number and nature of its real solutions. Analytical criteria for the unrealistic optimum are derived, and the selection of a realistic transfer trajectory under various conditions of the initial velocity vector is discussed and summarized in some simple rules. Various regions in the hodograph plane concerning the nature of the optimum transfer trajectories are established, and the effects of the initial velocity vector on such a trajectory are analyzed. An optimization chart is developed, and the construction of two versions of the optimum transfer hodograph are introduced. Several limiting cases including the vertical transfer, the 180° transfer, and the transfer to infinity are investigated, and the particular case of departure from a circular orbit is also reviewed. The analysis is basically two-dimensional with a brief presentation of the three-dimensional effects.

1. INTRODUCTION

The minimization of the fuel expenditure for the transfer between two terminal points by minimizing the initial impulse for a given initial velocity is a problem usually encountered in space flight when the primary objective is to impact a destination planet or to intercept a target in space. Such a problem has been previously treated by Battin[4] and Stark,[6] and numerical solutions for the case of an initial circular orbit have been worked out in the works of both. In particular, Stark's orthogonality consideration for the velocity vectors offers a simple approach to, and yields a general quartic equation for the solution of this problem. However, before such an equation can be broadly applied, several critical questions remain to be answered, regarding the existence of multiple real solutions of the quartic as well as the possibility of the arising of an unrealistic optimum trajectory (a trajectory leading toward the destination terminal point via infinity[1]). It will be shown here that, while the optimum solution is usually (though not always) unique and realistic when the initial velocity is elliptic and only the short transfers (range angle less than 180°) are considered, the situation may become quite complicated when the initial velocity is hyperbolic, and both short and long transfers are under consideration. The purpose of the present study is thus to investigate analytically Stark's quartic as to these vital questions so as to form a theoretical basis for the selection of a realistic optimum transfer trajectory under broad conditions of the prescribed initial velocity vector. Such an investigation will not only facilitate such a selection, but also reveal clearly the effects of the initial velocity vector on the optimum transfer trajectory.

Throughout the following analysis a geometrical approach in the hodograph space will be employed. However, to facilitate the investigation the chordal and radial pair of velocity coordinates will be used instead of the usual transversal and radial pair used by Stark. It will be seen later that such a coordinates pair will reduce Stark's quartic to a simpler form, and also enable the general findings previously found in Ref. (9) for a system of two-terminal trajectories to be readily applied to the present problem.

---

[1]Called "false optimum" in Ref. (6); see also Appendix A.

2. TWO-DIMENSIONAL ANALYSIS OF THE PROBLEM

2.1 FORMULATION OF THE PROBLEM

Consider a space vehicle, initially at the point Q_1 and having an initial velocity $\vec{V}_0$, to be transferred to a given point Q_2 by applying an instantaneous impulse at Q_1. The optimum transfer trajectory is defined as the one which requires the minimum impulse, which is equivalent to the minimum velocity increment at the initial terminal Q_1.

As we know, in an inverse-square central gravity field such transfer trajectories are Keplerian and all lie in the plane of the base triangle $OQ_1 Q_2$. Let us assume the initial velocity vector $\vec{V}_0$ also lies in this plane, then the problem is two-dimensional. Consider an arbitrary transfer trajectory from Q_1 to Q_2, and let $\vec{V}_1$ be the departure velocity at Q_1 along this trajectory (Fig. 1a). For convenience we will first restrict the vertex angle to be $0 < \psi < \pi$ so that the base triangle does not degenerate into a line segment. In such a case the departure velocity $\vec{V}_1$ must satisfy Godal's compatibility condition[5]

$$V_C V_R = \frac{\mu}{d} \tan \frac{\psi}{2} \qquad (1)$$

where V_C and V_R are the components of the terminal velocity V_1 along the direction of the chord line $Q_1 Q_2$ and the local radial direction respectively (Fig. 1b). The velocity increment vector is then

$$\Delta \vec{V} = \vec{V}_1 - \vec{V}_0 \qquad (2)$$

with its magnitude given by

$$|\Delta V|^2 = (V_C - V_{CO})^2 + (V_R - V_{RO})^2 - 2(V_C - V_{CO})(V_R - V_{RO})\cos\varphi_1 \qquad (3)$$

which simplifies to

$$|\Delta V|^2 = V_C^2 + V_R^2 - 2N_0 V_C - 2M_0 V_R + V_0^2 - 2K\cos\varphi_1 \qquad (3a)$$

2

(a) TRANSFER TRAJECTORY

(b) VELOCITY COMPONENTS

(c) THE CONSTRAINING HYPERBOLA
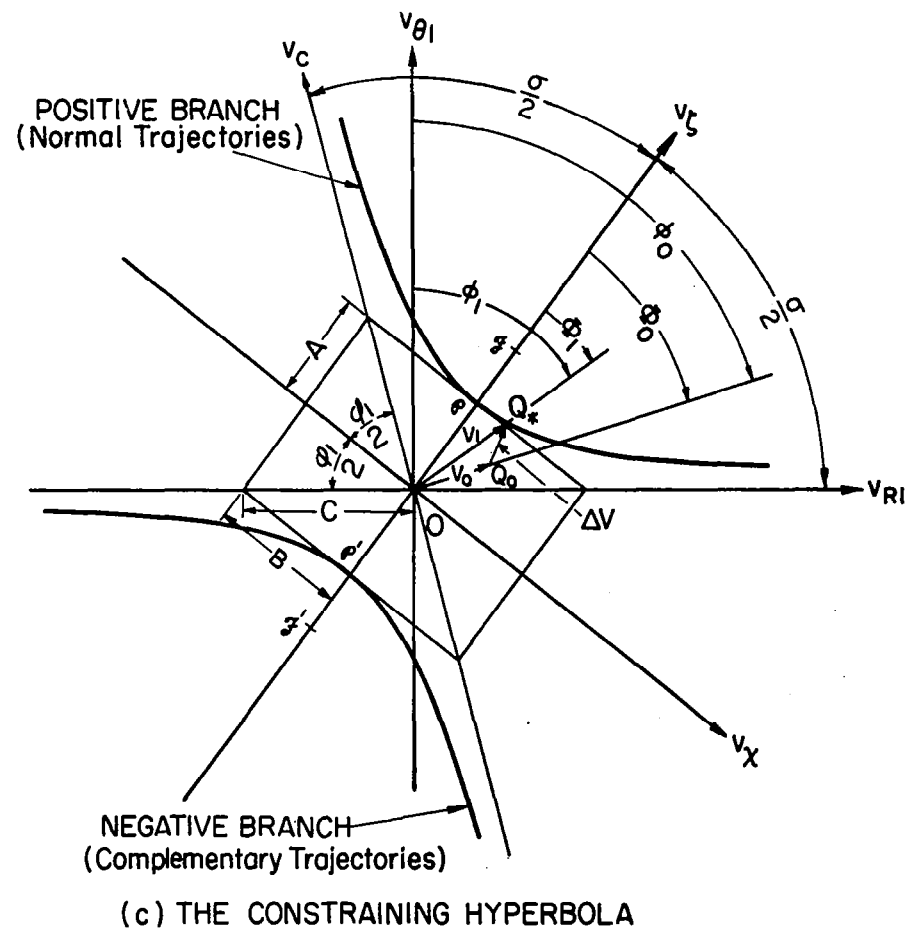
Fig. 1. The transfer trajectory and the constraining hyperbola in the hodograph plane.

where

$$K \equiv \frac{\mu}{d} \tan \frac{\psi}{2} \tag{4}$$

$$M_0 = V_{RO} - V_{CO} \cos\varphi_1 \quad , \quad N_0 = V_{CO} - V_{RO} \cos\varphi_1 \tag{5}$$

Thus the problem is to minimize $|\Delta V|$ under the constraint Eq. (1). It is to be noted that the parameters M_0 and N_0 here have the physical significance of being the orthogonal projections of the initial velocity vector $\vec{V}_0$ on the V_{R1}- and V_C-axes respectively, as is obvious from the geometry of the velocity vectors shown in Fig. 1b and c.

2.2   THE CONSTRAINING HYPERBOLA AND THE ORTHOGONALITY CONDITION

It is evident that the constraint Eq. (1) represents a hyperbola in the hodograph plane with the chordal and radial directions at Q_1 as its two asymptotic directions. Thus in order to insure that the trajectory will pass through the terminal point Q_2, the tip of the departure velocity vector $\vec{V}_1$ has to be constrained on this hyperbola, which in a given Newtonian gravity field is solely determined by the base triangle OQ_1Q_2. The problem is now reduced to finding the minimum distance from the tip Q_0 of the initial velocity vector $\vec{V}_0$ to the constraining hyperbola, and this requires the vector $\Delta\vec{V}$ to be normal to the hyperbola (Fig. 1c). This is the approach used by Stark[6] in which he employed the velocity coordinates V_θ and V_r to obtain an optimum equation by such an orthogonality consideration. In present coordinates this condition may be written

$$\frac{\Delta V_{C*} - \Delta V_{R*} \cos \varphi_1}{\Delta V_{R*} - \Delta V_{C*} \cos \varphi_1} = -\left(\frac{dV_R}{dV_C}\right)_* \tag{6}$$

where

$$\Delta V_{C*} = V_{C*} - V_{CO}$$

$$\tag{7}$$

$$\Delta V_{R*} = V_{R*} - V_{RO}$$

and $(dV_R/dV_C)_*$ is to be evaluated along the constraining hyperbola. The sub-

script * here indicates the point on the constraining hyperbola at which the normal line passes through the point Q_0. Such a point will be referred to as the ortho-point corresponding to Q_0. From Eq. (1) we have, at any point on the hyperbola,

$$\frac{dV_R}{dV_C} = -\frac{V_R}{V_C} \tag{8}$$

By substituting Eq. (7) into Eq. (6) and making use of Eq. (8) the orthogonality condition becomes

$$V_{C*}^2 - N_0 V_{C*} = V_{R*}^2 - M_0 V_{R*} \tag{9}$$

Further eliminating V_{R*} from Eqs. (9) and (1) yields an equation in the single variable V_{C*}:

$$V_{C*}^4 - N_0 V_{C*}^3 + K M_0 V_{C*} - K^2 = 0 \tag{10C}$$

The corresponding equation in V_{R*} is

$$V_{R*}^4 - M_0 V_{R*}^3 + K N_0 V_{R*} - K^2 = 0 \tag{10R}$$

Both Eqs. (10C) and (10R) are of the fourth degree, and in fact they are of the same form. They will be referred to as the orthogonality quartics, and their solutions the orthogonality solutions. Either of them can be solved in closed form by standard method of algebra, or by numerical approximations. With either of the unknown components V_{C*} or V_{R*} thus determined, the other component and the corresponding velocity increment $|\Delta V|$ can then be easily obtained from Eqs. (1) and (3a), and the principal elements of the transfer trajectory are then obtained from the usual orbital relations. However, it is to be noted that the real solution of either Eqs. (10C) or (10R) is not unique, since a quartic may give 4, 2 or no real solutions. Furthermore, the orthogonality condition expressed by such a quartic is neither sufficient nor necessary for the optimum solution of the problem. It is merely a necessary condition for an interior extremem, and it may yield maxima, minima, or neither. And even if it gives a local minimum, it may not be the absolute one; and even if it is absolute, the resulting trajectory may be unrealistic. Thus instead of going into numerical solutions the following vital questions are now posed:

(1) Under what condition will the orthogonality Eqs. (10C) or (10R) have a unique real solution, 2, 4 or no real solutions?

(2) If multiple solutions exist, is there any simple rule for the selection of an absolute minimum?

(3) Under what condition will the absolute minimum solution yield an unrealistic optimum? And if so, how to choose a realistic optimum trajectory for the problem?

These questions will be critically examined one by one in the sections that follow. Before proceeding to answering these questions, the dimensionless velocity parameter defined by

$$v = V/V_{S1} = V/ \sqrt{\frac{\mu}{r_1}} \qquad (11)$$

will now be introduced and the principal equations developed so far, be non-dimensionalized as summarized in Table 1.

Besides, formulas for the principal geometrical elements of the constraining hyperbola are presented in Table 2. Some essential features of the constraining hyperbola worthy of noting are as follows:

(1) The conjugate and transversal axes of the hyperbola (v_χ-, v_ζ-axes) are the bisectors of the interior and exterior angles at the initial terminal Q_1 of the base triangle respectively. The v_ζ-axis is in the direction of the minimum energy trajectory through the initial terminal according to Ref. (9) and may be called the minimum energy axis. The pair of directions (χ, ζ) together with the pair of the asymptotic directions (C,R_1) mentioned earlier and their respective normals to be introduced later constitute the most important reference directions of the present problem.

(2) The semi-transversal axis (A) of the constraining hyperbola is the minimum velocity satisfying the constraint, and therefore, the departure velocity along the minimum energy transfer trajectory.

(3) Of the two branches of the hyperbola, the one on which $V_C > 0$, and $V_R > 0$ is the constraint for the short transfer or the normal trajectory group,[2] and the other one on which $V_C < 0$ and $V_R < 0$ is the constraint for the long transfer, or the complementary group.

---

[2]For the definitions of these terms, see Appendix A.

TABLE 1

PRINCIPAL FORMULAS IN THE NONDIMENSIONAL
FORM FOR THE TERMINAL-TO-TERMINAL OPTIMUM TRANSFER

Compatibility Condition	$\nu_C \nu_R = \kappa$	(1')
Velocity Increment	$\lvert \Delta \nu \rvert^2 = \nu_C^2 + \nu_R^2 - 2\eta_0 \nu_C - 2 m_0 \nu_R + \nu_0^2 - 2\kappa \cos \varphi_1$	(3')
The Orthogonality Equation		
in ν_{C_*} , ν_{R_*}	$\nu_{C_*}^2 - \eta_0 \nu_{C_*} = \nu_{R_*}^2 - m_0 \nu_{R_*}$	(9')
in ν_{C_*}	$\nu_{C_*}^4 - \eta_0 \nu_{C_*}^3 + \kappa m_0 \nu_{C_*} - \kappa^2 = 0$	(10'-C)
in ν_{R_*}	$\nu_{R_*}^4 - m_0 \nu_{R_*}^3 + \kappa \eta_0 \nu_{R_*} - \kappa^2 = 0$	(10'-R)
The Constant Product	$\kappa \equiv \tan \dfrac{\psi}{2} \csc \varphi_1$	(4)
The Orthogonal Projections of the Initial Velocity Vector	$m_0 \equiv (\nu_R)_0 - (\nu_C)_0 \cos \varphi_1$ $\eta_0 \equiv (\nu_C)_0 - (\nu_R)_0 \cos \varphi_1$	(5')

TABLE 2

PRINCIPAL GEOMETRICAL ELEMENTS OF THE CONSTRAINING HYPERBOLA ($\nu_C \nu_R = \kappa$)

Element	Symbol	Formulas			Numbering
		In terms of $\kappa,\ \varphi_1$	In terms of $\psi,\ \varphi_1$	In terms of $\psi,\ n(\equiv r_2/r_1)$	
Included angle between the asymptotes	σ	$\pi - \varphi_1$	$\pi - \varphi_1$	$\sin^{-1}\left(\dfrac{2 \sin \frac{\psi}{2}}{\sqrt{\left(1 + \frac{1}{n}\right)^2 \sec^2 \frac{\psi}{2} - \frac{4}{n}}} \right)$	(12)
Semi-transversal axis	A	$2\sqrt{\kappa}\ \sin \frac{\varphi_1}{2}$	$\sqrt{2 \tan \frac{\psi}{2} \tan \frac{\varphi_1}{2}}$	$\sqrt{\sec \frac{\psi}{2} \sqrt{\left(1 + \frac{1}{n}\right)^2 \sec^2 \frac{\psi}{2} - \frac{4}{n}} - \left(1 + \frac{1}{n}\right) \sec^2 \frac{\psi}{2} + 2}$	(13)
Semi-conjugate axis	B	$2\sqrt{\kappa}\ \cos \frac{\varphi_1}{2}$	$\sqrt{2 \tan \frac{\psi}{2} \cot \frac{\varphi_1}{2}}$	$\sqrt{\sec \frac{\psi}{2} \sqrt{\left(1 + \frac{1}{n}\right)^2 \sec^2 \frac{\psi}{2} - \frac{4}{n}} + \left(1 + \frac{1}{n}\right) \sec^2 \frac{\psi}{2} - 2}$	(14)
Center-to-focus distance	C	$2\sqrt{\kappa}$	$2 \sqrt{\tan \frac{\psi}{2} \csc \varphi_1}$	$\sqrt{2 \sec \frac{\psi}{2} \sqrt{\left(1 + \frac{1}{n}\right)^2 \sec^2 \frac{\psi}{2} - \frac{4}{n}}}$	(15)
Eccentricity	e	$\csc \frac{\varphi_1}{2}$	$\csc \frac{\varphi_1}{2}$	$\left\{ \dfrac{2}{1 - \dfrac{\left(1 + \frac{1}{n}\right) - 2 \cos^2 \frac{\psi}{2}}{\sqrt{\left(1 + \frac{1}{n}\right)^2 - \frac{4}{n} \cos^2 \frac{\psi}{2}}}} \right\}^{1/2}$	(16)

(4) Points on the hyperbola which are symmetrical with respect to its transversal axis correspond to a pair of conjugate trajectories, and will be called the conjugate points; points symmetrical with respect to the origin correspond to a pair of complementary trajectories, and will be called the complementary points. Consequently, points symmetrical with respect to the conjugate axis correspond to a pair of complementary-conjugate trajectories. Such a point pair will be called a complementary conjugate pair.

For the convenience of later development the quadrants of the hodograph plane bounded by the symmetrical axes of the constraining hyperbola will be referred to as positive (+) or negative (-) according as it is on the positive or the negative side of the V_χ-axis; and high (H) or low (L) according as it is above or below the V_ζ-axis. The parts of the constraining hyperbola and all velocity vectors will also be so referred to according to the quadrant in which they lie. Such subdivisions are depicted in Fig. 2.
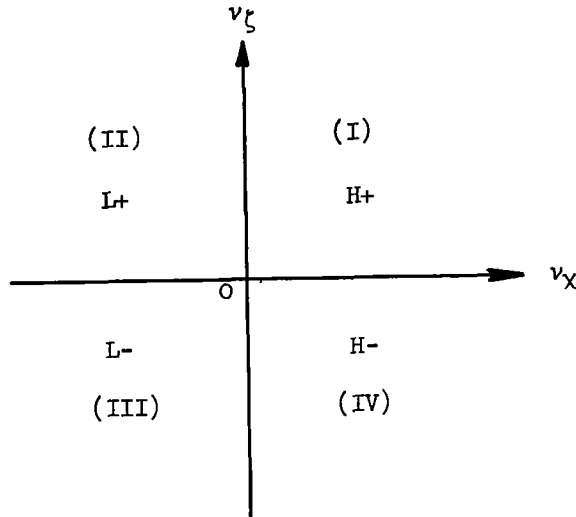
Fig. 2. Quadrants in the hodograph plane.

2.3 CRITERION OF THE NATURE OF THE REAL SOLUTIONS AND THE BOUNDARY EVOLUTE

In order to examine the nature of the solutions of the orthogonality quartic, either the V_{*C}-equation (10C) or the V_{*R}-equation (10R) may be used since they are identical in form and have essentially the same discriminant. To fix the idea the following discussion will be based on the V_{*C}-equation.

9

The discriminant for such a quartic is given by

$$\Delta \equiv I^3 - 27 J^2 \tag{17}$$

where

$$I \equiv \frac{1}{4} \kappa \left(m_0 n_0 - 4\kappa \right) \tag{18}$$

$$J \equiv \frac{1}{16} \kappa^2 \left(m_0^2 - \lambda_0^2 \right)$$

By using Burnside's criteria[2] together with Descartes' Rule of Signs we arrive at the conclusions in the first two columns of Table 3, classifying the nature of the real roots. Since multiple roots of the equation give identical solutions, they will be considered as one solution. From such considerations we arrive at the further conclusions in column IV, Table 3. The geometrical implication of such conclusions may be seen as follows.

With the expressions (17) and (18) the boundary condition $\Delta = 0$ may be written

$$4 \left(m_0 n_0 - 4\kappa \right)^3 - 27 \kappa \left(m_0^2 - \lambda_0^2 \right)^2 = 0 \tag{19}$$

Now introduce the polar coordinates (v, Φ) for the velocity vector $\vec{v}$ and express the parameters m_0 and n_0 for the initial velocity vector as

$$m_0 = v_0 \sin \left(\frac{\varphi_1}{2} + \Phi_0 \right)$$
$$n_0 = v_0 \sin \left(\frac{\varphi_1}{2} - \Phi_0 \right) \tag{20}$$

where Φ is the path angle referring to the minimum energy axis, and is related to the usual path angle ϕ by

$$\Phi = \phi - \frac{\varphi_1}{2} \tag{21}$$

By substituting these expressions into the boundary Eq. (19) we obtain

TABLE 3

NATURE OF THE REAL ROOTS (ν_{C_*} OR ν_{R_*}) OF THE ORTHOGONALITY
QUARTIC AND NUMBER OF REAL SOLUTIONS

(I)	(II)			(III)	(IV)		
	Real Roots				No. of Real, Distinct Orthogonality Solutions		
		Number			Positive Solutions	Negative Solutions	
Discriminant	Nature	Positive Roots	Negative Roots	Regions (see Fig. 3)	($\nu_C > 0$, $\nu_R > 0$)	($\nu_C < 0$, $\nu_R < 0$)	TOTAL
$\Delta < 0$	2 real roots, distinct	1	1	S_+ , S_-	1	1	2
$\Delta > 0$	4 real roots, all distinct	3	1	N_+	3	1	4
		1	3	N_-	1	3	4
$\Delta = 0$	4 real roots, not all distinct	3 (two equal)	1	H_+ L_+ } branches	2	1	3
		3 (all equal)	1	cusp G	1	1	2
		1	3 (two equal)	H_- L_- } branches	1	2	3
		1	3 (all equal)	cusp G'	1	1	2

$$[\bar{v}_o^2 (\cos 2\Phi_o - \cos\varphi_1) - 8\kappa]^3 - 54\kappa \ \bar{v}_o^4 \sin^2\varphi_1 \sin^2 2\Phi_o = 0 \qquad (22)$$

where $\bar{v}_o$ is the magnitude of the initial vector $\vec{v}_o$, which satisfies the boundary condition. This equation may be transformed into the following standard form in the rectangular coordinates (v_χ, v_ζ)

$$(A\bar{v}_\zeta)^{2/3} - (B\bar{v}_\chi)^{2/3} = C^{4/3} \qquad (23)$$

where the parameters A, B, and C have been given in Table 2. From Eq. (23) this boundary curve is recognized as one form of the Lamé curve,[3] which in the present case is the evolute of the constraining hyperbola. Some essential features of this curve are as follows (see Fig. 3):

(1) It is symmetrical with respect to both v_χ and v_ζ axes. Thus the boundary Lamé and the constraining hyperbola are co-axial.

(2) It is bounded between the v_θ- and v_d-axes which are normal to the asymptotic directions of the constraining hyperbola (the radial and chordal directions) respectively.

(3) It has two portions, one on each side of the v_χ-axis and each portion consists of two branches with a cusp (G,G') at its vertex given by the coordinates

$$(\bar{v}_o)_{G,G'} = 2\sqrt{\kappa} \ \csc \ \frac{\varphi_1}{2} \ , \ (\Phi_o)_{G,G'} = 0 \ , \ \pi \qquad (24)$$

It is well-known that an evolute of a given curve is the envelope of all normals of this curve, or conversely, the given curve is the involute of its evolute. Since to find solutions of the orthogonality quartic according to a pair of given values of m_o and n_o is equivalent to drawing normals to the constraining hyperbola from a given point in the hodograph plane, naturally its evolute should form the boundary separating the regions in which different number of such normals can be drawn. Directly from the concept of an evolute and the geometry of the hyperbola we see that

All points of intersections of the different normals to the constraining hyperbola are in the regions beyond the boundary Lamé, and no two normals to the hyperbola can intersect in the region between the two portions of the boundary Lamé.

The latter region will be referred to as simple (S), while the former, non-
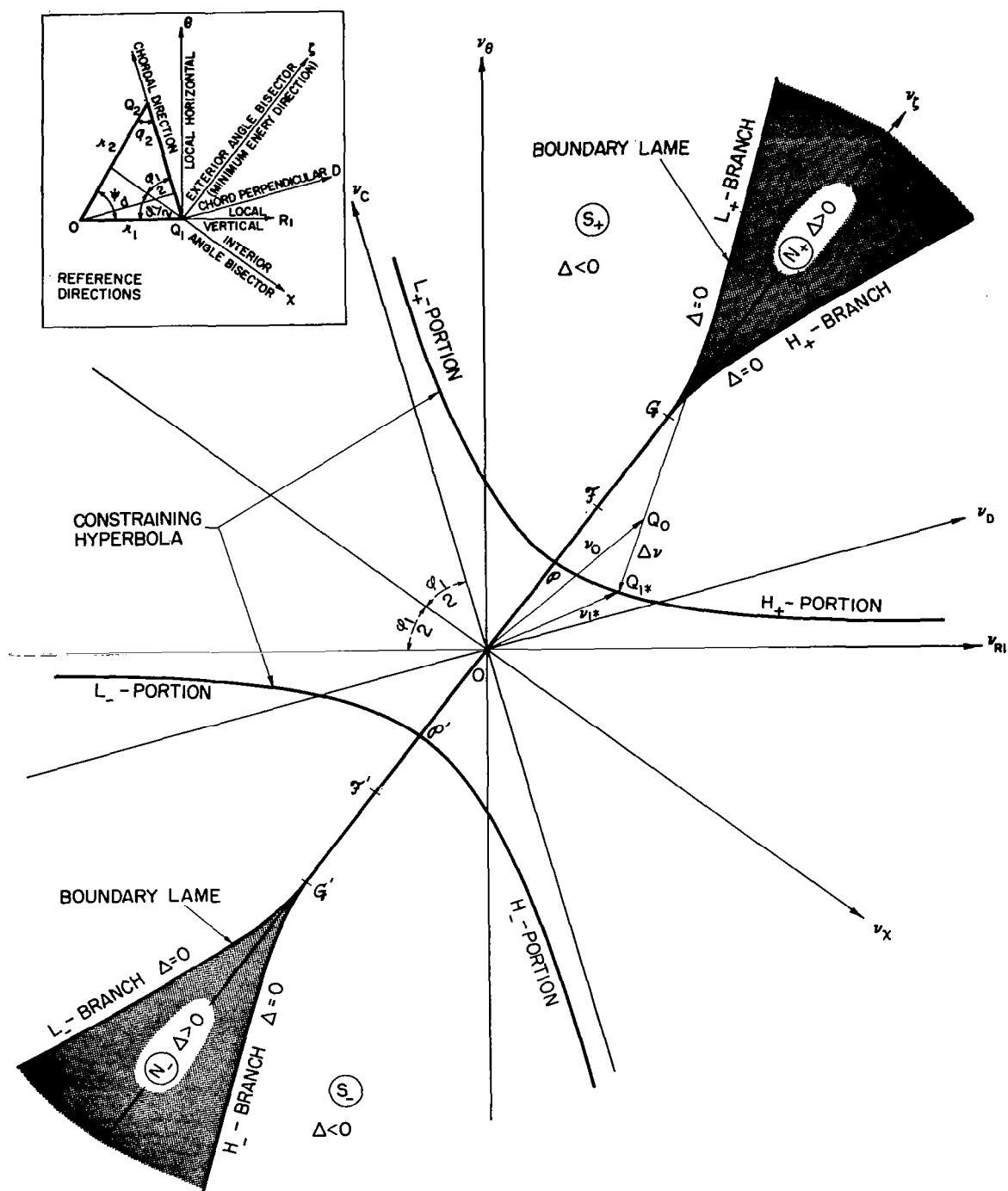
Fig. 3.   Geometry of the constraining hyperbola and the boundary Lamé.

13

simple (n). For convenience various portions of these regions, together with their boundaries, will be referred to as positive (+) or negative (-), and high (H) or low (L), according to the quadrant in which they are located, just as for the portions of the constraining hyperbola (Fig. 3).

With the foregoing understanding the conclusions previously derived from algebraic considerations may now be stated in geometrical terms as follows:

(A) Within the simple region one and only one normal can be drawn from a given point to each branch of the hyperbola.

(B) Within the non-simple region four distinct normals can be drawn from a given point, three to the nearer branch, and one to the farther branch.

(C) From any point on the boundary three distinct normals can be drawn: two to the nearer branch, and one to the farther branch except at the cusp, where only one normal can be drawn to each branch, both coinciding with the transversal axis.

Moreover, further examination of the geometry of a hyperbola shows that,

(D) The normals at points of the hyperbola in the same quadrant always intersect in the adjacent quadrant on the opposite side of the transversal axis of the hyperbola. (For example, two normals to the H+ part of the constraining hyperbola can meet only in the L+ portion of the N-region. This property is especially useful in the later treatment of the present problem; an analytical proof is given in Appendix B.)

Finally, it is to be noted that for a given vertex angle ψ the distance of either cusp of the boundary Lamé from the origin, $(\bar{v}_o)_{G,G'}$ decreases with increasing φ_1 or n, and it has the limiting value

$$(\bar{v}_o)_{G,G'} \to \sqrt{2} \; \sec^2 \frac{\psi}{2} > \sqrt{2} \quad \text{when} \quad \varphi_1 \to 0 \; (n \to \infty) \tag{25}$$

Thus multiple real solutions can occur in the half-plane ($v_\zeta > 0$ or $v_\zeta < 0$) only when the initial velocity is hyperbolic. Furthermore, owing to the presence of the asymptotic lines of the boundary Lamé, such a case cannot occur unless the initial velocity vector is directed above the local horizon but below its conjugate direction, the v_d-axis. A necessary and sufficient condition for the occurrence of such multiple solutions in the positive half-plane ($v_\zeta > 0$) may be precisely stated as follows:

$$v_o \geq \bar{v}_o \quad \text{and} \quad -\frac{\varphi_1}{2} < \Phi_o < +\frac{\varphi_1}{2} \tag{26}$$

where $\overline{v}_0$ is given by Eq. (22). Similar condition exists for the other half-plane $\left(v_\zeta < 0\right)$ by symmetry.

3. DETERMINATION OF THE OPTIMUM SOLUTION

3.1 THE ABSOLUTE MINIMUM SOLUTION

With the number of real and distinct solutions of the orthogonality quartic determined, the next task is to select the one for absolute minimum. For the time being let us disregard the question of unrealistic trajectory, and consider only the geometrical problem of determining the absolute minimum distance.[3] Such questions of maxima and minima can usually be settled by the second derivative test, and the absolute minimum determined by comparing the quantity to be minimized at these stationary points. However, it is simpler here to use a geometrical approach outlined below:

A. From the symmetrical nature of the hyperbola, it is evident that the minimum distance solution demands the optimum point on the constraining hyperbola to be in the same quadrant with the tip Q_O of the initial velocity vector. However, in view of the geometrical property of the hyperbola given by item (D) of the previous section, there is one and only one such a point on the constraining hyperbola in the same quadrant with the given point (see Figs. 4a, b, c) unless Q_O is on either of the symmetrical axes of the constraining hyperbola. This is true whether the point Q_O is in the simple or non-simple region. Thus when Q_O is off the symmetrical axes, the choice is clear, and the absolute minimum distance solution is unique. Furthermore, directly from this co-quadrant requirement it can be inferred immediately that the trajectory corresponding to such a solution always belongs to the same group (normal or complementary) and the same class (high or low) as the initial velocity vector.

B. In case Q_O lies on either of the symmetrical axes, then it is on the border of two adjacent quadrants. In such a case the minimum distance requirement is to have the optimum point lie in the half-plane of these two quadrants; and thus two solutions are possible.

(1) If Q_O lies on the v_χ-axis, then the optimum point must be on the same side of the v_ζ-axis with Q_O. The geometry in the hodograph plane shows that Q_O is in the simple region and equidistant from both branches of the hyperbola. Thus there are two and only two normals which can be drawn from Q_O, one to each branch, and they are of equal length. Consequently both ortho-points may be admitted, and there are two solutions for absolute minimum distance. The two corresponding trajectories require the same amount of Δv, and their departure velocities also have the same magnitude. Obviously

---

[3]The absolute minimum distance solution will be indicated by the subscript ** whenever it is to be distinguished from the orthogonality solution.

16
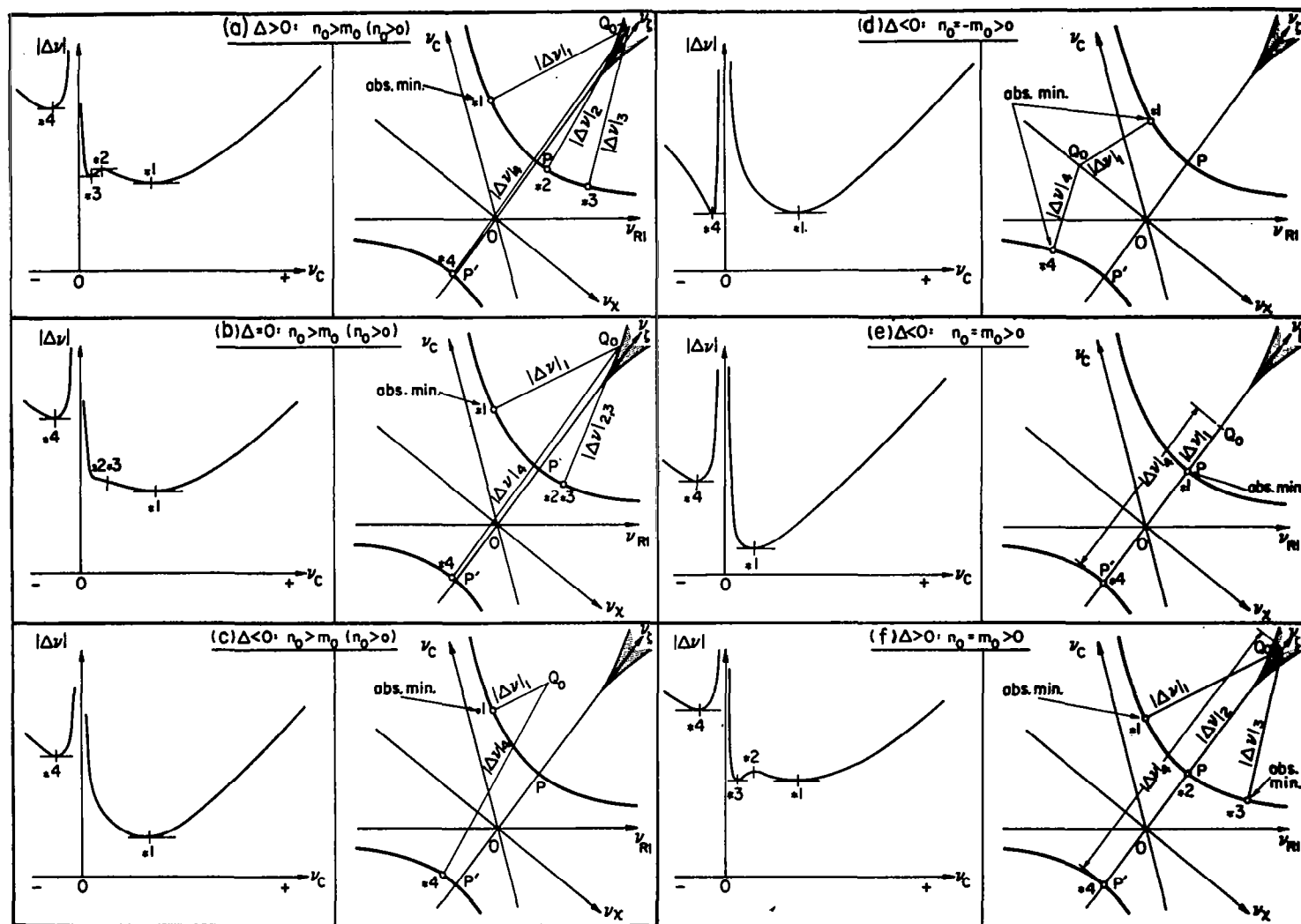
Fig. 4. Variation of $|\Delta \nu|$ and the corresponding geometry in the hodograph plane.

TABLE 4

THE REAL ROOTS OF THE ν_{C_*}-EQUATION AND THE NATURE
OF THE STATIONARY POINTS ON THE $|\Delta\nu|$-CURVE
(for the case $n_0 > 0$ and $n_0 \geq m_0$)

Designation of the root ν_{C_*}	$\Delta > 0$		$\Delta = 0$				$\Delta < 0$	
			$I^2 + J^2 \neq 0$		$I = 0, J = 0$			
	sign of ν_{C_*}	nature of $|\Delta\nu|$	sign of ν_{C_*}	nature of $|\Delta\nu|$	sign of ν_{C_*}	nature of $|\Delta\nu|$	sign of ν_{C_*}	nature of $|\Delta\nu|$
1	+	min	+	min	+ (all equal)	min	+	min
2	+	max	+ (equal)	neither			—	—
3	+	min					—	—
4	-	min	-	min	-	min	-	min

they constitute a complementary-conjugate pair, one belongs to the normal group, and the other, the complementary group. They will be either both high or both low according as the initial velocity vector is high or low. This situation is depicted in Fig. 4d.

(2) If Q_0 lies on the v_ζ-axis, then the optimum point must lie on the same side of the v_χ-axis. Now Q_0 may be either in the simple region (S) or the non-simple region (N).

i. Suppose Q_0 is in the S-region, that is, it lies between two cusps, G and G', of the boundary Lamé. Evidently the two and only two ortho-points now coincide with the vertices $\wp$ and $\wp'$ of the hyperbola, and there is only one on the same side of the v_χ-axis with Q_0. Thus the absolute minimum solution is again unique, and the corresponding trajectory is the minimum energy one. It will belong to the same group as the initial velocity vector. This situation is depicted in Fig. 4e.

ii. Suppose Q_0 is in the N-region, that is, it lies on the parts of the v_ζ-axis which are beyond the cusp points of the boundary Lamé in either direction. Then according to property (C) given in Section 2.3, there are three normals on the branch of the hyperbola on the same side of the v_χ-axis. It is evident from the symmetry of the hyperbola that among the three ortho-points, which are on the branch nearer to the initial point Q_0, one coincides with the vertex, while the other two are of a conjugate pair, and equidistant from Q_0. The fourth ortho-point coincides with the other vertex. This situation is depicted in Fig. 4f. Evidently, the fourth point should be rejected, and the choice will be between the point Q_{*2} and either of the points Q_{*1} and Q_{*3}. It can be shown that it is always the point Q_{*2} which is at a farther distance. (This can be easily proved by solving the orthogonality quartic with $m_0 = n_0$, and comparing the distances since in this particular case the quartic admits a simple solution.) Consequently, both points Q_{*1} and Q_{*3} may be admitted, and there are two solutions giving the same amount of Δv. The two corresponding trajectories are conjugate to each other, requiring the same magnitude of departure velocity, and they are both of the same group as the initial velocity vector. It is interesting to note here that the minimum energy trajectory is no longer the optimum transfer trajectory even though the initial velocity is in that direction; the two optimum directions are now inclined equally on either side of the minimum energy direction instead of lying along it.

iii. Finally when the point Q_0 is at either cusp of the boundary Lamé, then both conjugate points coincide with the nearer vertex, and the minimum distance solution is again unique, and the corresponding trajectory is again a minimum energy trajectory. This is the same as case i.

In conclusion,

(1)   Whenever the point Q_O is not on the conjugate axis of the hyperbola nor on the part of its transversal axis beyond the cusps of its evolute, the absolute minimum distance solution is unique. The corresponding trajectory will belong to the same group and same class as the initial velocity vector.

(2)   Whenever Q_O is on the conjugate axis of the constraining hyperbola there are two solutions with the same minimum distance. The corresponding trajectories are a complementary-conjugate pair of the same class as the initial velocity vector.

(3)   Whenever Q_O is on the transversal axis of the constraining hyperbola beyond the cusp points of the boundary Lamé, there are again two absolute minimum distance solutions. The corresponding trajectories are a conjugate pair of the same group as the initial velocity vector.

Based on such geometrical analysis we may now form the following "rules of thumb":

Rules—Geometric

(1)   Always choose the optimum point which is in the same quadrant with the point Q_O whenever no ambiguity arises. (One and only one solution.)

(2)   If ambiguity does arise such as when the point Q_O lies on either of the symmetrical axes of the constraining hyperbola, always choose the optimum point or points in the same half-plane with Q_O, and the ones off the minimum energy axis if they are present.

As shown above the geometrical rule for the selection of the absolute minimum solution is exceedingly simple. Such a geometrical analysis may in turn guide the selection of the appropriate root from the real solutions of the orthogonality quartic for an absolute minimum without calculating the magnitudes of the corresponding Δv's. In view of the symmetry of the constraining hyperbola it is sufficient to consider all the possible cases when Q_O is in one certain quadrant, say the second, and center our attention on the variation of $|\Delta v|$ with one variable, say c_*, when Q_O is in this quadrant. The geometry of such cases are illustrated in Fig. 4, and the corresponding variation of $|\Delta v|$ with v_{c_*} and the nature of its stationary points as obtained from usual algebraic analysis are also graphically shown in Fig. 4 for each case, and summarized in Table 4 for reference.

It is to be noted that the present restriction of Q_O in quadrant II is equivalent to saying $n_O > m_O$ and $n_O > 0$ in the orthogonality quartic. Keeping this in mind and without going into algebraic details, an examination of the geometry of the hodograph plane shows that:

When $m_0 \neq \pm n_0$ (Q_0 off the symmetrical axes), the optimum point in the hodograph plane always corresponds to the highest root v_{C*1} of the orthogonality quartic (see Fig. 4a, b, c).

When $m_0 = n_0$ (Q_0 on v_ζ-axis), the co-half-plane requirement from geometrical considerations indicates that the optimum root v_{C**} must agree in sign with the initial value v_{ζ_0}. Thus, under the present assumption, only the positive roots need be considered. The hodograph shows that there may be either one or three such roots corresponding to the one or three ortho-points on the positive branch of the constraining hyperbola. In the former case the only positive root is necessarily the optimum one. In the latter case the geometry of the hodograph shows that the pair of optimum points correspond to the highest and the lowest roots respectively (see Fig. 4f). Thus both roots may be chosen. It is to be noted that the prerequisite to have v_{C**} agree in sign with v_{ζ_0} hold in general whenever $m_0 = n_0$.

When $m_0 = -n_0$ (Q_0 on v_χ-axis), the two optimum points in the hodograph plane, one on each branch, correspond to the two and only two real roots of the quartic, one positive and one negative (see Fig. 4d). Thus again both roots may be chosen.

All the foregoing observations were made on the L_+ portion of the constraining hyperbola. The symmetry of the hyperbola with its conjugate axis shows that the same is true for the L_- portion if we take the magnitude of the root algebraically. Thus the same conclusions hold in the low-half-plane where $n_0 \geq m_0$. In the high-half-plane, we have $n_0 \leq m_0$. By the symmetrical nature of the hyperbola with its transversal axis, whatever is true for v_C in the low-half-plane is equally true for v_R in the high-half-plane. Or, in view of the reciprocal relation between v_C and v_R (Eq. (1)) we may say that whatever is true for the largest v_C (algebraic) in the low-half-plane is equally true for the smallest v_C (algebraic) in the high-half-plane. Based on such observations we may form some algebraic rules of thumb as follows:

Rules—Algebraic

(1) If $m_0 \neq \pm n_0$, always choose the root which agrees in sign with the initial value of v_ζ; and if more than one such root is present, choose the largest one if $n_0 \gtrless m_0$ and the smallest one if $n_0 < m_0$ (one solution only).

(2) If $m_0 = n_0$, choose both the largest and the smallest roots which agree in sign with v_{ζ_0} (two solutions).

(3) If $m_0 = -n_0$, only two real roots are present, both may be chosen (two solutions).

The magnitudes of roots are being considered algebraically. All rules (1) to (3) hold for the v_{R*}-equation (10R) if we interchange the words m_0 and n_0.

3.2 LINES OF CONSTANT OPTIMUM TRAJECTORY AND LINES OF CONSTANT VELOCITY INCREMENT

Before we take up the question of unrealistic trajectories, it is essential to note that when the tip Q_O of the initial velocity vector moves along a straight line normal to the constraining hyperbola, the absolute minimim point Q_{**} remains intact, and consequently the corresponding transfer trajectories are the same as long as Q_O remains in the same quadrant. Such a trajectory will be the optimum trajectory for the present problem unless it is unrealistic. Thus the part of the normal line intercepted by the symmetrical axes of the constraining hyperbola (e.g., line **a'b** in Fig. 5) may be regarded as a line of constant optimum trajectory. As soon as the normal line crosses either axis the absolute minimum point will shift to the other side of the axis and move along the constraining hyperbola resulting in a different trajectory for each point on the extended part of this normal line. It is to be noted that along a line of constant optimum trajectory the velocity-increment required varies from point to point depending on the position of Q_O on this line, the farther Q_O is from the constraining hyperbola, the larger the velocity-increment (absolute value) required.

In such a connection we may conceive that, when Q_O moves along a curve running parallel to the constraining hyperbola, the amount of velocity increment required will remain the same while the optimum transfer trajectory changes from point to point. Thus such parallel curves may be regarded as lines of constant optimum velocity-increment. As known in geometry, all these parallel curves have the same normal lines and a common evolute. In the present case the boundary Lamé is this common evolute, and each of the parallel curves, including the constraining hyperbola is its involute. Thus the lines of constant optimum trajectory and the lines of constant velocity-increment are normal to each other, forming an orthogonal net in the hodograph plane. Such a net will be useful in developing hodograph charts for the present problem, which will be presented after the question of unrealistic trajectories has been cleared up. For the time being it is to be noted that such parallel curves though quite similar to the original curve (the constraining hyperbola) when they are close to it, may look radically different from it when they are farther from the hyperbola, especially when they enter the non-simple region. The mathematic equation for the curves parallel to a hyperbola is in general of the eighth degree.[1] A few such typical curves are shown in Fig. 6.

3.3 THE CRITICAL CONDITION AND THE UNREALISTIC TRAJECTORIES

From the foregoing consideration of the lines of constant transfer trajectories it is evident that when the tip Q_O of the initial velocity vector moves along such a line which passes through a critical point ($v = \sqrt{2}$) on the constraining hyperbola, the absolute minimum distance solution will call for a parabolic trajectory. Such lines will be called the critical lines. Figure 7 shows the four critical lines, one through each of the four critical points
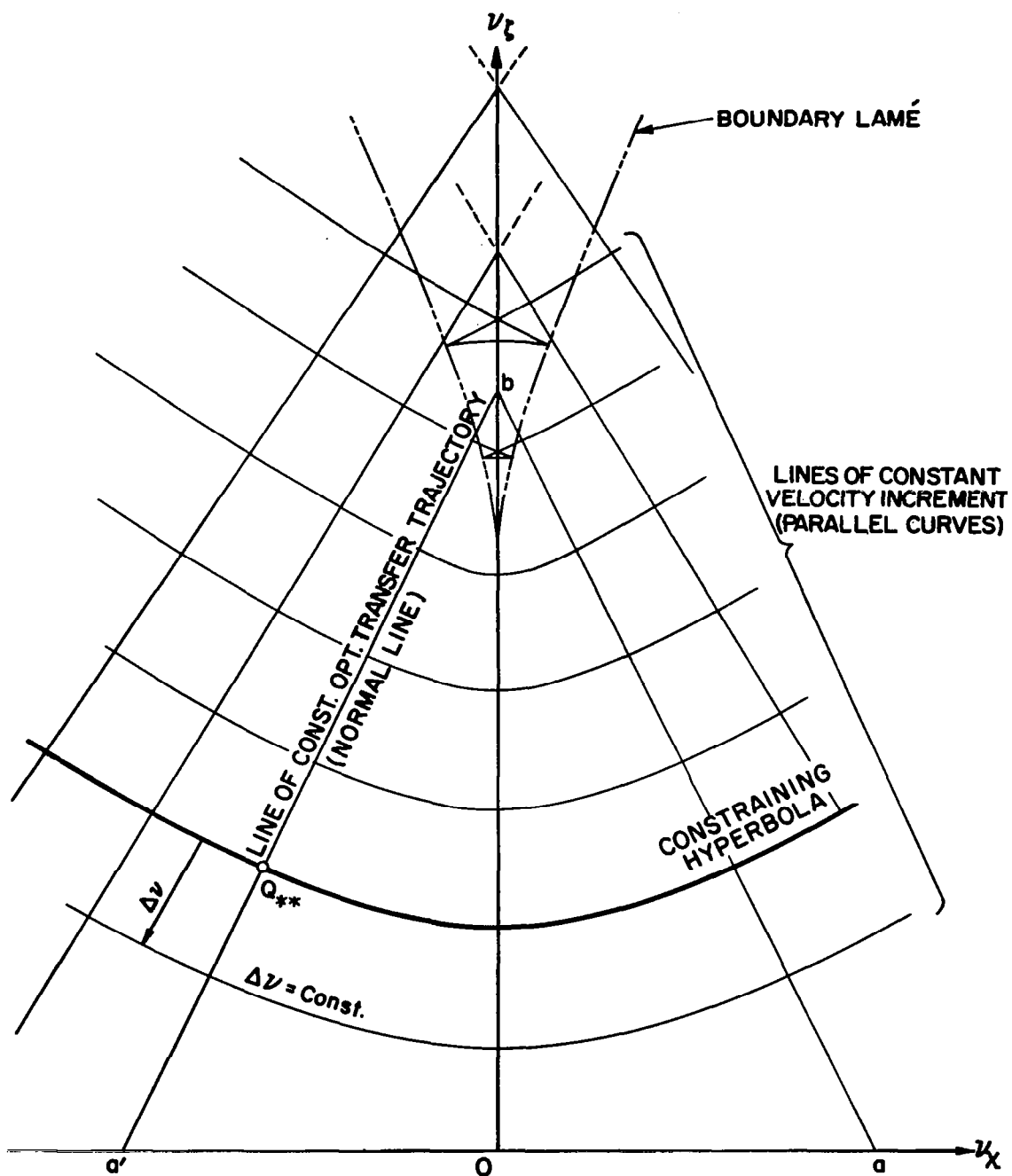
Fig. 5. Lines of constant optimum transfer trajectory and lines of constant optimum velocity-increment.

$\Delta \nu =$ Const.

ν_ζ

A'

B'

C'

φ'

$\Delta \nu$

$\Delta \nu$

$\Delta \nu$

$\Delta \nu$

A

L⁺ PORTION

B

C

φ

HYPERBOLA

H⁺ PORTION

(a) Correspondence Between the Hyperbola and It's Parallel Curve.

$\Delta \nu_{III} =$ Const.

$\Delta \nu_{II} =$ Const.

$\Delta \nu_{I} =$ Const.

N

I

III

II

BOUNDARY LAMÉ

(b) Three Parallel Curves Passing Through a Point in the Non-Simple Region.

Fig. 6. Geometry of the parallel curves.

(H) Hyperbolic Transfer (Realistic)

Constraining Hyperbola

CRITICAL CIRCLE
Radius = $\sqrt{2}$

(E) Elliptic Transfer (Realistic)

ECVI Line

(U) Region of Unrealistic Transfer

(U₁)

▨▨	Initial hyperbolic orbit requires elliptic optimum
░░░	Initial elliptic orbit requires hyperbolic optimum
▨▨	Initial elliptic orbit requires unrealistic optimum
U₁	Unrealistic region: no definite alternate realistic optimum
U₂	Unrealistic region: definite alternate realistic optimum exists
ECVI Line	Equi-critical-velocity-increment line

Fig. 7. Regions of the hodograph plane and the nature
of the optimum transfer trajectory.

25

on the constraining hyperbola, forming a critical circuit a-b-a'-b'-a. These four critical points are given by the intersections of the hyperbola with the critical circle centered at the hodograph origin and having the radius $\sqrt{2}$. When Q_O moves along such a circuit, the trajectory corresponding to the absolute minimum distance solution will first be a parabola of the high class and normal group when Q_O remains on ab, and as soon as it passes the point b, the trajectory will shift to its conjugate, and so forth.

As seen from the hodograph geometry, as long as Q_O is inside the rhomboid-shaped region bounded by the four critical lines, the corresponding absolute minimum point on the constraining hyperbola will remain inside the critical circle, consequently the transfer trajectory will be elliptic. This region will therefore be called the elliptic region. When Q_O is on the boundary of this rhomboid and beyond, the corresponding absolute minimum distance trajectory will first become parabolic and then hyperbolic. Thus the regions beyond the critical boundaries are hyperbolic regions. As shown in Ref. (9), a transfer trajectory between two fixed terminal points will be unrealistic only when it is parabolic or hyperbolic, and of the high class. Consequently the hyperbolic region on the high side is the region for unrealistic optimum transfer, and will be called the unrealistic region, while that on the low side, and the elliptic region in between are regions for realistic optimum transfer, and will be called the realistic region. Thus the boundary b-a'-b' separates the region for hyperbolic transfer from that for elliptic transfer, all realistic; while the boundary b'-a-b separates the elliptic realistic region from that of unrealistic transfer. Hence the two critical lines on the high side will hereafter be referred to as the realistic barrier. Beyond the vertices b and b' of the rhomboid aba'b' the realistic and the unrealistic regions are further separated by the v_ζ-axis, which itself belongs to the realistic region. In short, the broken line b'-a-b and the part of v_ζ-axis beyond either b or b' form the entire realistic barrier which divides the whole hodograph plane into two main regions, the realistic region and the unrealistic region for the optimum transfer. With such a partition established in the hodograph plane we may say that the absolute minimum distance solutions obtained in the preceding analysis is actually the optimum solution of the problem whenever the tip Q_O of the initial velocity vector lies in the realistic region. It ceases to be the optimum only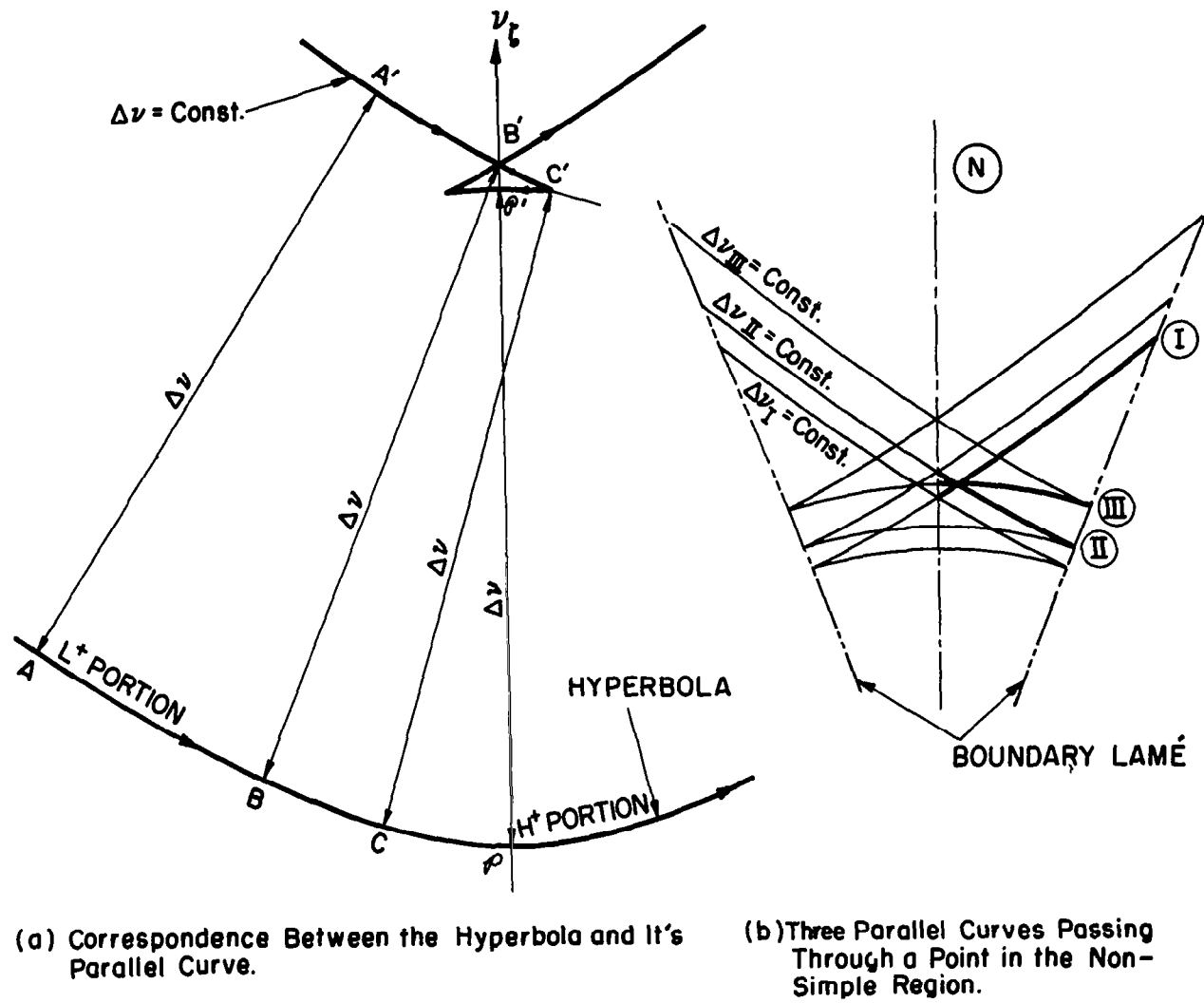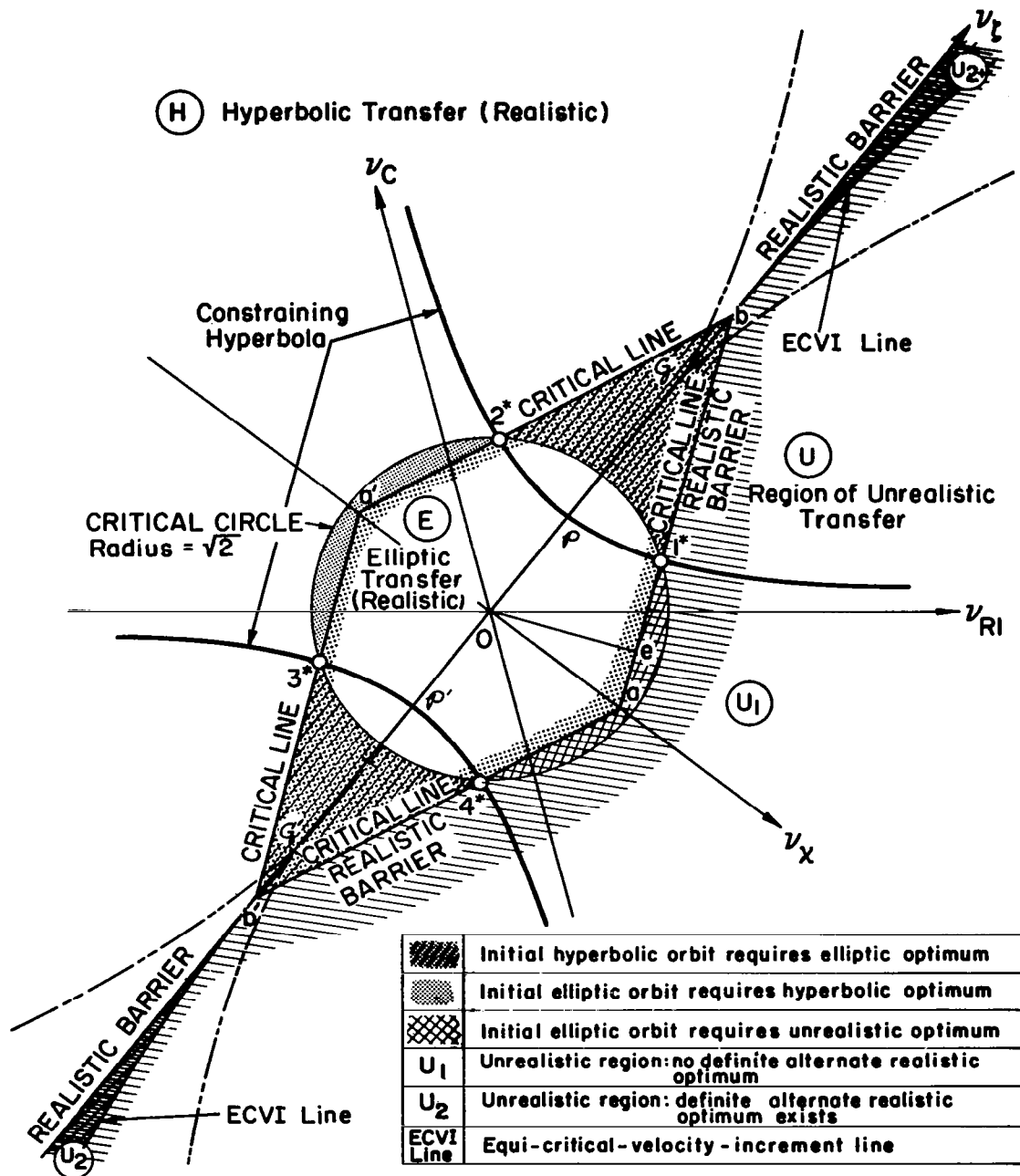 when Q_O is beyond the realistic barrier, or on the boundary b'-a-b, excluding the two end points b and b'. The various regions in the hodograph plane are shown in Fig. 7, and further divisions of the unrealistic region will be presented in the next section.

It is interesting to note that the type of the optimum transfer trajectory, whether elliptic, parabolic, or hyperbolic does not necessarily agree with that of the initial velocity. The shaded region beyond the critical lines on the low side but within the critical circle is the region where the initial velocity is elliptic, but the optimum solution calls for a hyperbolic transfer. Similarly, the shaded region beyond the critical circle but within the rhomboid is the region where a hyperbolic initial velocity calls for an optimum elliptic transfer.

It is also evident from the hodograph that even an elliptic initial velocity, if at sufficiently high path angle, may introduce an unrealistic optimum. The geometrical criterion for an unrealistic optimum transfer obtained so far will be analytically formulated as follows:

First, we note that there always exist such critical points, where $v = \sqrt{2}$, on the constraining hyperbola, because the minimum velocity along this hyperbola is always elliptic according to Eq. (13), Table 2,

$$v_{min} = A = \sqrt{2 \tan \frac{\psi}{2} \tan \frac{\varphi_1}{2}} < \sqrt{2} \tag{27}$$

since $\varphi_1 < \pi - \psi$. The condition to be satisfied by the initial velocity vector in order that its tip lies on the critical line through a critical point (v_C^*, v_R^*) is then, according to Eq. (9'),

$$n_o\, v_C^* - m_o\, v_R^* = v_C^{*2} - v_R^{*2} \tag{28}$$

Proceeding from the oblique coordinates (v_C, v_R) to the rectangular coordinates (v_χ, v_ζ), Eq. (28) may be transformed into

$$v_\chi^* v_{\zeta o} \sin^2 \frac{\varphi_1}{2} + v_\zeta^* v_{\chi o} \cos^2 \frac{\varphi_1}{2} = v_\chi^* v_\zeta^* \tag{29}$$

which finally reduces to the polar form

$$v_o \left(v_\chi^* \cos \Phi \sin^2 \frac{\varphi_1}{2} + v_\zeta^* \sin \Phi \cos^2 \frac{\varphi_1}{2} \right) = v_\chi^* v_\zeta^* \tag{30}$$

with

$$v_{\chi o} = v_o \sin \Phi_o$$
$$v_{\zeta o} = v_o \cos \Phi_o \tag{31}$$

The coordinates of the four critical points as given by the intersection of the critical circle and the constraining hyperbola are found as follows:

27

	v_X^*	v_ζ^*
1*	$+\sqrt{X*}$	$+\sqrt{Y*}$
2*	$-\sqrt{X*}$	$+\sqrt{Y*}$
3*	$-\sqrt{X*}$	$-\sqrt{Y*}$
4*	$+\sqrt{X*}$	$-\sqrt{Y*}$

$$(32)$$

where

$$X* = 2 \sec \frac{\psi}{2} \cos \frac{\varphi_1}{2} \cos \frac{1}{2}(\psi + \varphi_1)$$

$$(33)$$

$$Y* = 2 \sec \frac{\psi}{2} \sin \frac{\varphi_1}{2} \sin \frac{1}{2}(\psi + \varphi_1)$$

The four points are numbered according to the quadrant they are in (see Fig. 7). Let $\vec{v}_0^*$ be the initial velocity vector satisfying Eq. (30) then by inserting Eqs. (32,33) into Eq. (30) we may express the critical condition along the boundary a-b-a'-b'-a as summarized below (where the usual subscripts H+ etc. are used to indicate the quadrant where the tip of Q_0 lies):

along a-b $(0 \leq \phi_0 \leq \frac{\pi}{2})$	$(v_0)_{H+}^* (C_1 \cos \phi_0 + C_2 \sin \phi_0) = 1$ $\qquad$ (34-1)
along b-a' $(-\frac{\pi}{2} \leq \phi_0 \leq 0)$	$(v_0)_{L+}^* (C_1 \cos \phi_0 - C_2 \sin \phi_0) = 1$ $\qquad$ (34-2)
along a'-b' $(-\pi \leq \phi_0 \leq -\frac{\pi}{2})$	$(v_0)_{L-}^* (C_1 \cos \phi_0 + C_2 \sin \phi_0) = -1$ $\qquad$ (34-3)
along b'-a $(\frac{\pi}{2} \leq \phi_0 \leq \pi)$	$(v_0)_{H-}^* (C_1 \cos \phi_0 - C_2 \sin \phi_0) = -1$ $\qquad$ (34-4)
$C_1 \equiv \sqrt{\dfrac{\sin^3 \frac{\varphi_1}{2} \cos \frac{\psi}{2}}{2 \sin \frac{1}{2}(\psi+\varphi_1)}}, \quad C_2 \equiv \sqrt{\dfrac{\cos^3 \frac{\varphi_1}{2} \cos \frac{\psi}{2}}{2 \cos \frac{1}{2}(\psi+\varphi_1)}}$ $\qquad$ (35)	

28

Recalling that the realistic barrier is along b'-a-b, a criterion for unrealistic optimum transfer may now be stated as follows:

$$0 < \Phi_0 \leq \frac{\pi}{2} : \quad v_0 \geq (v_0^*)_{H+}$$

$$\frac{\pi}{2} \leq \Phi_0 < \pi : \quad v_0 \geq (v_0^*)_{H-} \tag{36}$$

Similarly, recalling that the realistic critical boundary is along b-a'-b', and that realistic hyperbolic transfer exists along the v_ζ-axis beyond b and b', a criterion for parabolic and hyperbolic optimum transfer is

$$-\frac{\pi}{2} \leq \Phi_0 < 0 : \quad v_0 \geq (v_0^*)_{L+}$$

$$-\frac{\pi}{2} \geq \Phi_0 > -\pi : \quad v_0 \geq (v_0^*)_{L-} \tag{37}$$

$$\Phi_0 = 0, \pi : \quad v_0 \geq v_{b,b'}$$

By setting $v_{\chi 0} = 0$ in Eq. (29) and using formulas (32) and (33) we find the distance from the origin to either corner point, b or b',

$$v_{b,b'} = \overline{Ob} = \sqrt{2 \sec \frac{\psi}{2} \csc^3 \frac{\varphi_1}{2} \sin \frac{1}{2}(\psi + \varphi_1)} \tag{38}$$

It can be shown by comparing Eq. (38) with Eq. (24) that,

$$v_{b,b'} > v_{G,G'}$$

That is, the corners of the elliptic region always extend into the non-simple regions. This should be expected since either point b or b' is an intersection of two normals to the constraining hyperbola. This situation implies that two realistic optimum solutions exist in the elliptic region when the initial velocity is in the minimum energy direction, and has the magnitude

$$v_{G,G'} < v_0 < v_{b,b'}$$

As discussed before, the optimum solution in such a case does not give the minimum energy trajectory, but instead it gives a conjugate pair of two trajectories. And, within the present range of v_0 they are both elliptic of course. The same situation exists when $v_0 \geq v_{b,b'}$ except that the optimum trajectory is now hyperbolic, and the realistic optimum solution is unique since its conjugate becomes unrealistic.

Finally, as the hodograph shows, there is a minimum initial speed $(v_o^*)_L$ below which neither a critical nor an unrealistic optimum can occur, for whatever the path angle may be. This is given by the length of the perpendicular drawn from the origin to any of the critical lines, e.g., the line segment oe in Fig. 7. From the trigonometry of the triangle oab, we find

$$(v_o^*)_L = \overline{oe} = \sqrt{\frac{\sec \frac{\psi}{2} \sin(\psi+\varphi_1)}{\sin^3 \frac{\varphi_1}{2} \cos \frac{1}{2}(\psi+\varphi_1) + \cos^3 \frac{\varphi_1}{2} \sin \frac{1}{2}(\psi+\varphi_1)}} \tag{39}$$

For example, if $\psi = 60°$, $\varphi_1 = 75°$ (corresponding to the transfer to a target point at the distance ratio $n = 1.366$) we have $(v_o^*)_L = 1.22$. Besides, it is evident that unrealistic optimum cannot occur when the initial velocity vector is in the low half-plane ($\Phi_o \le 0$).

3.4 CHOICE OF THE REALISTIC OPTIMUM TRANSFER TRAJECTORY

From the preceding analysis the absolute minimum solution of the orthogonality quartic is the optimum solution of the problem whenever the tip Q_o of the initial velocity vector is in the realistic region. However, whenever Q_o is outside this region, the absolute minimum solution is an unrealistic optimum, from the physical point of view, and it remains to select a realistic optimum trajectory for the problem. Such a selection will depend on whether the point Q_o is in the simple or non-simple region of the hodograph plane.

A. Suppose Q_o is in the simple region and off the v_χ-axis. Then the absolute minimum distance solution is unique. In such a case it is evident that the best choice will be the point on the constraining hyperbola sufficiently close to the critical point in the same quadrant with the initial point Q_o but still within the elliptic region. Thus, strictly speaking, there is no definite optimum solution for the problem in this case. The transfer trajectory so chosen will necessarily be highly eccentric, of the same class (high) and same group as the initial velocity vector. If Q_o is on the v_χ-axis, then the two critical points on the realistic barrier, one on each side of the v_χ-axis may be the reference points, and points close to either critical point may be chosen.

B. Suppose Q_o is in the non-simple region. We recall that in such a region three normals can be drawn from the point Q_o to the nearer branch of the constraining hyperbola. For definiteness let us assume Q_o is the H_+ portion of the region N (see Fig. 8). Then the three ortho-points on the constraining hyperbola will be distributed as follows:

Fig. 8. Choice of the realistic optimum trajectory: initial
velocity vector in the unrealistic region.

Ortho-Point	Branch of the Constraining Hyperbola	Nature of the Solution
*1	H+	Min., absolute, unrealistic
*2	L+	Max.
*3	L+	Min., local, realistic

Thus, besides the unrealistic minimum there is a second minimum for consideration, which is realistic. Let $|\Delta v|_3$ and $|\Delta v|^*$ be the velocity-increments required at the point 3 and the critical point under consideration (e.g., point 1* in Fig. 8) respectively. Then the choice will depend on the magnitudes of these two quantities.

(1) If $|\Delta v|_3 \leq |\Delta v|^*$, then the optimum trajectory is definite and unique, as given by the point *3.

(2) If $|\Delta v|_3 > |\Delta v|^*$, then some point close to the critical point but within the elliptic region should be chosen. This case is the same as case A.

C. Suppose Q_0 is on the boundary Lamé, then the points *2 and *3 coincide, giving neither minimum nor maximum, leaving the unrealistic point *1 to be the only minimum solution. This case is again the same as case A.

In making the foregoing comparison, the concept of constant velocity-increment introduced in Section 3.2 is helpful. It is to be noted that while such lines are curves parallel to the constraining hyperbola in the realistic region, they are concentric circles centered at the reference critical point in the unrealistic region, since in this latter region the velocity increment at the critical point is the standard for comparison. The point in the unrealistic region at which

$$|\Delta v|_3 = |\Delta v|^*$$

is then given by the intersection of such a circle with one of the parallel curves of the same constant $|\Delta v|$ as illustrated in Fig. 9. Of course only these intersections within the non-simple region are of interest at present. The locus of all such points of intersections in the unrealistic region will be called the line of equi-critical-velocity-increment (E-C-V-I line for short), and there is one such line on either side of the v_χ-axis. As shown in Fig. 7 these two lines further divide the unrealistic region into the following subregions: the one (U_2) bounded by each E-C-V-I line and the v_t-axis is the one in which we have $|\Delta v_3| < |\Delta v|^*$ and therefore the realistic optimum solution is definite and unique; and the one (U_2) bounded between these two lines is the subregion in which either $|\Delta v_3| > |\Delta v|^*$ or Δv_3 does not exist, therefore the realistic optimum solution of the problem is definite. On the boundary $|\Delta v_3| = |\Delta v|^*$ the realistic optimum solution is
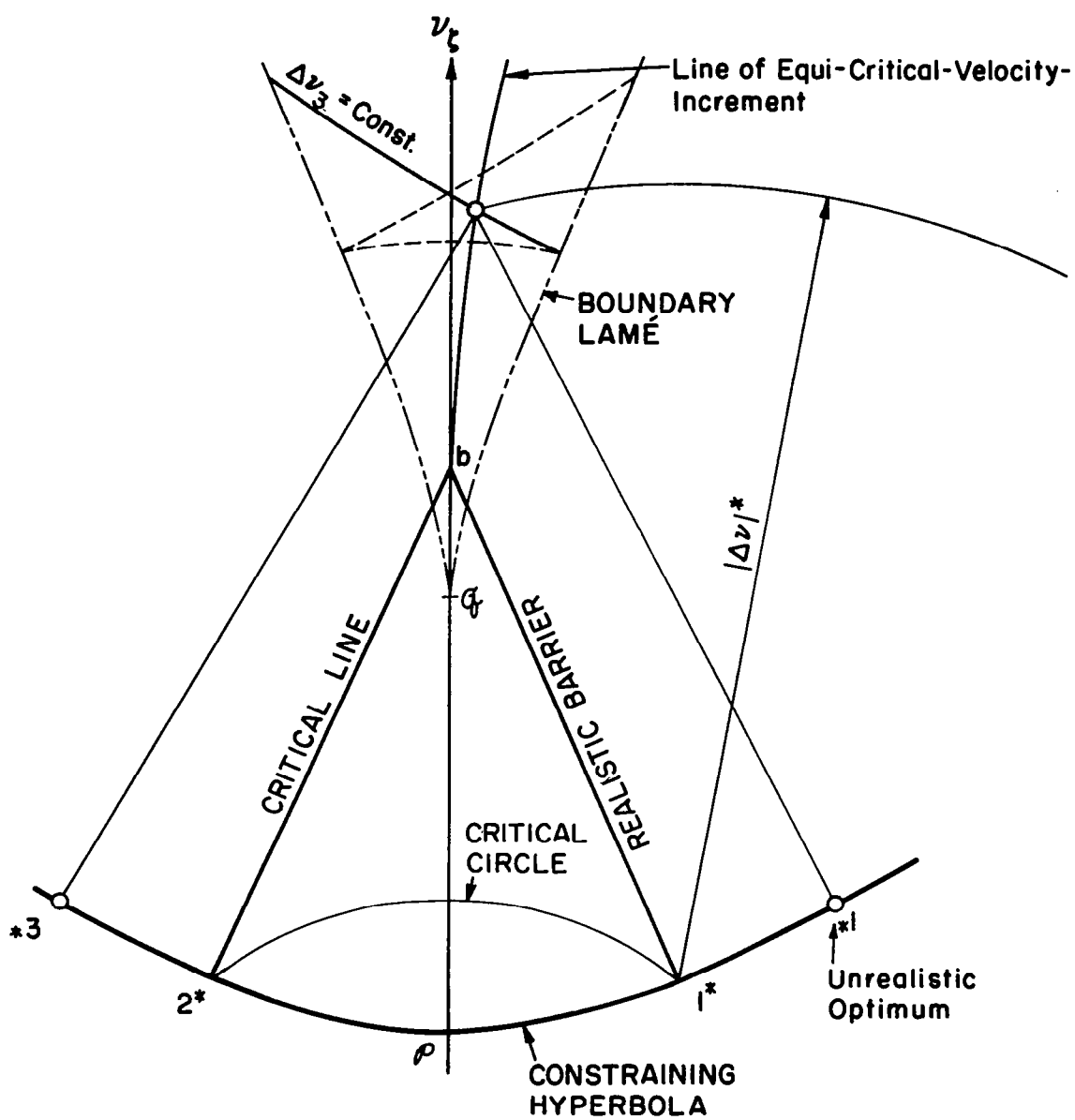
Fig. 9. Determination of the boundary point, $|\Delta v|_3 = |\Delta v|^*$

TABLE 5

REGIONS IN THE HODOGRAPH PLANE AND THE NATURE OF THE OPTIMUM TRANSFER TRAJECTORIES

Region				Number of Realistic Optimum Solutions	Nature of the Realistic Optimum Transfer Trajectory
Name	Designation	Description	Subregion		
Elliptic Region	(E)	Within the rhomboid aba'b'	Off ν_χ, ν_ζ -axes	1	Elliptic
			On ν_χ -axis: between a and a'	2	Elliptic, complementary-conjugate pair
			On ν_ζ -axis: between and at $\mathscr{g}$ and $\mathscr{g}'$	1	Elliptic, minimum energy
			On ν_ζ -axis: between $\mathscr{g}$ and b or $\mathscr{g}'$ and b'	2	Elliptic, conjugate pair
Critical Line	b-a'-b'	Including end points b and b'		1	Parabolic
Hyperbolic Region	(H)	On the low side of the line b-a'-b' and the ν_ζ-axis	Off ν_χ, ν_ζ -axes	1	Hyperbolic
			On ν_χ-axis: beyond a'	2	Hyperbolic, complementary-conjugate pair
Realistic Barrier	ν_ζ-axis	Beyond b or b'		1	Hyperbolic
	Line b'-a-b	Excluding end points b and b'		Indefinite	Elliptic, highly eccentric, close to the unrealistic parabolic trajectory
Unrealistic Region	(U)	On the high side of the line b'-a-b and the ν_ζ-axis	Between the two lines of equi-critical-velocity-increment (U_1)	Indefinite	Elliptic, highly eccentric, close to the unrealistic parabolic trajectory
			Between the ν_ζ-axis and each line of equi-critical-velocity-increment (U_{2+}, U_{2-})	1	Hyperbolic

also definite and unique. The subregion U_2 falls entirely within the non-simple region of course. Following the previous analysis we see that in this subregion the realistic optimum solution is to be found by following the normal line through the initial point Q_0 to the constraining hyperbola in the low half plane. This practically extends the applicability of the normal lines originated from the low-half plane to the high half-plane until the E-C-V-I-line. Evidently the same is true for the parallel curves. Furthermore, the geometry of the hodograph shows that, whenever a definite realistic optimum solution exists while the tip Q_0 of the initial velocity vector is in the unrealistic region the optimum transfer trajectory will always be hyperbolic of the low class, since the two E-C-V-I lines terminate at the corners b and b' of the elliptic region.

The foregoing analysis completes the discussion on the selection of the realistic optimum transfer trajectory for the problem. All the previous conclusions on such selections are summarized in Table 5.

3.5 THE MINIMUM VELOCITY-INCREMENT OF THE OPTIMUM SOLUTION

Following the previous analysis the realistic optimum solution of the problem is indefinite whenever Q_0 is in the region U_1, and is definite everywhere else. The definite optimum solution is provided by the orthogonality Eq. (10'-C or 10'-R), and the corresponding minimum velocity-increment is given by Eq. (3'), which may be written alternately,

$$|\Delta v_*|^2 = 2v_{C*}^2 - 3n_0 v_{C*} - \frac{m_0^\kappa}{v_{C*}} + v_0^2 - 2 \tan \frac{\psi}{2} \cot \varphi_1 \qquad (3'\text{-C})$$

$$= 2v_{R*}^2 - 3m_0 v_{R*} - \frac{n_0^\kappa}{v_{R*}} + v_0^2 - 2 \tan \frac{\psi}{2} \cot \varphi_1 \qquad (3'\text{-R})$$

by using Eqs. (10'-C,R). The indefinite optimum solution may be written approximately,

$$\vec{v}_* \cong \vec{v}^* \qquad (40)$$

$$|\Delta v_*| = |\Delta v^*|^+$$

where $\vec{v}^*$ is the critical velocity vector co-quadrant with $\vec{v}_0$, and $|\Delta v^*|$ is given by

$$|\Delta v^*| = |\vec{v}^* - \vec{v}_0| = \sqrt{v_0^2 - 2\sqrt{2} \cos(\Phi_0 - \Phi^*) + 2} \qquad (41)$$

where Φ_O and Φ^* are the path angles of $\vec{v}_O$ and $\vec{v}^*$ respectively, both referring to the minimum energy direction at the initial terminal.

For a given base triangle the effects of the initial velocity vector $\vec{v}_O$ on the magnitude of $\vec{\Delta v}_*$ may be easily seen from the hodograph geometry. Let us first consider the case when $\vec{v}_O$ has a constant direction but varying magnitude, that is, when Q_O moves along a directed straight line through the hodograph origin at an arbitrary angle Φ_O such as the $\mathcal{L}$-lines in Fig. 10a. When Q_O moves from the origin outward, the hodograph shows that $|\Delta v_*|$ first decreases and then increases. In the realistic region, it will have its least value when Q_O is closest to the constraining hyperbola. The point of closest approach, Q_C, will be at the intersection of the $\mathcal{l}$-line and the hyperbola if they do intersect. This will be the case when the $\mathcal{L}$-line falls in neither of the inner and outer forbidden regions for the direction of departure[4] (like $\mathcal{L}_1$ and $\mathcal{L}_2$ in Fig. 10a). In such a case, $\Delta v_* = 0$, and the initial velocity is the correct departure velocity along the given direction for the two terminal transfer. If the $\mathcal{L}$-line falls within the inner forbidden region, no such an intersection is possible; however, Q_C may still exist on the $\mathcal{L}$-line (see $\mathcal{L}_3$ in Fig. 10a), but the corresponding Δv_* will not be zero. If the $\mathcal{L}$-line falls within the outer forbidden region, then it lies partly in an unrealistic region, and $|\Delta v_*|$ will be least when Q_O is closest to the critical point in the same quadrant with the $\mathcal{L}$-line. The point of closest approach, Q_C, will then be given by the foot of the perpendicular drawn from this critical point to the $\mathcal{L}$-line if the foot lies also in the unrealistic region. A rectangular plotting of $|\Delta v_*|$ versus v_O is shown in Fig. 10b. To avoid confusion the constant Φ_O lines have been separated into two groups: $|\Phi_O| = 0$ to Φ^*, and $|\Phi_O| = \Phi^*$ to $\pi/2$, where Φ^* is the critical angle indicated in Fig. 10a.

It is worth noting that, in the elliptic region, due to the symmetry of the hodograph geometry with respect to the v_ζ-axis, $|\Delta v_*|$ remains the same when Φ_O changes to $-\Phi_O$ at the same v_O. Thus, in this region the $|\Delta v_*|$ versus v_O curves are identical for $\pm\Phi_O$. However, after v_O reaches its value on the critical boundary a-b-a'-b'-a, such a symmetry no longer exists due to the presence of the unrealistic region, and $|\Delta v_*|$ in the high half-plane is higher than its conjugate part in the low half-plane. Consequently the $|\Delta v_*|$ vs v_O curves splits into two branches, one for the $+\Phi_O$ and one for the $-\Phi_O$ as shown in Fig. 10b. It is also to be noted that, on the positive branch, the optimum solution is indefinite, and the values used in the plotting are in fact those of $|\Delta v^*|$ which is the lower limit of the indefinite $|\Delta v_*|$. Finally it should be mentioned that, as the hodograph geometry is symmetrical with respect to the v_χ-axis in both the realistic and the unrealistic regions, each constant Φ_O curve also holds for its supplementary angle of the same sign (e.g. the curves for $\Phi_O = 70°$ and $110°$ are indentical, and so are those for $-70°$ and $-110°$).

---

[4]For terminology see Appendix A and Ref. 9, pp. 10-12.

(a) Hodograph Geometry

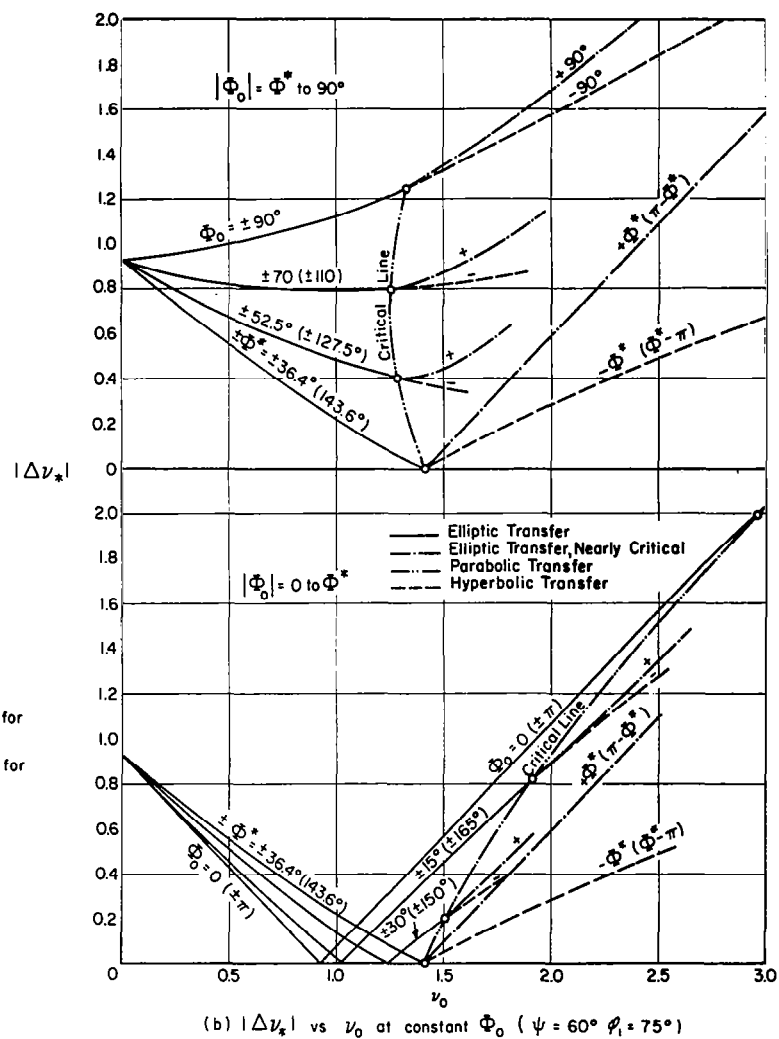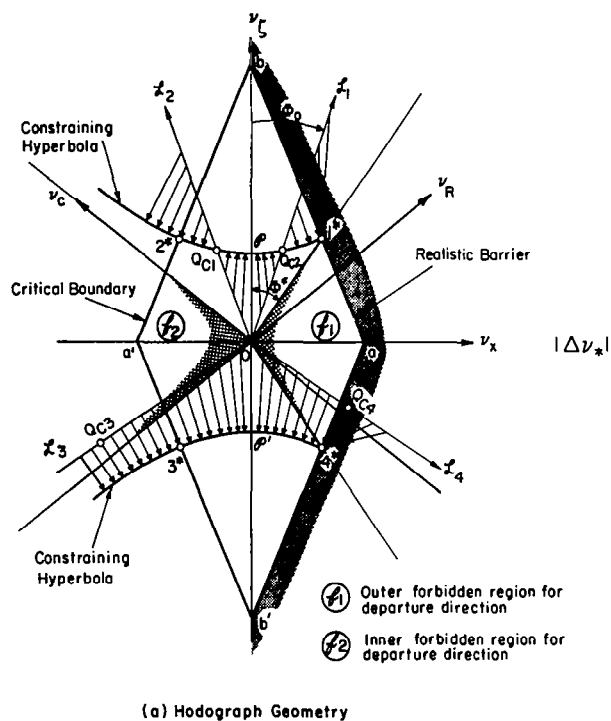(b) $|\Delta \nu_*|$ vs ν_0 at constant Φ_0 ($\psi = 60°$ $\varphi_1 = 75°$)

Fig. 10. Variation of the minimum velocity increment with the initial velocity vector at constant direction and varying magnitude.

Now let us consider the case when $\vec{v}_0$ has a constant magnitude but varying direction, that is, when Q_0 moves along a circle centered at O with the radius v_0. There are several sub-cases to be distinguished.

a. When $v_0 < (v_0)_L$, the v_0-circle is entirely within the boundary aba'b' and the transfers are all elliptic.

(a-1) $v_0 \leq A$ First suppose $v_0 < A$, then as the hodograph shows (Fig. 11a-1), the v_0-circle intersects the constraining hyperbola at no point, and Q_0 is closest to the hyperbola when it is at the point D or its complementary point D' (not shown in Fig. 11). Consequently $|\Delta v_*|$ is least at $\Phi_0 = 0$ or $\pm \pi$, and is given by

$$|\Delta v_*|_{min} = A - v_0 \qquad (42)$$

Thus the best direction for the initial velocity vector is the local minimum energy direction. The same is true when $v_0 = A$ except that the v_0-circle now touches the constraining hyperbola at its vertices $\mathcal{P}$ and $\mathcal{P}'$. Thus the points D and D' coincide with $\mathcal{P}$ and $\mathcal{P}$ respectively, and $\Delta v_* = 0$.

(a-2) $v_0 > A$ The v_0-circle now intersects the constraining hyperbola at four distinct points, one in each quadrant (two of them are shown in Fig. 11a-2), where $\Delta v_* = 0$. Consequently the best directions for $\vec{v}_0$ shifts from the minimum energy direction to either of the four directions determined by these four points. They are the correct directions for the 2-terminal transfer at the departure speed v_0. There is one pair of such directions, a conjugate pair, for each of the trajectory groups, the normal and the complementary.

b. When $v_0 \geq (v_0)_L$, a part of the v_0-circle is outside the boundary aba'b' and the transfers are not all elliptic.

(b-1) $v_0 < \sqrt{2}$ Four points of intersection of the v_0-circle with the constraining hyperbolic exist in the elliptic region like in case (a-2). (see Fig. 11 b-1)

(b-2) $v_0 \geq \sqrt{2}$ The v_0-circle will intersect the constraining hyperbola in the realistic region at two points only, both in the low half-plane (one of them is shown in Fig. 11b-2 as Q_{C2}). Thus there are two optimum directions for the low transfer with zero velocity-increment. In the high half-plane the v_0-circle extneds partly into the unrealistic region, and $|\Delta v_*|$ will be least when Q_0 is closest to either of the critical points 1^* and 4^*. As the hodograph shows, it is given by the point where the v_0-circle intersects the radial line through each of these critical points. Thus the optimum directions for $\vec{v}_0$ for high transfer are given by $\Phi_0 = \Phi^*$ and $\pi - \Phi^*$. The corresponding minimum $|\Delta v_*|$ will be nonzero unless $v_0 = \sqrt{2}$.

Figure 11 also shows the rectangular plottings of $|\Delta v_*|$ versus Φ_0 for several constant values of v_0. Note that the portions of the $|\Delta v_*|$-curve beyond the critical points in the high and low half-planes are not symmetrical. This asymmetry is negligible when v_0 is close to $(v_0^*)_L$ (Fig. 11b-1), but becomes increasingly obvious as v_0 grows (Fig. 11b-2).
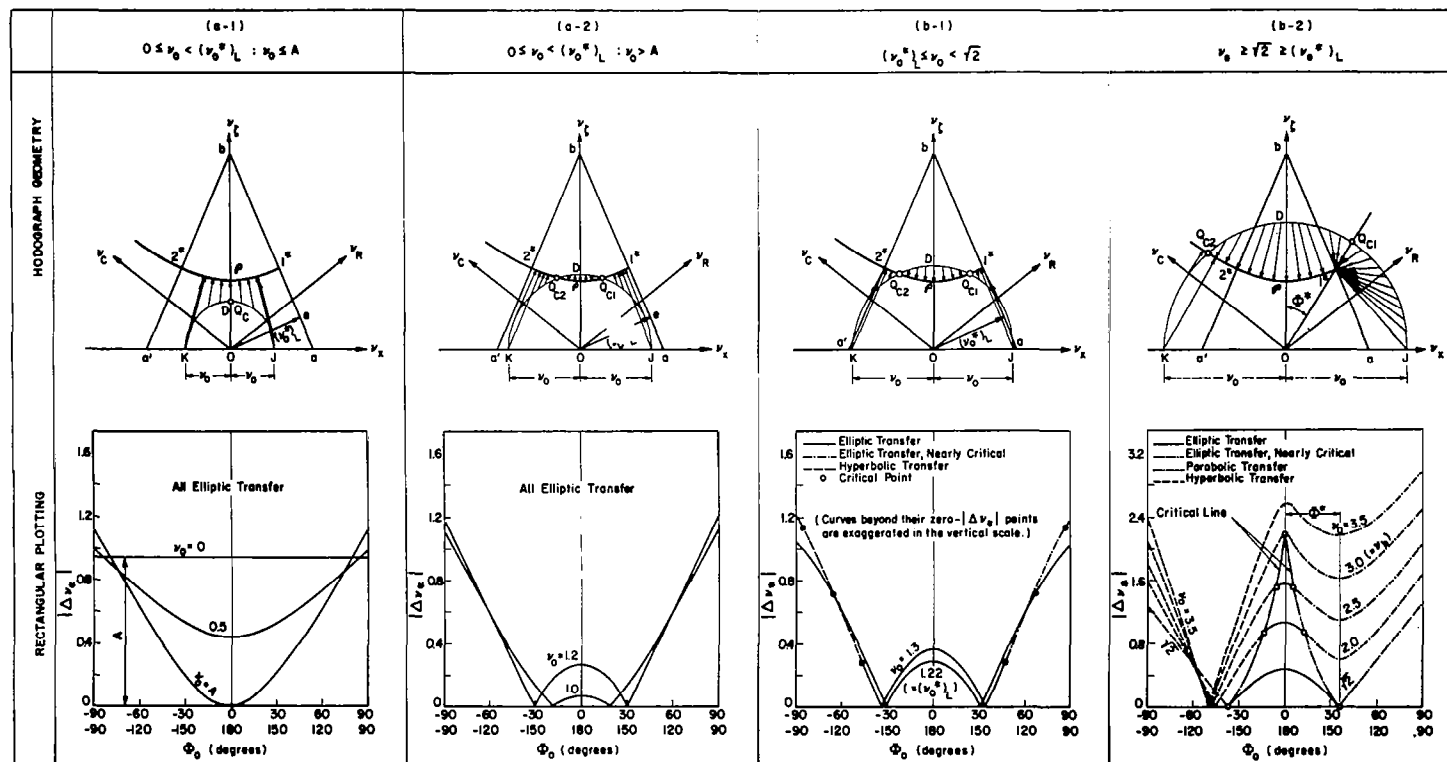
Fig. 11. Variation of the minimum velocity-increment with the initial velocity
vector of constant magnitude and varying direction.

Finally it is interesting to note that $|\Delta v_*|$ is a local maximum when Q_O is at the point J or K ($\Phi_O = \pm \pi/2$) in all the previous cases. In the case (a-1) it is also the absolute maximum since no other local maximum is present. Consequently the worst direction for $\vec{V}_O$ in this case is along the v_χ-axis, which is the bisector of the base angle φ_1. This is also true in the case (a-2) even here a second local maximum for $|\Delta v_*|$ exists at D or D', corresponding to the local minimum energy direction. This second local maximum is also present in case b. As shown in Fig. 11b-1,2, it grows as v_O increases, and it may eventually become the absolute maximum. Its location will shift to the high side of the v_ξ-axis instead of lying on it when $v_O > v_b$. Thus the minimum energy direction and its neighbourhood in the high half-plane may become the worst direction for $\vec{V}_O$ at high initial speed.

3.6 EFFECTS OF THE INITIAL VELOCITY VECTOR ON THE OPTIMUM SOLUTION: SUMMARY OF FINDINGS

As seen from the preceding analyses the optimum solution for the problem is determined by the geometry of the base triangle and the initial velocity vector. Based on the previous findings the effects of the initial velocity vector on the optimum solution for a given base triangle may be summarized as follows:

(1) Corresponding to every initial velocity vector $\vec{V}_O$ there exists at least one definite realistic optimum trajectory for the problem provided by the orthogonality quartic unless the tip of $\vec{V}_O$ exceeds the realistic barrier in the hodograph plane. Such a barrier is analytically defined by Eqs. (34-1) and (34-4).

(2) If such a limit is not exceeded, the initial velocity vector is said to be in the realistic region, then the realistic optimum solution is unique whenever $\vec{V}_O$ is not directed along the bisector of either the interior or the exterior base angle at the initial terminal.

If this is the case, then the optimum trajectory will be of the same group and the same class with the initial velocity vector $\vec{V}_O$. However, the type of the trajectory, whether elliptic, parabolic, or hyperbolic, does not necessarily agree with that of V_O, but is determined by the particular region in the hodograph plane in which its tip Q_O lies (see Table 5 and Fig. 7).

(3) In a realistic region, if $\vec{V}_O$ is directed along the interior base angle bisector, then there are two optimum solutions for the problem, corresponding to a complementary-conjugate pair of trajectories of the same class with the initial velocity vector, and of the same type which is determined by the region in which the tip Q_O lies.

(4) The minimum energy direction of departure is along the exterior base angle bisector. If $\vec{V}_0$ is directed along this direction, then the optimum solution may be unique or not, depending on the magnitude of $\vec{V}_0$ or the location of its tip, Q_0. Consider $\vec{V}_0$ in the positive half of the hodograph plane (see Fig. 7):

(a) When Q_0 moves from the origin up to the cusp G of the boundary Lame along the minimum energy direction such that $0 < V_0 < V_G$ (where V_G is given by Eq. (24)), the optimum solution is unique, the trajectory is elliptic, and of minimum energy, and the velocity-increment vector is to be directed along the minimum energy axis.

(b) When Q_0 moves between the cusp G and the point b, where the boundary of the elliptic region meets the minimum energy axis such that $V_G < V_0 < V_b$ (where V_b is given by Eq. (38)), then there are two optimum solutions for the problem corresponding to a conjugate pair of trajectories of the same group with the initial velocity vector. They are both elliptic, but no longer of minimum energy, and the optimum directions for the velocity-increment vector deviate from the minimum energy direction with equal inclinations on either side of it even though the initial velocity vector is along that direction.

(c) When Q_0 moves further along the minimum energy direction such that $V_0 \geq V_b$ the realistic optimum is again unique. Like case (b) the optimum ΔV is no longer in the minimum energy direction, and the trajectory is no longer the minimum energy one. It is parabolic when $V_0 = V_b$, and hyperbolic when $V_0 > V_b$.

Situations similar to the foregoing three cases (a) to (c) exist when $\vec{V}_0$ is in the other half plane.

(5) Different initial velocity vectors may call for the same optimum transfer trajectory. This statement is necessarily true when these velocity vectors all lie on the same normal line in the same quadrant in the realistic region.

(6) Similarly, different initial velocity vectors may call for the same amount of velocity increment. This statement is necessarily true when these velocity vectors all lie in the realistic region and on the curve parallel to the constraining hyperbola with the same common distance on either side of it.

(7) No unrealistic optimum will arise when the initial velocity is directed below the minimum energy direction regardless of its magnitude, or when its magnitude is below the lower critical limit $(V_0^*)_L$ (given by Eq. 39)) regardless of its direction.

(8) When the tip Q_O of the initial velocity vector exceeds the real-
istic barrier, it is said to be in the unrealistic region. In such a region a
definite realistic optimum solution can be found only when Q_O is inside or on
the boundary of the strip bounded by the v_ξ-axis and the line of equi-critical-
velocity-increment (see Fig. 7). In such a subregion the realistic optimum
trajectory is hyperbolic of the same group with the initial velocity vector,
but of the low class. Outside this subregion no definite optimum solution
can be found. The possible choice will be an elliptic one, of high eccentri-
city, close to the unrealistic parabolic trajectory given by the critical
point or points nearer to Q_O.

(9) For a given direction of the initial velocity, there is a best
magnitude for which the optimum velocity-increment is an overall minimum. This
is given by the point of closest approach on the direction line to the constrain-
ing hyperbola in the realistic region, or to the critical point co-quadrant with
the direction line in an unrealistic region. This best magnitude will be the
correct departure speed in the given direction for the 2-terminal transfer if
it falls in neither of the inner and outer forbidden regions for the direction
of departure. The velocity-increment required is thus zero.

(10) For a given magnitude v_O the best direction for the initial
velocity from the initial impulse standpoint is in the local minimum energy
direction only if v_O is not greater than A, which is the departure speed along
the minimum energy trajectory. When v_O exceeds A, the best directions are those
for a realistic transfer (long or short) with v_O as the departure speed. The
corresponding velocity-increment is again zero   From the same standpoint, the
worst direction for the initial velocity is that along the bisector of the base
angle at the initial terminal, either inward or outward, when v_O is less than
A. At higher initial speed a second worse direction exists in the minimum
energy direction; it and its neighbourhood in the high side may eventually
become the worst when v_O grows.

4.   HODOGRAPHIC REPRESENTATION OF THE TWO-DIMENSIONAL OPTIMUM TRANSFER

4.1   THE ORTHOGONAL NET IN THE HODOGRAPH PLANE AND THE OPTIMIZATION CHART

As seen from the previous analysis the normal lines to the constraining hyperbola and its parallel curves form an orthogonal net in the hodograph plane. Such a net may be looked upon as the curvilinear coordinates of the initial velocity vector, and it forms naturally the basis for the development of the optimization chart for the present problem. A typical example of such a chart is shown in Fig. 12,[5] which is constructed for the case of $\psi = 60°$ and $\varphi_1 = 75°$ corresponding to a transfer distance ratio of n = 1.366. As soon as the tip Q_o of the initial velocity vector is located on the chart, the optimum velocity increment vector and the optimum departure velocity vector can be readily determined by noting the normal line and the parallel curve passing through this initial point Q_o. In case unrealistic optimum arises it can be seen at once from the chart, and in such a case a realistic optimum solution may also be obtained directly from the chart by noting the subregion (U_1 or U_2 in Figs. 12 and 12A) in which the point Q_o is located, and the rules given in Section 3.4. The type of the optimum transfer trajectory, elliptic, parabolic, or hyperbolic, will be indicated by the region in which the selected optimum point lies. To illustrate the use of this chart an example is given below:

Consider a transfer from an initial point to a target point at a distance of $r_2 = 1.366\ r_1$, an angle of separation 60°, and an initial velocity given by

$$v_o \;=\; 0.80 \quad,\quad \phi_o \;=\; -25°$$

By locating the initial point Q_o according to (v_o,φ_o) in Fig. 12 , we find the optimum solution approximately as follows:

Velocity increment:	magnitude	$\lvert \Delta v_* \rvert$	= 0.672
	direction	$\phi_{\Delta v_*}$	= 54.5°
Departure velocity:	magnitude	v_{1*}	= 1.14
	direction	ϕ_{1*}	= 11°

The transfer trajectory is elliptic.

---

[5] Only one half of the hodograph plane is shown owing to symmetry; the normal lines are arbitrarily numbered for convenience.
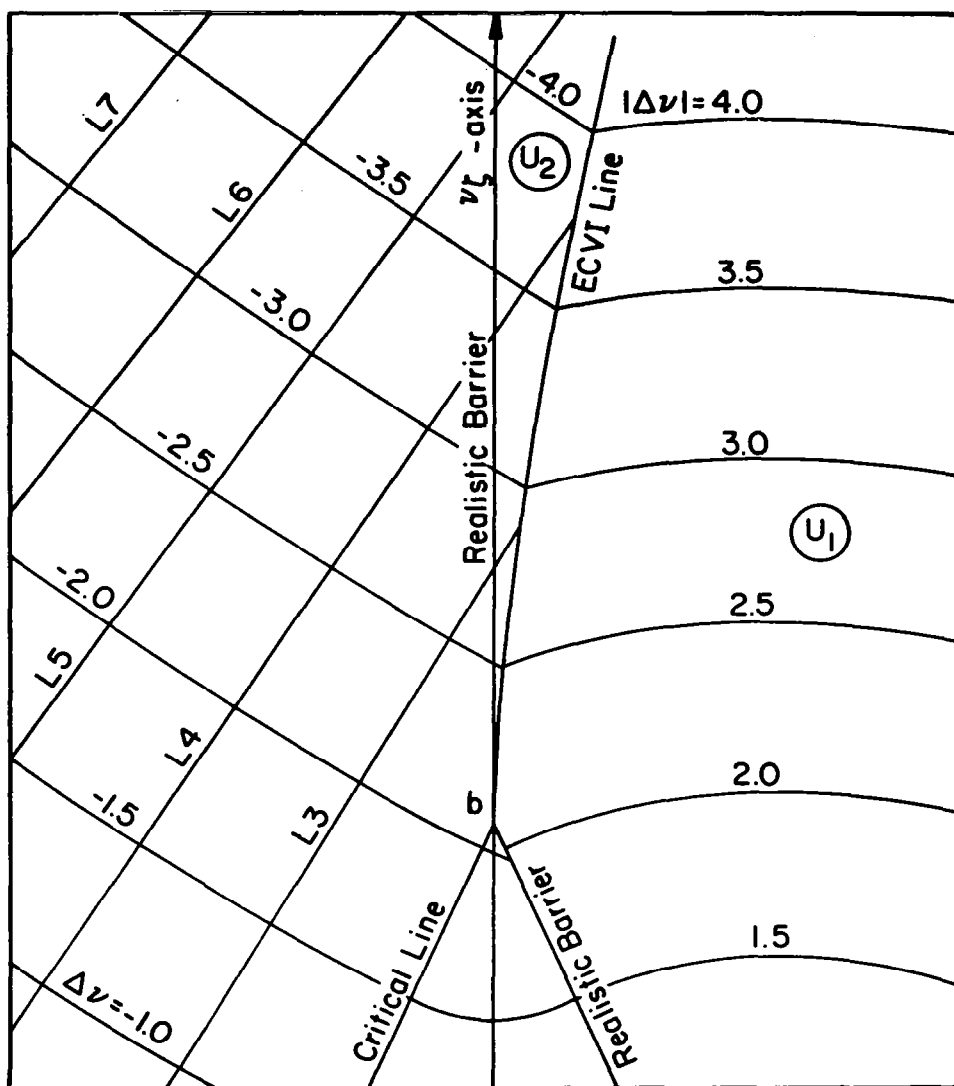
Fig. 12. The optimization chart for minimum initial impulse terminal-to-terminal transfer ($\psi = 60°$, $\varphi_1 = 75°$).

Fig. 12A. The equi-critical-velocity-increment line in the hodograph plane. ($\psi = 60°$, $\varphi_1 = 75°$).

45

While such a chart yields immediately the optimum solution corresponding to a specified initial velocity vector, it does not give directly the principal elements of the transfer trajectory except its type. For such information the hodograph circle for the transfer trajectory should be constructed, and it will be presented in the next section. Finally it is to be noted that although such a chart is constructed on the basis of a hyperbolic constraint, it may well be applied when the departure velocity is constrained not on this hyperbola, but on any one of its parallel curves, since all of them have common normals and the same Lamé as their involute. The only change necessary is to shift the datum curve, on which $\Delta v = 0$, from the hyperbola to the new constraining curve and to make corresponding adjustment on the constant value of Δv on each of the parallel curves. Graphical techniques on the extensive use of such optimization charts, however, will not be elaborated here.

4.2 THE CONSTRUCTION OF THE TRANSFER HODOGRAPH

With the optimum departure velocity vector determined analytically or graphically, the hodograph for the transfer trajectory may be constructed by using the terminal relations given in Ref. 9,

$$\vec{V}_{C1} = \vec{V}_{C2} \; , \quad V_{R1} = V_{R2} \tag{43}$$

from which we see that once the hodograph image of the initial terminal Q_1 is determined, so is that of the final termina Q_2. In fact the point Q_2 in the hodograph plane is also constrained on a hyperbola defined by

$$V_C \, V_R = -K \tag{44}$$

which is Godal's compatibility condition applied at the second terminal. The negative sign here signifies the fact that the vector $\vec{V}_{R2}$ is directed in the negative direction of the local vertical at Q_2. However, the construction of this second constraint is not necessary since following Eq. (43), the point Q_2 may be easily located in the hodograph plane by completing the two velocity parallelograms with the common side V_C and the other sides of equal length V_R lying along the directions of $\vec{r}_1$ and $\vec{r}_2$ respectively as shown in Fig. 13. With the two terminals on the transfer hodograph thus determined, the next step is to locate the center of the hodograph circle. According to the general correlation established in Ref. 7 this center must lie on the local horizontal line at each terminal. Thus by drawing the lines perpendicular to the local radial directions at Q_1 and Q_2 respectively we find their intersection at C, and by using C as center the hodograph circle can be drawn to pass through
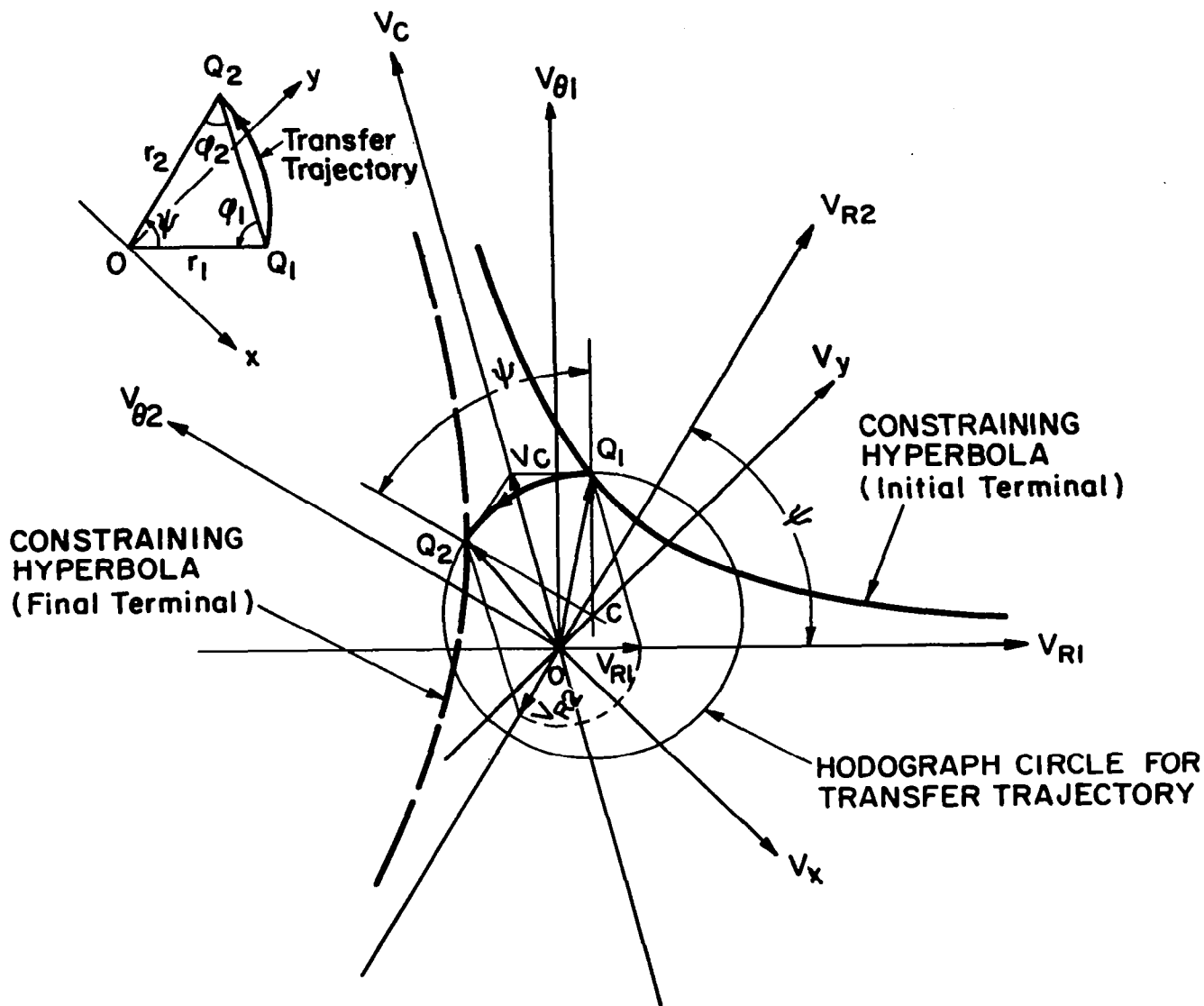
Fig. 13. Construction of the transfer hodograph in the $\vec{V}$-plane.

the points Q_1 and Q_2.[6] This completes the construction, and the circular arc between the points Q_1 and Q_2 subtending a central angle ψ represents the transfer trajectory. The principal geometric as well as kinematic elements of the trajectory can then be determined from the hodograph according to the correlation given in Ref. 7.

4.3 THE HODOGRAPH OF OPTIMUM TRANSFER TRAJECTORIES IN THE $\vec{\mathcal{U}}$-PLANE

So far the analysis has been made exclusively in the $\vec{v}$-plane. Such a hodograph, though nondimensionalized, is essentially different from the dimensionless hodograph in the $\vec{\mathcal{U}}$-plane defined by

$$\vec{\mathcal{U}} \equiv \frac{h}{\mu} \vec{v} \qquad\qquad (45)$$

where h is the angular momentum per unit orbiting mass and μ is the Newtonian gravitational constant, as introduced in Ref. 7. To distinguish the two we will call them the $\vec{v}$-hodograph and the $\mathcal{U}$-hodograph respectively according to their planes. In a $\vec{v}$-plane the velocity is nondimensionalized by dividing through by the circular speed at a fixed point, which is a constant in the problem. Thus the $\vec{v}$-hodograph is in fact the same as the hodograph in the usual $\vec{V}$-plane, except for the scale of plotting. However, in the $\mathcal{U}$-plane the velocity is being divided through by the parameter μ/h which varies from one trajectory to another. Such a nondimensionalization has the advantage of reducing the hodograph of all Keplerian orbits into a unit circle. Having made the analysis and representation of the present problem in the $\vec{v}$-plane, it is appropriate to introduce here the hodographic representation of the same optimum solution of the problem in the $\mathcal{U}$-plane.

The locus of the hodograph origins in the $\vec{\mathcal{U}}$-plane, as shown in Ref. 9, is a straight line for all two-terminal trajectories of the same group. Thus, the two straight lines parallel to the chord of the base triangle in the $\vec{\mathcal{U}}$-plane are comparable to the two branches of the constraining hyperbola in the $\vec{v}$-plane, one for each group (see Fig. 14). Thus while the tip of the departure velocity vector is constrained on the two branches of the hyperbola in the $\vec{v}$-plane, the origin of the transfer hodograph is confined on these two straight lines in the $\vec{\mathcal{U}}$-plane. Detailed discussion on the lines of origins are found in Ref. 9.

Consider a normal group. Let O be an arbitrary point on the straight line locus, and ρ its distance from the radical center T as shown in Fig. 15. Then by definition

---

[6]Note here the vector $\vec{V}_2 - \vec{V}_1$ is in the direction of the bisector of the vertex angle ψ in the physical plane, see Ref. 5 or 7, pp. 897-898.

Constraining Hyperbola (Normal Group)

ν_ζ

ν_c

2^* 1^*

$\sqrt{2}$

ν

$\dfrac{\varphi_1}{2}$

$\dfrac{\varphi_1}{2}$

O

ν_x

ν_τ

3^* 4^*

Constraining Hyperbola (Complementary Group)

$$\nu \equiv \vec{V}\sqrt{\dfrac{\lambda_1}{\mu}}$$

Q_2

φ_2

Q_1

λ_2 φ_1

ψ λ_1

O

Base Triangle

Line of Origins (Complementary Group)

Hodograph Circle

4^*

Q_1

φ_1

T

1^* ν

φ_2

O

Q_2 ψ C Q'_2

1 3^*

T'

2^* Q'_1

Line of Origins (Normal Group)

$$\vec{\nu} \equiv \dfrac{\hbar}{\mu}\vec{V}$$

++++++++ unrealistic constraint

(a) The $\vec{\nu}$- plane   (b) The $\vec{\nu}$- plane
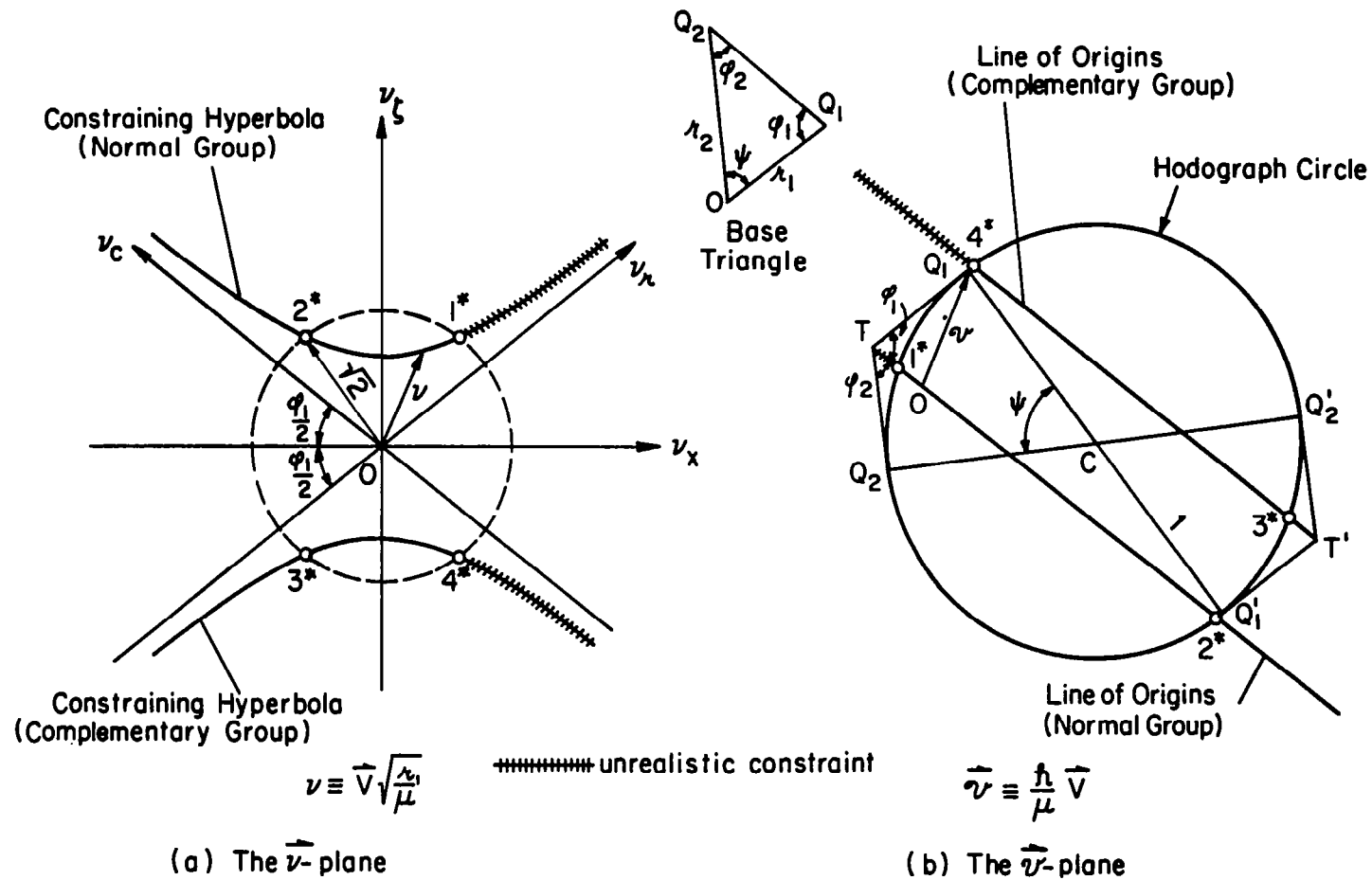
Fig. 14. Geometric representation of the two-terminal constraint in the $\vec{\nu}$ - and $\vec{\nu}$-planes.
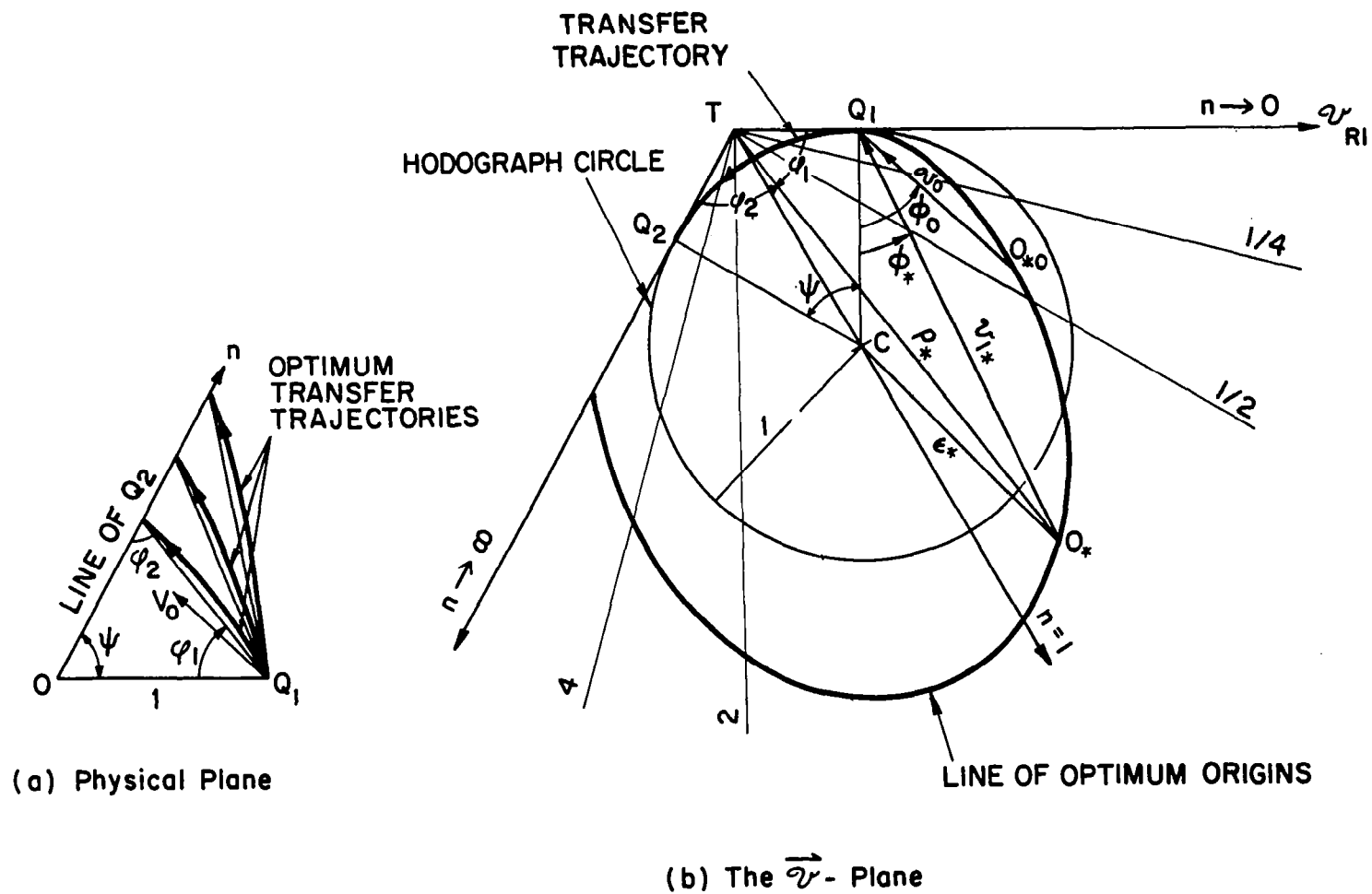
(a) Physical Plane

(b) The $\vec{v}$- Plane

Fig. 15. Hodograph of optimum transfer trajectories in the $\vec{v}$-plane (ψ = Const.).

$$\rho = \frac{h}{\mu} v_C \qquad (46)$$

Comparing this with the definition of v given by Eq. (11), and noting here,

$$h = v_C d = v_C r_1 \sin \varphi_1 \qquad (47)$$

we find the relation

$$\rho = v_C^2 \sin \varphi_1 \qquad (48)$$

Thus corresponding to each optimum value of v_{C*} for a given base triangle and a given initial velocity vector there is a unique value of ρ_*, from which the origin $O*$ of the optimum transfer hodograph is determined. Such an origin will be called the optimum origin for the present problem, and the locus of such origins in the $\vec{\nu}$-plane, the locus of optimum origins, or simply the O_*-locus. A typical example of such a locus for a constant vertex angle ψ is shown in Fig. 15b. By substituting Eq. (48) into the orthogonality Eq. (10c) we find the ρ_*-equation

$$(\rho_*^2 - \tan^2 \tfrac{\psi}{2})^2 = \rho_* \sin \varphi_1 \, (\eta_o \rho_* - m_o \tan \tfrac{\psi}{2})^2 \qquad (49)$$

where

$$\begin{aligned} m_o &= v_o \sin \phi_o \\ \eta_o &= v_o \sin (\varphi_1 - \phi_o) \end{aligned} \qquad (50)$$

according to Eqs. (20) and (21). For constant ψ such an equation may be looked upon as the polar equation of the ρ_*-vector with the angle φ_1 as the polar angle, and the directed tangent line $T \, Q_1$, its polar axis. It represents the O_*-locus whenever the orthogonality Eq. (10) yields a realistic optimum solution. Some essential features of a ρ_*-curve are to be noted as follows:

(1) It is bounded between the two tangent lines at Q_1 and Q_2 on the hodograph circle since for a given vertex angle ψ the angle φ_1 can only vary between 0 and $\pi-\psi$.

(2) For a constant ψ each value of the angle φ_1 corresponds to a

unique value of the distance ratio n. Thus the radial lines drawn from the radical center T are also the lines of constant n.

(3) The point Q_1 lies on the ρ_*-curve since the ρ_*-equation (49) is satisfied by $\varphi_1 = 0$ and $\rho_* = \tan \psi/2$ there.

(4) The origin of the initial orbit as given by the initial velocity vector $\vec{\nu}_0$ in the $\vec{\nu}$-plane lies on the ρ-curve, as its coordinates also satisfy the ρ_*-equation (49). The corresponding values of φ_1 and n at this point give the configuration of the base triangle such that the initial orbit passes through the final terminal Q_2, and thus itself may be regarded as the optimum transfer trajectory.

(5) The point where the ρ_*-curve intersects the hodograph circle is the critical point, and the portion of the curve beyond it is hyperbolic.

(6) From the critical point beyond, the ρ_*-curve will be unrealistic (corresponding to unrealistic optimum trajectories) if it is on the high side, otherwise it is realistic.

(7) When the ρ_*-curve is unrealistic, it ceases to represent the O_*-locus, and should be modified according to its corresponding realistic optimum value of ν_{C_*}.

(8) The point where the O_*-locus meets the bounding line $T\,Q_2$ gives the optimum transfer trajectory from Q_1 to infinity. Such a transfer will be further discussed in Section 5.3.

Finally it is to be noted that the orthogonality principle does not directly apply in a $\vec{V}$-plane since the initial velocity and the velocity along the transfer trajectory to be optimized are not represented by the same scale there. However, it has the advantage over the $\vec{\nu}$- or $\vec{V}$-hodograph in that it shows the totality of the optimum transfer trajectories for all possible configurations of the base triangle (given by the variable φ_1 or n) under a given vertex angle ψ and a prescribed initial velocity vector (see Fig. 15a). Furthermore, unlike in the $\vec{\nu}$-plane where a hodograph circle is to be drawn for each transfer trajectory, the $\vec{\nu}$-hodograph enables one to use the same arc of the unit circle for all transfer trajectories between the fixed terminal points Q_1 and Q_2, and from which all the principal geometrical as well as the kinematic elements of the transfer trajectory associated with a particular optimum origin can be readily determined according to the correlations given in Ref. 7.

All the foregoing features are also true for the ρ_*-curve or the O_*-locus of the complementary group. Such a hodographic representation can be easily obtained by turning the corresponding hodograph for the normal group through 180°.

5. ANALYSIS OF SOME LIMITING CASES

So far the analysis has been restricted to $0 < \psi < \pi$, and $0 < n < \infty$. An examination of each of these limiting cases is now in order.

5.1 THE CASE $\psi = 0$

Physically this case corresponds to a vertical descent if $r_1 > r_2$ and a vertical ascent if $r_1 < r_2$. In either case the base triangle OQ_1Q_2 degenerates into a line segment with Q_1 and Q_2 on the same side of O. The geometry in the physical plane and that in the hodograph plane for each case are shown in Fig. 16. The constraining hyperbola also degenerates in each case, and its principal elements are as follows:

	$r_1 > r_2$ $(n < 1)$	$r_1 < r_2$ $(n > 1)$
σ	π	0
A	0	$\sqrt{2\left(1 - \dfrac{1}{n}\right)}$
B	$\sqrt{2\left(\dfrac{1}{n} - 1\right)}$	0
e	∞	1

$$(51)$$

(a)   Vertical Descent: $r_1 > r_2$ $(n < 1)$

The degenerate constraining hyperbola is a straight line parallel to the line OQ_1Q_2 in the physical plane. Consequently all normal lines are parallel to the local horizontal at Q_1 and Q_2, the orthogonal net becomes rectangular, and the transfer trajectory is a vertical straight line. The entire hodograph plane is divided into three main regions as usual: the hyperbolic region on the low side, the unrealistic region on the high side, and the elliptic region between them. However, it is to be noted that the usual closed elliptic region is now open since its sides are parallel. Furthermore, as a straight line trajectory is identical to its conjugate, as well as its complementary-conjugate, the optimum solution is unique everywhere in the realistic region even on the v_χ-axis which now coincides with the v_{r_1}-axis.

The optimum solution of the problem is very simple in this particular case. As seen from the hodograph (Fig. 16a) Q_o is in the realistic region whenever
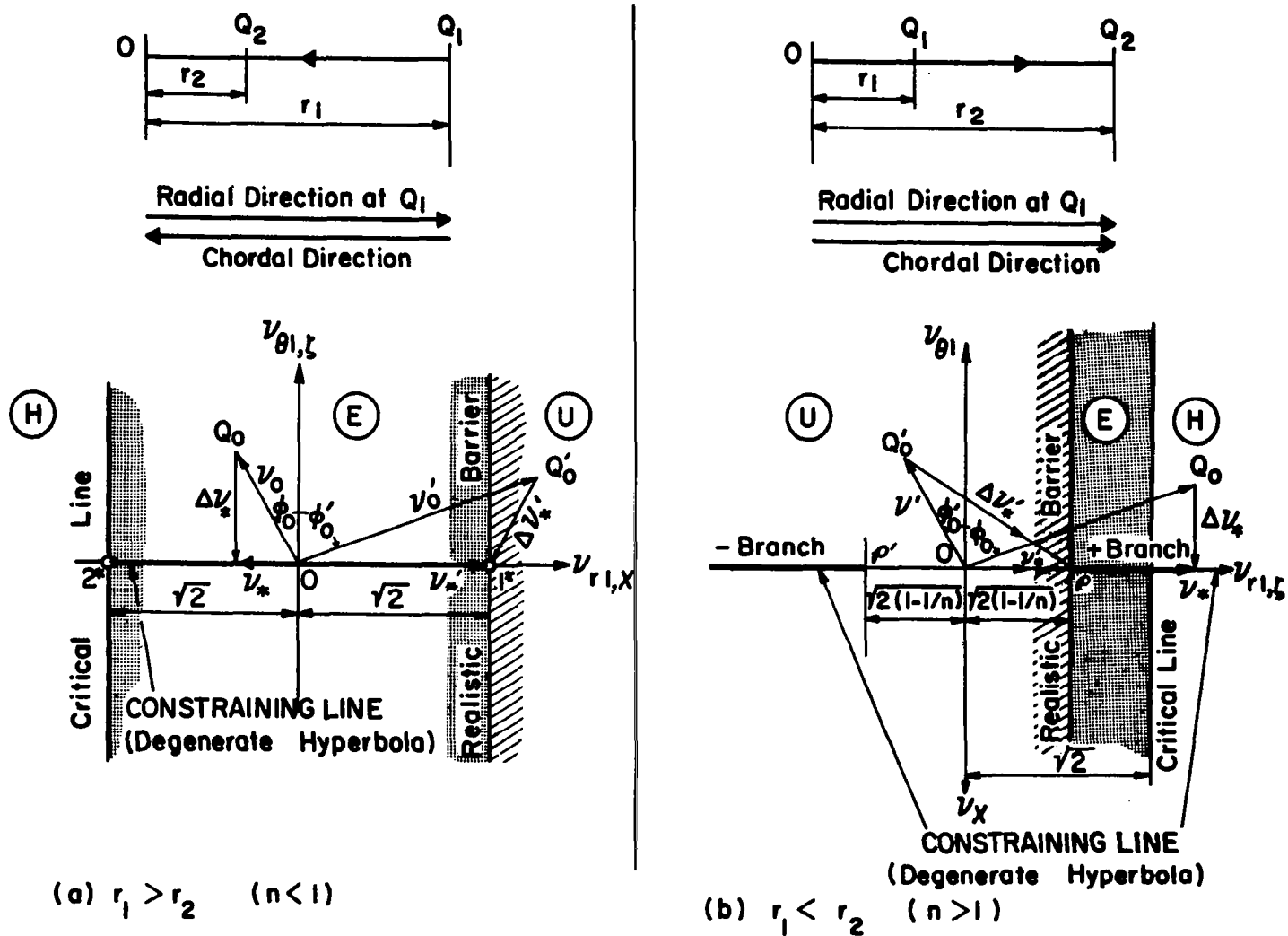
$$v_o \sin \phi_o < \sqrt{2}$$

53

Fig. 16. Optimization of vertical transfer ($\psi = 0$).

and the geometry of the hodograph gives readily the solution summarized in Table 6, column a. As seen from the hodograph the optimum velocity increment vector in this region is everywhere in the local horizontal direction. It is simply to nullify the horizontal component of the initial velocity if any—a fact which is evident from physical considerations. However, whenever

$$v_o \sin \phi_o \geq \sqrt{2} \tag{52-2a}$$

Q_o is in the unrealistic region, the point on the v_{r1}-axis close to the critical point 1* but inside the elliptic region has to be chosen as discussed in Section 3.4. No second choice is possible at present since no evolute exists for a straight line and the hodograph plane is simple everywhere. Consequently, the optimum velocity increment vector is no longer in the normal direction, and in addition to nullifying the horizontal component of the initial velocity, it has a vertical component opposed to that of the initial velocity so as to keep the resultant velocity below that for escape. The optimum solution in this case is indefinite, and, as seen from the geometry in the hodograph plane, it may be written approximately as summarized in Table 6.

(b) Vertical Ascent: $r_1 < r_2$ (n > 1)

This case looks similar to the previous one, but there are some radical differences: 1) the constraining hyperbola degenerates into two semi-infinite lines along the radial axis instead of a single line as in case (a); and between the vertices $\mathcal{P}$ and $\mathcal{P}'$ of these two branches of the velocity constraint, there is a gap of length 2A where no normal lines to the constraint line can be drawn, and consequently the orthogonality principle cannot apply there; 2) trajectories of the complementary group are out of the question since in such a transfer all physically realistic trajectories must go in one direction only, that is, from Q_1 to Q_2 not through 0. Thus the negative portion of the degenerate constraining hyperbola is meaningless. Consequently the straight line normal to the positive branch of the constraining line at its vertex $\mathcal{P}$ forms a realistic barrier instead of the usual critical line.[7] The geometry of the hodograph plane and various regions are shown in Fig. 16b.

As seen from the hodograph, whenever

$$v_o \sin \phi_o \geq A \tag{52-1b}$$

Q_o is in the realistic region, the solution is definite and unique, and formulas are identical to those for case (a) in Table 6. Whenever

$$v_o \sin \phi_o < A \tag{52-2b}$$

---

[7]Note here in the region between the horizontal lines through $\mathcal{P}$ and $\mathcal{P}'$ there exists no optimum solution, realistic or unrealistic, and in the region to the left of the horizontal line through $\mathcal{P}'$ (not shown in Fig. 16b) the unrealistic solution consists of elliptic trajectories in addition to the hyperbolic ones as encountered in the case of $\psi \neq 0$, owing to the consideration 2).

TABLE 6

OPTIMUM SOLUTIONS FOR VERTICAL TRANSFER ($\psi = 0$)

		(a)	(b)
		$r_1 > r_2$ (n < 1) Vertical Descent	$r_1 < r_2$ (n > 1) Vertical Ascent
REALISTIC REGION	Condition on v_0	$v_0 \sin \phi_0 < \sqrt{2}$ (52-1a)	$v_0 \sin \phi_0 \geq \sqrt{2(1 - \frac{1}{n})}$ (52-1b)

	Velocity-Increment
	    r-component $(\Delta v_r)_{opt.}$
	    θ-component $(\Delta v_\theta)_{opt.}$
		0
		 $-v_0 \cos \phi_0$
			(53-1)

	Departure Velocity
	    r-component $(v_r)_{opt.}$
	    θ-component $(v_\theta)_{opt.}$
		$v_0 \sin \phi_0$
		 0
			(54-1)

UNREALISTIC REGION	Condition on v_0	$v_0 \sin \phi_0 \geq \sqrt{2}$ (52-2a)	$v_0 \sin \phi_0 < \sqrt{2(1 - \frac{1}{n})}$ (52-2b)

	Velocity-Increment $(\Delta v)_{opt.}$
	    r-component $(\Delta v_r)_{opt.}$
	    θ-component $(\Delta v_\theta)_{opt.}$
		$\cong \Delta v^*$
		 $\cong \sqrt{2} - v_0 \sin \phi_0$ (53-2a)
		 $- v_0 \cos \phi_0$
			$= (\Delta v)_P$
			 $= \sqrt{2(1 - \frac{1}{n})} - v_0 \sin \phi_0$ (53-2b)
			 $- v_0 \cos \phi_0$

	Departure Velocity
	    r-component $(v_r)_{opt}$
	    θ-component $(v_\theta)_{opt.}$
		$\cong \sqrt{2}$ (54-2a)
		 0
			$= \sqrt{2(1 - \frac{1}{n})}$ (54-2b)
			 0

Q_0 is in the unrealistic region, the orthogonality principle no longer applies. In such a case the vertex ρ should be chosen as the optimum point, giving

$$v_{opt.} = A = \sqrt{2(1 - \frac{1}{n})} \qquad (54\text{-}2b)$$

which is the minimum departure velocity for such a transfer (see item (2) on the "Constraining Hyperbola," Section 2.2). Formulas for this optimum solution are summarized in Table 6, column b.

5.2 THE CASE $\psi = \pi$

The case is of practical importance. Like the previous one the base triangle degenerates again into a line segment but with the two terminal points on the opposite sides of O. The elements of the constraining hyperbola have the following limiting values according to Table 2:

$$
\begin{aligned}
\sigma &\longrightarrow \pi \\
A &\longrightarrow \sqrt{\frac{2n}{n+1}} \\
B &\longrightarrow \infty \\
e &\longrightarrow \infty
\end{aligned}
\qquad (55)
$$

Thus the constraining hyperbola degenerates into two straight lines parallel to the v_{r1}-axis at the distances $\pm$ A. Consequently, all normal lines are again in the horizontal direction everywhere in the hodograph plane, the orthogonal net is again rectangular, and the plane is divided into the three regions, elliptic, hyperbolic, and unrealistic, by the two critical lines just as in the case $\psi = 0$, and $r_1 > r_2$. With the absence of the boundary Lamé the entire hodograph is again simple, and a definite and unique optimum solution exists everywhere in the realistic region except on the v_{r1}-axis along which a complementary-conjugate pair of optimum solutions exist. The geometry in the physical plane and that in the hodograph plane are shown in Fig. 17.

As seen from the hodograph, Q_0 is in the realistic region whenever

$$v_0 \sin \phi_0 < \sqrt{\frac{2}{n+1}} \qquad (56\text{-}1)$$

and in this region the optimum direction of $\overrightarrow{\Delta v}$ is horizontal everywhere. The optimum solution can be readily obtained from the geometry of the hodograph, and is summarized in Table 7, column 1.

Whenever

$$v_0 \sin \phi_0 \geq \sqrt{\frac{2}{n+1}} \qquad (56\text{-}2)$$

TRANSFER
TRAJECTORY

ΔV_* V_* ϕ_0

$180°$

V_0 ϕ_*

O

Q_2 Q_1

r_2 r_1

Radial Direction at Q_1

Chordal Direction

(a) Physical Plane

VELOCITY CONSTRAINT
(Degenerate Hyperbola)

$v_{\theta 1, \zeta}$

H E U

2^* Q_x 1^*

Δv_* v_* ϕ'_0 $\Delta v'_*$

$\sqrt{\dfrac{2n}{n+1}}$ ϕ_0 v'_* Q'_0

v_0 ϕ_* ϕ'_*

$\sqrt{\dfrac{2n}{n+1}}$ v'_0

O $v_{R1,X}$

CRITICAL LINE

$\sqrt{2}$

REALISTIC
BARRIER

3^* 4^*

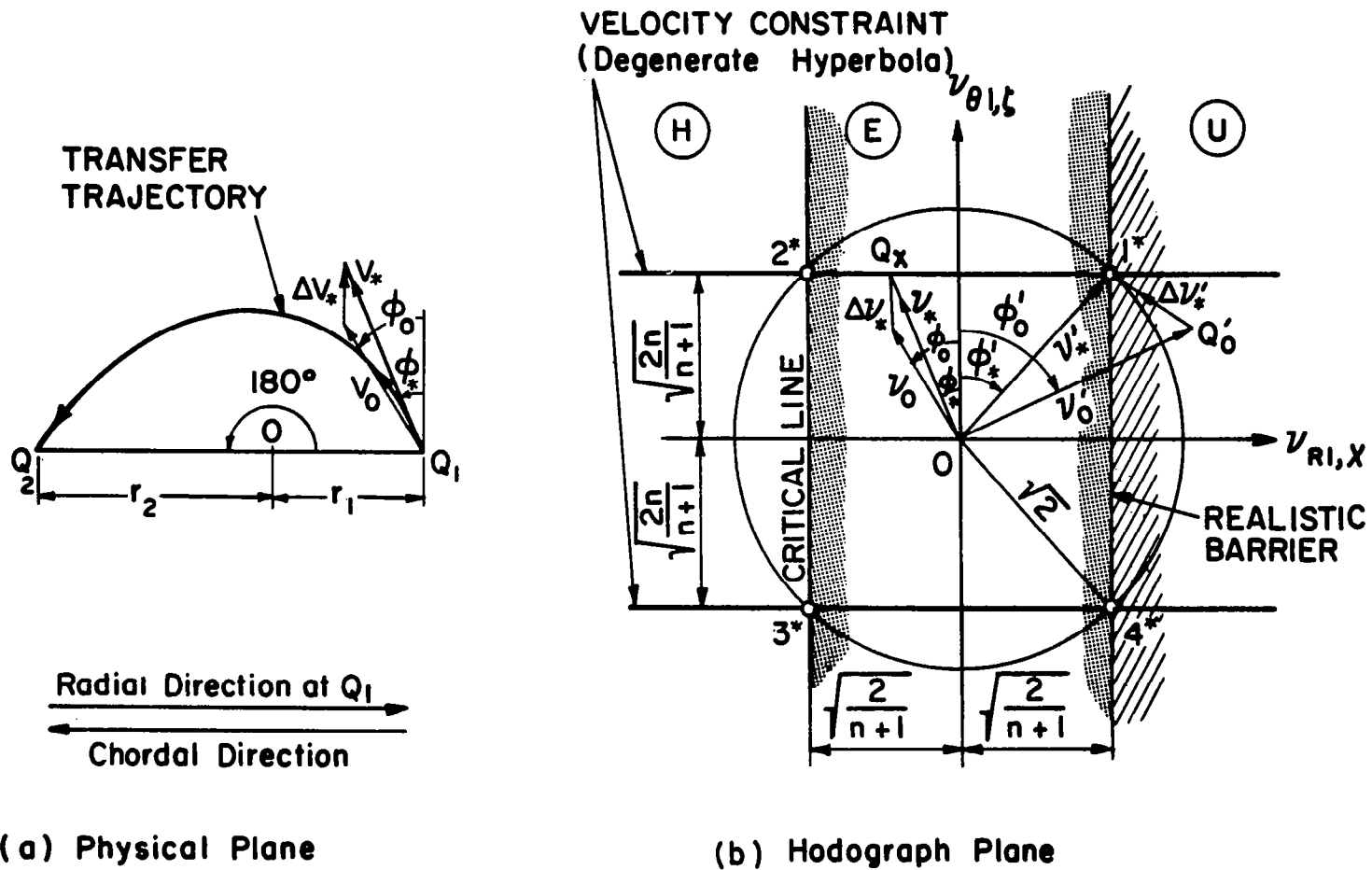$\sqrt{\dfrac{2}{n+1}}$ $\sqrt{\dfrac{2}{n+1}}$

(b) Hodograph Plane

Fig. 17. Optimization of $180°$ transfer $(\psi = \pi)$.

TABLE 7

OPTIMUM SOLUTIONS FOR 180° TRANSFER $(\psi = \pi)$

	(1) Realistic Region	(2) Unrealistic Region
Condition on $\vec{v}_0$	$v_0 \sin\phi_0 < \sqrt{\dfrac{2}{n+1}}$ (56-1)	$v_0 \sin\phi_0 \gtreqless \sqrt{\dfrac{2}{n+1}}$ (56-2)
Velocity-Increment $(\vec{\Delta v})_{opt.}$		$\cong \vec{\Delta v}^*$
r-component $(\Delta v_r)_{opt.}$	0	$\cong \sqrt{\dfrac{2}{n+1}} - v_0 \sin\phi_0$ (57-2)
θ-component $(\Delta v_\theta)_{opt.}$	$\pm \sqrt{\dfrac{2n}{n+1}} - v_0 \cos\phi_0$ (57-1)	$\pm \sqrt{\dfrac{2n}{n+1}} - v_0 \cos\phi_0$
Departure Velocity $(\vec{v})_{opt.}$		$\cong \vec{v}^* \; (v^* = \sqrt{2})$
r-component $(v_r)_{opt.}$	$v_0 \sin\phi_0$	$\cong \sqrt{\dfrac{2}{n+1}}$
θ-component $(v_\theta)_{opt.}$	$\pm \sqrt{\dfrac{2n}{n+1}}$ (58-1)	$\pm \sqrt{\dfrac{2n}{n+1}}$ (58-2)

NOTE: For the double sign: take the upper sign when $(v_\theta)_0 > 0$. $(|\phi_0| < \frac{\pi}{2})$ (1 solution)

take the lower sign when $(v_\theta)_0 < 0$ $(|\phi_0| > \frac{\pi}{2})$ (1 solution)

take both signs when $(v_\theta)_0 = 0$ $(|\phi_0| = \frac{\pi}{2})$ (2 solutions)

Q_0 is in the unrealistic region. Since no non-simple region exists, the only choice for the optimum is then the one close to the nearer critical point, 1* or 4*, and remains in the elliptic region. The optimum solution is again indefinite, and may be written approximately as summarized in Table 7, column 2.

With v_{1*} thus determined the hodograph for the transfer trajectory can be constructed in the $\vec{v}$-plane by noting that for a 180° trajectory we have

$$v_{\theta 1} : v_{\theta 2} = n : 1 \tag{59}$$

Thus once the image point Q_1 is determined in the hodograph plane, so is the image point Q_2. Since the center of the hodograph circle is necessarily halfway between Q_1 and Q_2, the hodograph of the transfer trajectory is now completely determined, as shown in Fig. 18a. It is interesting to note that, in a $\vec{v}$-plane the center of the hodograph circle for such transfer trajectories is constrained on a line also parallel to the v_{r1}-axis and at a distance $(1-n)/\sqrt{2n(n+1)}$ from it, which follows directly from Eqs. (55) and (59).

In the $\vec{v}$-plane the radical center T recedes to infinity, and all constant-n-lines become parallel. Consequently, ρ_* also tends to infinity and the ρ_*-equation is no longer suitable for the description of the O_*-locus. In such a case the use of an alternate coordinate system is necessary. A convenient choice is a rectangular system with its axes coinciding with the directed lines $\overrightarrow{TQ_1}$ and $\overrightarrow{Q_2Q_1}$ in the $\vec{v}$-plane (which are in the local horizontal and vertical directions at Q_1 respectively). Let ρ_*' be the radius vector from the point Q_1 to the optimum origin O_*, then evidently, (see Fig. 18b).
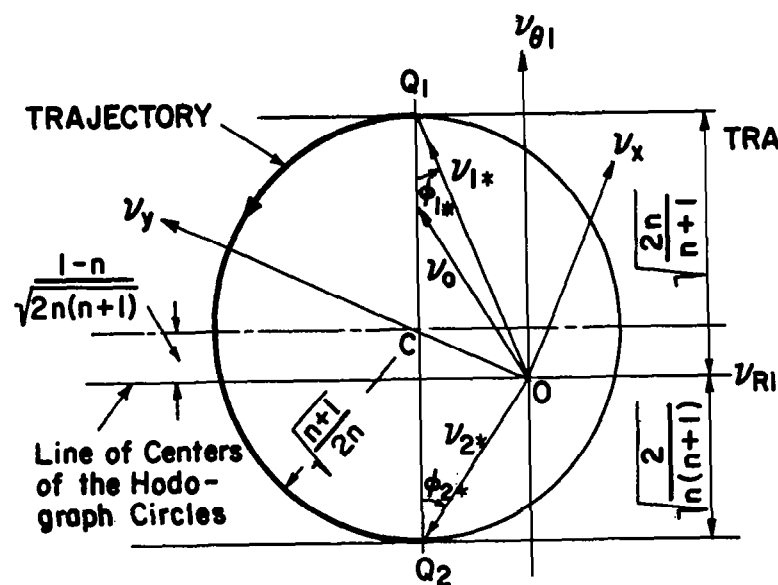
$$\vec{\rho_*'} = - \vec{v}_{1*} \tag{60}$$
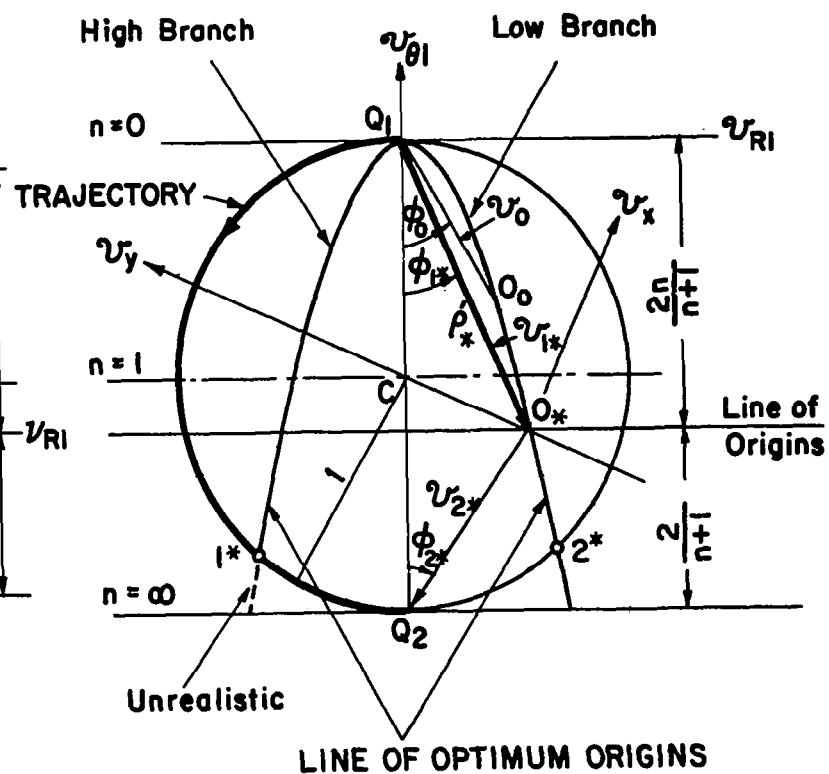
with their rectangular coordinates related by

$$\begin{aligned}
(\rho_*')_r &= - v_{r*} \\
(\rho_*')_\theta &= - v_{\theta*}
\end{aligned} \tag{60a}$$

Temporarily let us consider only the trajectories of the normal group, that is we restrict v_θ to be non-negative $(-\pi/2 \leq \phi_0 \leq \pi/2)$, then directly from their definitions the components of $\vec{v}$ and $\vec{v}$ are related by

$$\begin{aligned}
v_\theta &= v_\theta^2 \\
v_r &= v_r v_\theta
\end{aligned} \tag{61}$$

(a) The $\widetilde{\nu}$ – Hodograph

(b) The $\widetilde{\upsilon}$ – Hodograph

Fig. 18. The optimum trajectory hodograph for 180° transfer.

It follows that

$$\frac{v_r^2}{v_\theta} = v_r^2 \tag{62}$$

But according to Eqs. (58-1) and (50) we have for realistic optimum,

$$v_{r*} = v_0 \sin \phi_0 = m_0 \tag{63}$$

Substituting Eq. (63) into Eq. (62) gives

$$v_{r*}^2 = m_0^2 \, v_{\theta*} \tag{64}$$

In terms of ρ_r' and ρ_θ' , this becomes

$$(\rho_*')_r^2 = -m_0^2 (\rho_*')_\theta \tag{65}$$

Thus the ρ_*'-equation is a parabola tangent to the v_{r1}-axis at Q_1 and having the $v_{\theta1}$-axis as its axis of symmetry (see Fig. 18b). Note that the line of optimum origins must pass through the initial point O_0 determined by the initial velocity vector $\vec{v}_0$, according to Section 4.3. Thus the positive branch of this parabola corresponds to initial velocity vectors at negative path angles ($\phi_0 < 0$) and will be designated as the low branch; while the negative branch corresponds to those at positive path angles ($\phi_0 > 0$) and will be designated as the high branch. The low branch therefore always gives a realistic optimum, and its portion beyond the hodograph circle is the hyperbolic portion. The high branch corresponds to a realistic optimum only up to the critical point, and beyond that the optimum origin will move closely around the circumference of the hodograph circle, but remain inside it.

It is to be noted that, when the initial velocity is directed in the local horizontal direction ($\phi_0 = 0$), the ρ_*'-parabola degenerates into the line Q_1Q_2, and all optimum transfer trajectories are realistic and elliptic. As is evident from both the $\vec{v}^2$-hodograph and the $\vec{v}$-hodograph, such an optimum transfer trajectory is always the Hohmann transfer ellipse independent of the magnitude of the initial velocity vector.

When the path angle of the initial velocity vector exceeds the limit $\pm \pi/2$, the optimum solution calls for a trajectory of the complementary group. The corresponding transfer hodograph can be obtained by rotating the present one for the normal group through 180° as usual.

5.3 THE CASE $n \to \infty$ ($r_2 \to \infty$)

When r_2 increases indefinitely while the angle ψ is fixed, the final terminal point Q_2 recedes to infinity along a given direction, and the problem becomes an escape from a given point Q_1 along a given asymptotic direction

specified by ψ. The base triangle is now open with

$$\varphi_1 \to \pi - \psi \; , \quad \varphi_2 \to 0 \tag{66}$$

and the principal elements of the constraining hyperbola have the following limiting values according to Table 2:

$$\sigma \; \to \; \psi$$

$$A \; \to \; \sqrt{2}$$

$$B \; \to \; \sqrt{2} \tan \frac{\psi}{2} \tag{67}$$

$$e \; \to \; \sec \frac{\psi}{2}$$

Besides, the boundary Lamé has its cusps G and G' given by

$$\nu_{G,G'} \to \sqrt{2} \, \sec^2 \frac{\psi}{2} \tag{68}$$

The geometry in the physical plane and that in the hodograph plane are shown in Fig. 19 a,b. The minimum velocity along the constraining hyperbola, as given by A, is the escape speed; thus all possible transfer trajectories are hyperbolic, or at least parabolic, a fact which is self evident. In the hodograph plane the critical circle now touches the constraining hyperbola at its vertices φ and φ', and the entire hodograph plane is divided into the realistic (all hyperbolic) and the unrealistic regions by the $\nu\zeta$-axis.

It is to be noted that, although nonsimple regions exist in the hodograph plane for the present case, no realistic conjugate optimum solutions exist along the $\nu\zeta$-axis since no elliptic region exists, and the high half-plane is all unrealistic. Furthermore, a parabolic trajectory should not be admitted as a solution since it has no definite asymptotic direction as required by the problem. Thus whenever the tip Q_0 of the initial velocity vector lies between the points G and G' on the $\nu\zeta$-axis, a point on the constraining hyperbola in the realistic region and close to the nearer critical point, φ or φ' is to be chosen as the optimum point. For points on the $\nu\zeta$-axis beyond either G or G', of course hyperbolic realistic optimum solutions always exist. A simple criterion for realistic optimum transfer is then

$$-\frac{1}{2}(\pi+\psi) < \phi_0 < \frac{1}{2}(\pi-\psi) \; (-\pi < \Phi_0 < 0) \quad : \quad \text{any } \nu_0$$

$$\phi_0 = \frac{1}{2}(\pm\pi-\psi) \; (\Phi_0 = 0,-\pi) \quad : \quad \nu_0 > \sqrt{2} \sec^2 \frac{\psi}{2} \tag{69}$$

Note that the E-C-V-I lines here coincide with the $\nu\zeta$-axis, and the subregion U_2 does not exist. Consequently, the optimum solution is indefinite whenever Q_0 is in the unrealistic region, and such a solution is given by Eqs. (40,41) with $\Phi^* = 0$. The optimum solution when Q_0 is in the realistic region
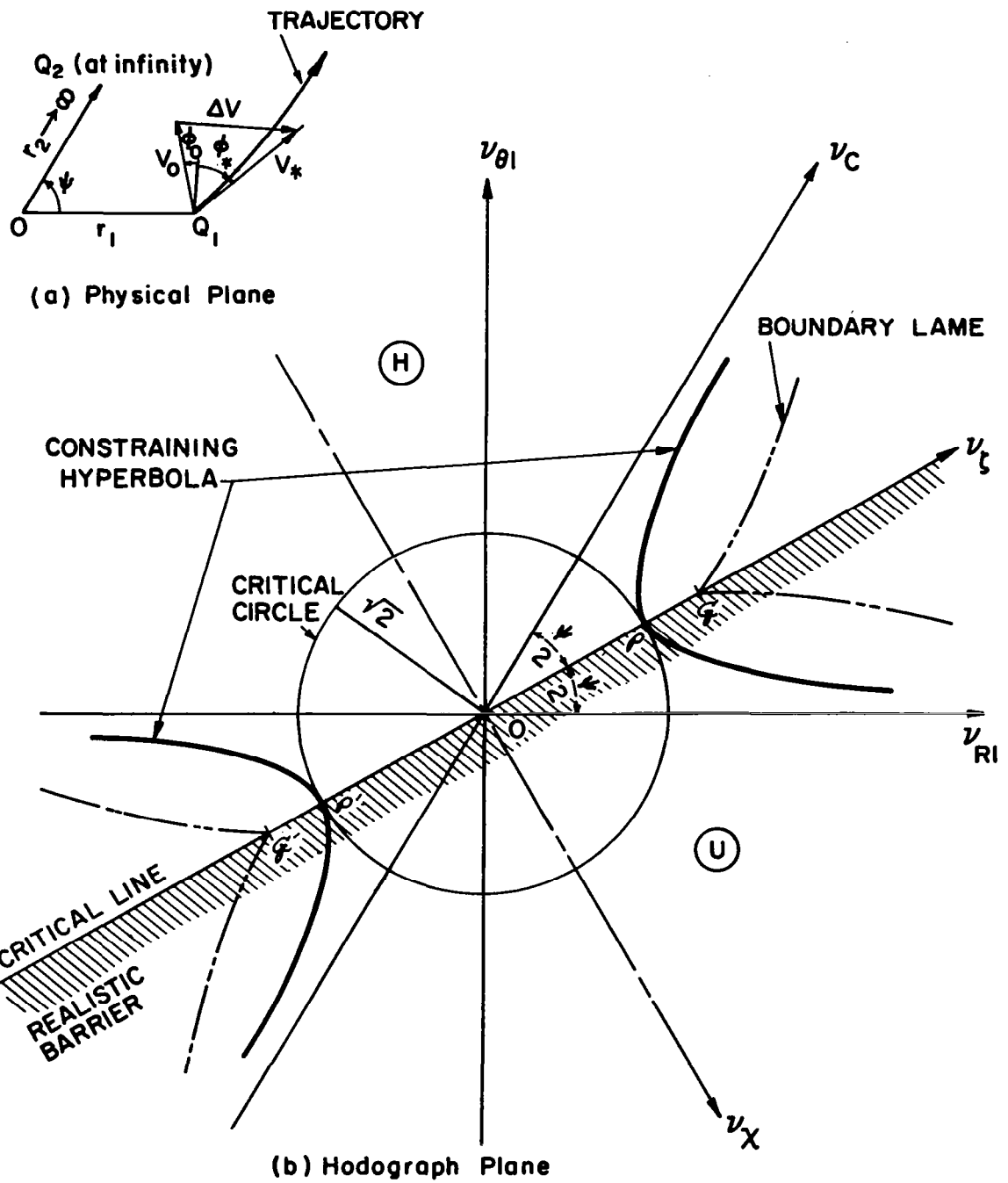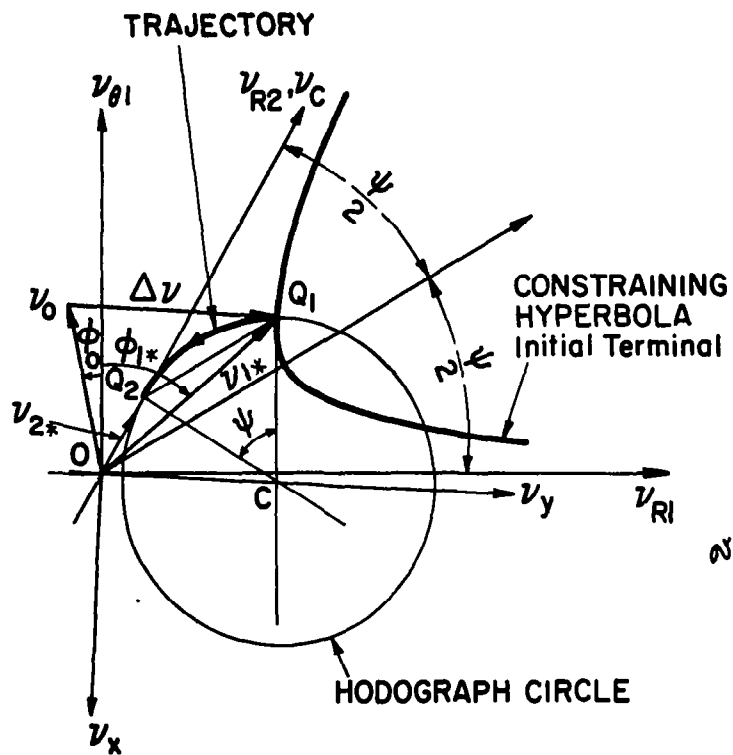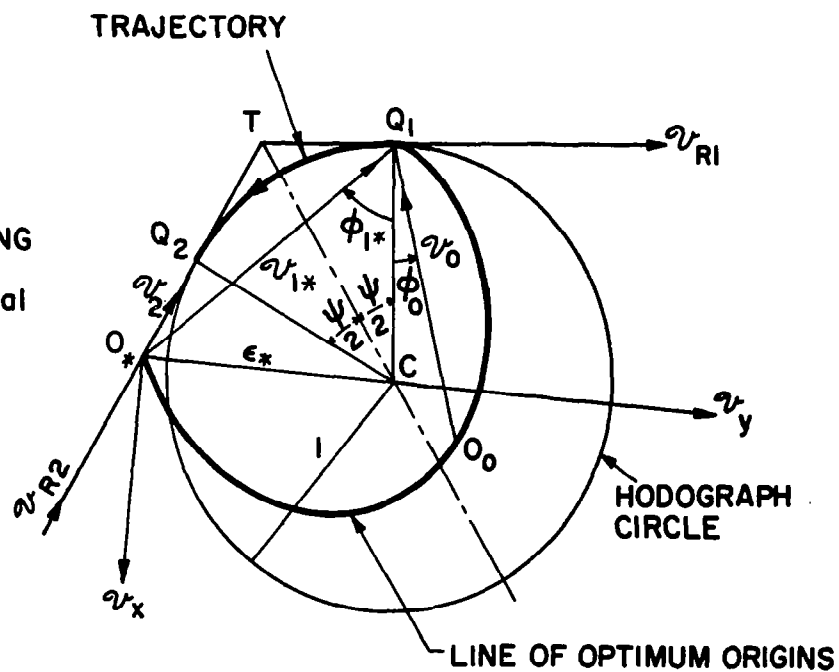
63

Fig. 19. Optimization of transfer to infinity $(r_2 \to \infty)$.

(a) The $\vec{\nu}$ - Hodograph

(b) The $\vec{\mathcal{V}}$ - Hodograph

Fig. 20. The optimum trajectory hodograph for transfer to infinity.

cannot be readily written from the geometry in the $\vec{v}$-plane as was done in the previous particular cases. However, it is given by the point where the line of the optimum origins meets the line TQ in the $\vec{v}$-plane as shown in Fig. 20b, and essential information concerning the transfer trajectory can be obtained from the $\vec{v}$-hodograph. For example, the eccentricity of the optimum trajectory is given by $\overline{O*C}$, its apsidal axis by the line normal to $\overrightarrow{O*C}$, and the residual velocity, the vector $\overrightarrow{O*Q_2}$.

The $\vec{v}$-hodograph can be constructed as usual. In this case the point Q_2 in the hodograph plane can be easily located by drawing a straight line passing through Q_1 and parallel to the bisector of the angle ψ.[8] The point where this line meets the v_{r2}-axis gives the point Q_2 required (see Fig. 20a). The hodograph circle will of course be tangent to the v_{r2}-axis.

5.4 THE CASE $n \to 0$ $(r_2 \to 0)$

In this case the final terminal Q_2 is approaching the field center O, and the constraining hyperbola in the hodograph plane is approaching the v_{r1}-axis. In the limit the situation reduces to that of a vertical descent analyzed in Section 5.1a with $r_2 = 0$. The hodograph geometry is the same, the transfer trajectory is again a vertical line segment, and all formulas of Section 5.1a apply to the present case.

[8]See footnote 6.

6. TRANSFER FROM A CIRCULAR ORBIT

Since the transfer from an initial circular orbit is of frequent occurrence in space flight problems, it is worth a brief treatment in the light of the present analysis. For the time being the two-dimensional case will be considered, that is, the final terminal will be restricted to the plane of the initial orbit.

6.1 ANALYSIS

The initial condition for the transfer from a circular orbit to a coplanar point is as follows (Fig. 21a):

Short transfer $\quad\quad v_o = 1 , \quad \phi_o = 0 \quad\quad\quad\quad$ (70a)

Long transfer $\quad\quad\quad v_o = 1 , \quad \phi_o = \pi \quad\quad\quad\quad$ (70b)

As is evident from the optimization chart (Fig. 12), an unrealistic optimum is possible only for a long transfer. Thus a definite realistic optimum solution exists for a short transfer, and also for a long transfer before the realistic barrier is reached. Such a solution is provided by the orthogonality Eq. (10'-R), which takes the simple form
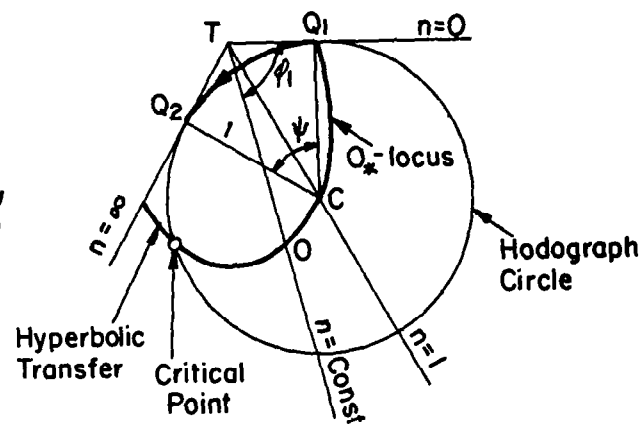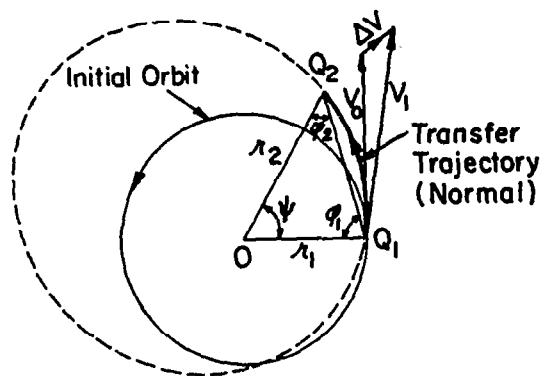
$$v_{R*}^4 \pm v_{R*} \tan \frac{\psi}{2} - \kappa^2 = 0 \quad\quad\quad\quad (71)$$

under the conditions (70a,b). The upper sign in Eq. (71) pertains to the short transfer, and the equation has one positive real root (according to Table 3) giving the optimum solution. Similarly, the lower sign pertains to the long transfer, and the equation has one negative real root for the optimum solution. Evidently, these two roots differ in sign only and the two solutions are a complementary pair. The corresponding O_*-locus in the $\vec{v}$-plane is given by Eq. (49), which reduces to

$$\left(\rho_*^2 - \tan^2 \frac{\psi}{2} \right)^2 = \rho_*^3 \sin^3 \varphi_1 \quad\quad\quad\quad (72)$$

for the present case. The locus passes through the center of the hodograph circle as shown in Fig. 21b. Whenever an unrealistic optimum arises from Eq. (71) in the case of a long transfer, the realistic optimum solution becomes indefinite, and is given by Eqs. (40,41). The corresponding O_*-locus is then to follow the arc of the hodograph circle but remain inside it as discussed in Section 4.3, item (7). Formulas for the minimum velocity-increment for both the defi-

Short Transfer

Initial Orbit

Q_2

V_b

V_1

ϕ_2

r_2

Transfer Trajectory (Normal)

ψ

ϕ_1

ΔV

O

r_1

Q_1

T

Q_1

n=0

Q_2

l

ϕ_1

ψ

O_*-locus

C

n=∞

O

Hodograph Circle

Hyperbolic Transfer

Critical Point

n=1

n=Const

Long Transfer

Initial Orbit

Q_2

ϕ_2

r_2

ψ

ϕ_1

O

r_1

Q_1

V_1

V_0

ΔV

Transfer Trajectory (Complementary)

Physical Plane

n=1

n=Const

Critical Point

Hodograph Circle

O

n=∞

C

l

Unrealistic Transfer

O_*-locus

ψ

Q_2

ϕ_1

n=0

Q_1

T
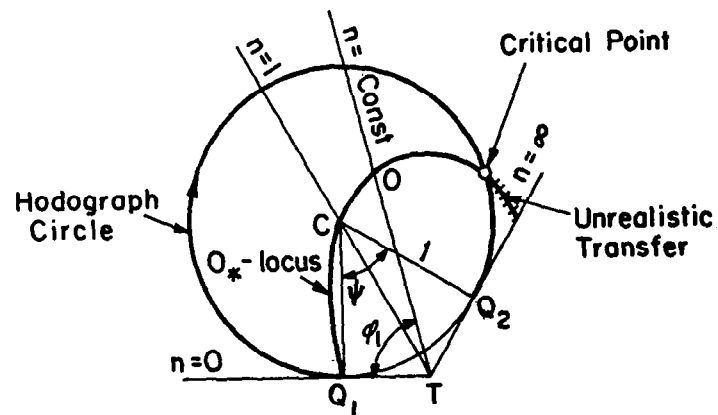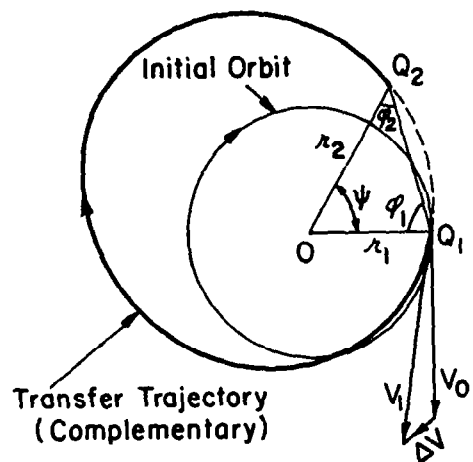
Hodograph Plane $(\dot{x}, \dot{y})$

Fig. 21. Transfer from a circular orbit to a coplanar point.

nite and indefinite optimums as specialized to the circular case are summarized in Table 8, and the variation of the minimum velocity-increment under various configurations of the base triangle is shown in Fig. 22.

In view of the foregoing analysis it is of importance to safeguard the occurrence of an unrealistic optimum in the case of a long transfer. An analytical criterion for the occurrence of a critical optimum (including both the realistic and unrealistic cases) has been derived by Battin (4) in an approximate form. An exact form of such a criterion can be obtained here by applying the circular condition (70a) or (70b) to the general critical condition (28), which, after some trigonometric simplifications, reduces to

$$\cos^4 \frac{\psi}{2} - \cos^2 \frac{\psi}{2} - 4(\frac{1}{n*})^{\frac{3}{2}} \cos \frac{\psi}{2} + \frac{2}{n*} (1 + \frac{1}{n*}) = 0 \tag{75}$$

where ψ is the vertex angle of the base triangle, and is related to the range angle Ψ by

$$\Psi = \begin{cases} \psi & \text{for short transfer} \\ 2\pi - \psi & \text{for long transfer} \end{cases} \tag{76}$$

and n*, the critical distance ratio, is the value of n which satisfies the critical criterion (75) for a given ψ. For a fixed initial terminal Q_1, Eq. (75) defines for the final terminal Q_2 in the physical plane a boundary on which the optimum transfer trajectory given by Eq. (10'-R) would be parabolic. Such a boundary is shown in Fig. 23. It is the critical boundary for a short transfer, but an unrealistic barrier for a long transfer. For convenience the configuration of the base triangle will be called sub-critical, critical, or super-critical according as Q_2 is below, on, or above this boundary. As Fig. 23 shows, along this boundary n* extends to infinity at $\phi = 0, \pi$, and it has a minimum value of approximately 3.845 at $\psi \cong 71°$. Such a boundary line has also been depicted in Fig. 22. The $|\Delta v_*|$-curve at a constant ψ, as Fig. 22 shows, holds for both the short transfer and the long transfer before it reaches the critical line, that is, the curve for a range angle ψ also holds for the range angle $2\pi - \psi$. However, this breaks down after it crosses the critical line, and the $|\Delta v_*|$-curve splits into two branches, one for the short transfer, and one for the long transfer with the latter branch above the former one. Thus the region enclosed by the critical boundary is the region of definite hyperbolic optimum for short transfers, but of indefinite elliptic optimum for long transfers.

TABLE 8

MINIMUM VELOCITY INCREMENT $|\Delta v_*|$ FOR THE TRANSFER FROM
A CIRCULAR ORBIT TO A COPLANAR POINT

	Definite Optimum For short transfer $0 \leq n < \infty$ or long transfer with $n < n^*$		Indefinite Optimum For long transfer with $n \geq n^*$	
$0 < \psi < \pi$	$\left[2v_{R*}^2 - \dfrac{1}{|v_{R*}|} \tan \dfrac{\psi}{2} - (1 + \dfrac{1}{n}) \sec^2 \dfrac{\psi}{2} + 3\right]^{\frac{1}{2}}$	(73a)	$\left[3 - 2\sqrt{2} \cos (\Phi^* - \dfrac{\varphi_1}{2})\right]^{\frac{1}{2}}$	(73b)
$\psi = 0$	$\begin{array}{ll} 1 & (n < 1) \\ 0 & (n = 1) \\ \sqrt{3 - 2/n} & (n > 1) \end{array}$	(73a-1)	———	
$\psi = \pi$	$\left\| 1 - \sqrt{\dfrac{2n}{n+1}} \right\|$	(73a-2)	———	
$n = 0$	1	(73a-3)	———	
$n \to \infty$	$\left[2v_{R*}^2 - \dfrac{1}{|v_{R*}|} \tan \dfrac{\psi}{2} - \sec^2 \dfrac{\psi}{2} + 3\right]^{\frac{1}{2}}$	(73a-4)	$\left[3 - 2\sqrt{2} \sin \dfrac{\psi}{2}\right]^{\frac{1}{2}}$	(73b-4)
Auxiliary Equations	$v_{R*}^4 \pm v_{R*} \tan \dfrac{\psi}{2} = \sec^2 \dfrac{\psi}{2}\left[\dfrac{1}{4}(1 + \dfrac{1}{n})^2 \sec^2 \dfrac{\psi}{2} - \dfrac{1}{n}\right]$ (71')		$\cot \Phi^* = \sqrt{\tan \dfrac{\varphi_1}{2} \tan \dfrac{1}{2}(\psi + \varphi_1)}$ $(0 \leq \Phi^* \leq \dfrac{\pi}{2})$	(74)

Note: 1) For indefinite optimum, the formula listed in each case is its lower limit, $|\Delta v_*|$.
2) For the double sign in Eq. (71'), the upper sign is for the short transfer, while the lower one, the long transfer.
3) n^* is defined by Eq. (75).

Minimum Velocity-Increment $|\Delta v_*| \equiv \Delta v_* / v_{s1}$

DISTANCE RATIO $n \equiv \lambda_2 / \lambda_1$

Elliptic Transfer
Elliptic Transfer, Nearly Critical
Parabolic Transfer
Hyperbolic Transfer

Inner Transfer ← → Outer Transfer

$\Psi = 0°$

$\Psi = 0°$

$30°, 330°$

$60°, 300°$

$90°, 270°$

$120°, 240°$

$180°$

Critical Line $(n = n^*)$

$(n^*)_{min} = 3.845$

$300°$
$60°$
$270°$
$90°$
$240°$
$120°$

$\left(\text{Horizontal Scale: } n<1 : 5" = 1 \text{ unit}\right)$
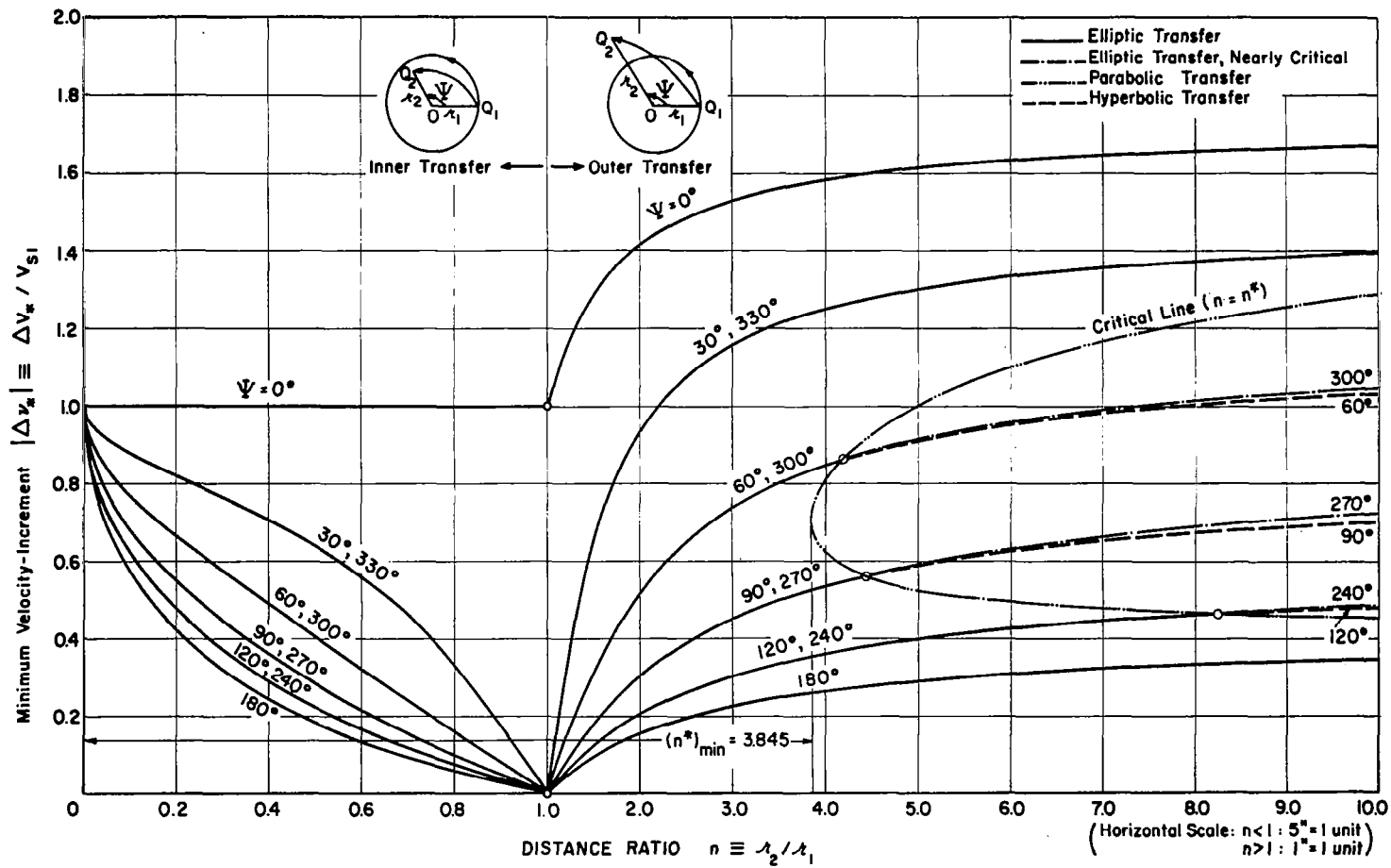$\left(\qquad\qquad\qquad n>1 : 1" = 1 \text{ unit}\right)$

Fig. 22. Minimum velocity-increment for the transfer from a
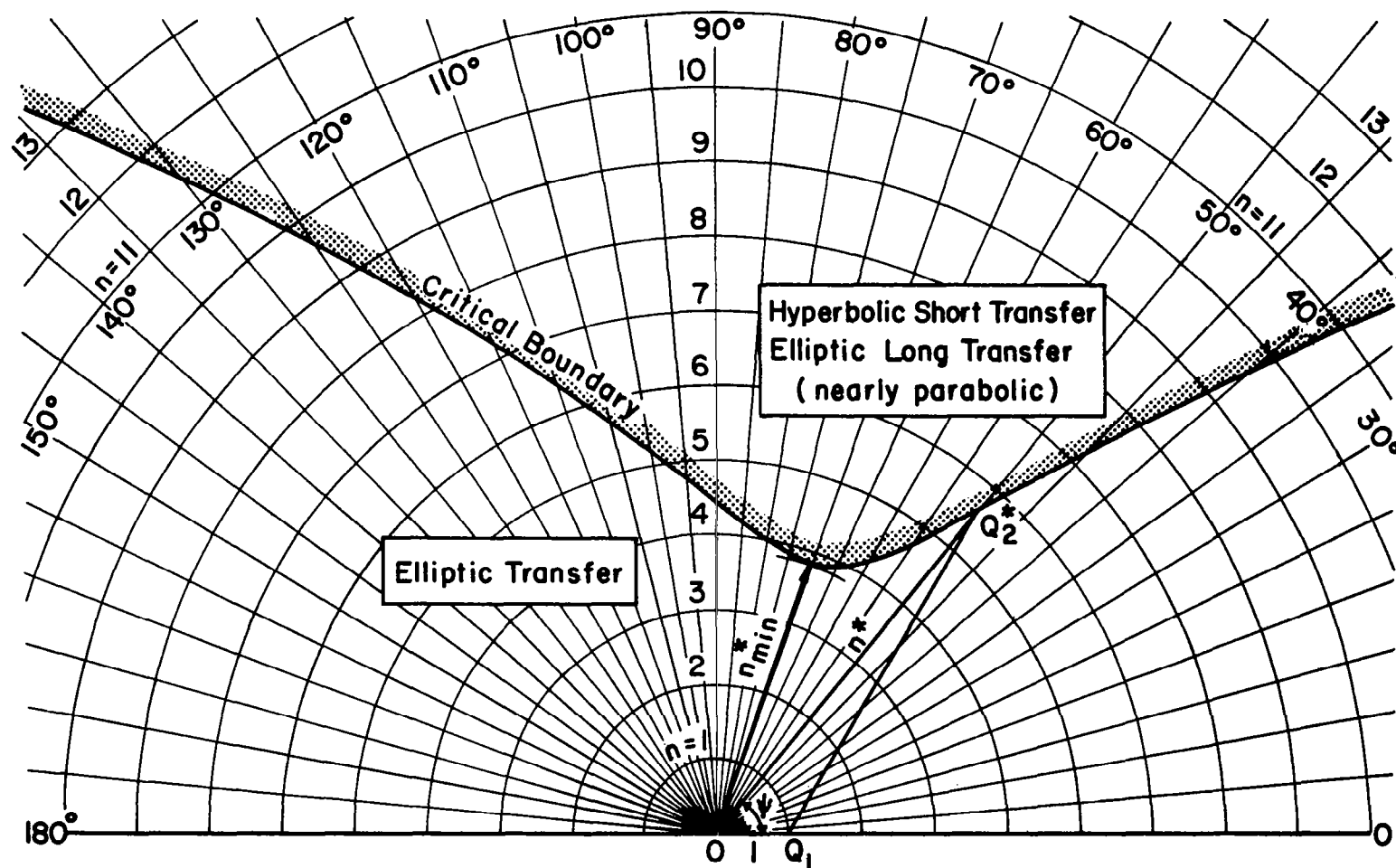circular orbit to a coplanar point.

Fig. 23. The critical configuration of the base triangle for the optimum transfer from a circular orbit.

6.2 SOME OBSERVATIONS

Based on the foregoing analysis and the graphs of Figs. 22 and 23, a number of observations may now be made as summarized below:

(1) There exist definite configurations of the base triangle for which the optimum trajectory is parabolic, which will be realistic for the short transfer, but unrealistic for the long transfer. Such critical configurations are defined by Eq. (75).

(2) For a base triangle of sub-critical configuration, the optimum trajectory is elliptic, and the minimum velocity-increment is the same whether the transfer is short or long. (see Fig. 22)

(3) For a base triangle of critical or super-critical configuration the realistic optimum will be definite, parabolic or hyperbolic for the short transfer, and it will be indefinite, elliptic but nearly parabolic for the long transfer. (see Fig. 22) The minimum velocity-increment is higher in the latter case.

(4) For each vertex angle ψ between 0 and π, there is a minimum distance ratio, n^*, below which no critical optimum, realistic or unrealistic, may occur (see Fig. 23). An overall minimum $n^* \cong 3.845$ exists, below which no such a critical optimum may occur for whatever the vertex angle ψ. In the solar system this distance ratio corresponds to a transfer from the earth orbit to somewhere between the orbits of Mars and Jupiter.

(5) No critical optimum, realistic or unrealistic, may arise for either a vertical transfer or an 180° transfer, through any finite distance ratio since $n^* \to \infty$ in both cases.

(6) For a given distance ratio $n > n^*$, there are two critical values of ψ beyond which no critical optimum, realistic or unrealistic, may occur (see Figs. 22, 23). Thus the two values of ψ define a range of ψ for the definite hyperbolic optimums for the short transfers or the indefinite elliptic optimums for the long transfers, both will be referred to as the critical range for brevity. Definite parabolic optimum exists at the end points in the case of the short transfers of course. In the solar system such a critical range exists in the interplanetary transfer from the earth orbit to that of Jupiter and beyond. Values of these critical angles together with some numerical data pertaining to the solar system as obtained from the present analysis are shown in Table 9. These angles related to Jupiter, Saturn, and Neptune confirm the previous results of Battin (4).

(7) At a constant distance ratio n, the closer the range angle to 180° the smaller the minimum velocity-increment required (see Fig. 22). Thus, from the viewpoint of fuel economy, transfer close to 180° range is desirable. In the limiting case of 180° transfer, the optimum trajectory will be an Hohmann ellipse.

73

(8) At a constant range angle, the closer the values of r_1 and r_2 to each other, the smaller the minimum velocity-increment required. The overall minimum $|\Delta v_*|$ is zero at $r_1 = r_2$ for all values of the range angle, since in this case the initial orbit passes through the final terminal point. (Note in Fig. 22, the $|\Delta v_*|$-curve for $\psi = 0$ is discontinuous at $n = 1$ with an isolated point at $n = 1$, and $|\Delta v_*| = 0$ in accordance with Eqs. (73a-1).)

(9) As the distance ratio n increases indefinitely at a constant range angle, the minimum velocity-increment increases and approaches a finite limit depending on the range angle according to Eqs. (73a,b-4). Similarly, when n decreases indefinitely, the minimum velocity-increment also increases; however, it approaches the value of unity as its limit regardless of the range angle. (see Eq. 73a-3 and Fig. 22)

(10) There exists an overall upper limit for the minimum velocity-increment for all possible configurations of the base triangle. It is given by

$$\left|\Delta v_*\right|_{\psi=0,\ n\to\infty} \longrightarrow \sqrt{3} \quad \text{or} \quad \left|\Delta V_*\right|_{\text{upper limit}} = \sqrt{3}\ V_{s1} \qquad (77)$$

according to Eq. (73b-4). Thus, in principle, any propulsion device capable of producing a velocity-increment of $29.8\sqrt{3} \cong 51.6$ Km/sec will be enough for the transfer from the earth orbit (orbital speed = 29.8 Km/sec) to any terminal point in the solar system.

All the foregoing observations are made on the assumption of the two-dimensional transfer from an initial circular orbit. The three-dimensional effects will be presented in the chapter that follows.

TABLE 9

MINIMUM VELOCITY INCREMENT REQUIRED AND THE CRITICAL RANGE ANGLES FOR INTERPLANETARY
FLIGHT IN THE SOLAR SYSTEM FROM THE EARTH ORBIT

Destination Planet	Mean Distance Ratio $n = \dfrac{r_2}{r_1}$	Minimum Velocity Increment Required $\psi = 180°$ (Orbital Speed of Earth = 29.8 $\frac{km}{sec}$)		Critical Range Angle			
				Short Transfer		Long Transfer	
		$\lvert \Delta v_* \rvert = \dfrac{\lvert \Delta V_{1*} \rvert}{V_{s1}}$	$\lvert \Delta V_{1*} \rvert$	ψ_L^*	ψ_U^*	ψ_L^*	ψ_U^*
Mercury	0.39	0.250	7.45	—	—	—	—
Venus	0.72	0.085	2.53	—	—	—	—
Mars	1.52	0.098	2.92	—	—	—	—
Jupiter	5.20	0.295	8.79	52.0°	100.2°	259.8°	308.0°
Saturn	9.54	0.346	10.3	40.2°	124.8°	235.2°	319.8°
Uranus	19.19	0.379	11.3	30.3°	142.1°	217.9°	329.7°
Neptune	30.07	0.392	11.7	25.1°	150.0°	210.0°	334.9°
Pluto	39.46	0.397	11.8	22.3°	153.9°	206.1°	337.7°

7. THE THREE-DIMENSIONAL EFFECTS ON THE OPTIMUM TRANSFER

7.1 THE THREE-DIMENSIONAL ANALYSIS

When the initial velocity vector is not coplanar with the base triangle, the problem is three-dimensional. In such a case the in-plane and out-of-plane components of the velocities are to be considered. Thus Eq. (1) may be written.

$$\vec{\Delta V} = \vec{V}_1 - (\vec{V}_{op} + \vec{V}_{on}) \tag{78}$$

where

$$
\begin{aligned}
V_{op} &= V_o \cos \omega \\[2ex]
V_{on} &= V_o \sin \omega
\end{aligned}
\tag{79}
$$

and ω is the inclination angle of the initial velocity V_o with the plane of the base triangle. The geometry of the transfer is shown in Fig. 24.
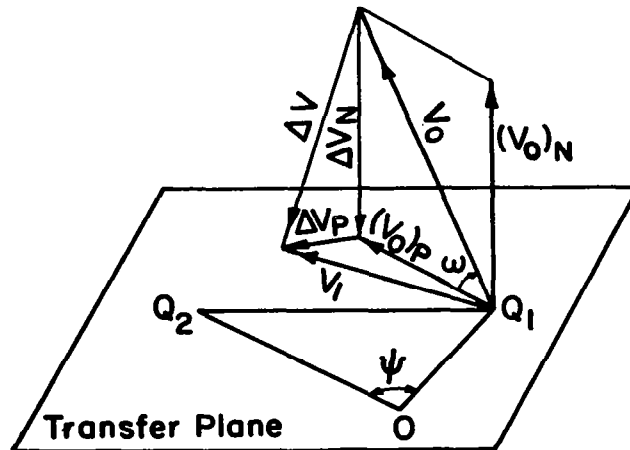

Fig. 24 Geometry of the three-dimensional transfer.

76

In view of the fact that the departure velocity $\vec{V}_1$ along the transfer trajectory must be in the plane of the base triangle, Eq. (78) may be written

$$\vec{\Delta V} \;=\; \vec{\Delta V}_p \;-\; \vec{V}_{on} \tag{78a}$$

where $\vec{\Delta V}_p$ is the in-plane velocity-increment, defined by

$$\vec{\Delta V}_p \;=\; \vec{V}_1 \;-\; \vec{V}_{op} \tag{80}$$

The magnitude of the total velocity-increment is then given by

$$|\Delta V|^2 \;=\; |\Delta V_p|^2 \;+\; V_{on}^{\;2} \tag{81}$$

For a given initial velocity vector and a given base triangle, $\vec{V}_{on}$ is constant. Thus the optimization of $|\Delta V|$ amounts to the optimization of $|\Delta V_p|$, and the problem becomes two-dimensional. Consequently we have

$$|\Delta V_*|^2 \;=\; |\Delta V_{p*}|^2 \;+\; V_{on}^{\;2} \tag{82}$$

where $|\Delta V_{p*}|$ is given by the two-dimensional optimum solution corresponding to the initial velocity vector $\vec{V}_{op}$. Thus by replacing $\vec{V}_o$ by $V_o \cos \omega$ we obtain ΔV_{p*} from the previous two-dimensional analysis, and the three-dimensional solution follows from Eqs. (78a and 82). Such a reduction of the three-dimensional case to the two-dimensional case has been pointed out by Stark and some numerical solutions are found in (6). Thus no elaborate analysis is necessary here. However, in the light of the present analysis a few remarks on the three-dimensional effects will be given below.

7.2 THE THREE-DIMENSIONAL EFFECTS

First, the effect of tilting the initial velocity vector from the plane of the base triangle may be investigated by using Eq. (82). Let $|\Delta V_*|_{3D}$ and $|\Delta V_*|_{2D}$ be the minimum velocity-increments for the three-dimensional and two-dimensional problems respectively, both referring to the same base triangle and the same initial speed and path angle (V_o, ϕ_o) except $\omega = 0$ in the latter case. When ω is small, we have $V_{op} \cong V_o$, $|\Delta V_{p*}| \cong |\Delta V_*|_{2D}$ and Eq. (82) may be written

$$|\Delta V_*|_{3D} \;\cong\; \sqrt{|\Delta V_*|_{2D}^2 + V_{on}^{\;2}} \tag{83}$$

from which we see that the presence of the out-of-plane component V_{on} is of
importance when the term $|\Delta V_*|_{2D}$ is comparatively small. Thus we may say that,
the smaller the two-dimensional solution, the more significant the three-di-
mensional effect. In the case of the transfer from an initial circular orbit,
such is the situation in the neighborhood of n = 1. That is, the closer the
distances r_1 and r_2 are to each other, the more significant is the effect of
the inclination between the orbital plane and the plane of the base triangle.
As Fig. 25a shows, the maximum deviation of $|\Delta V_*|_{3D}$ from $|\Delta V_*|_{2D}$ occurs at
n = 1, and is the same regardless of the range angle. It is in fact equal
to the magnitude of the out-of-plane component of the initial velocity. The
same reasoning accounts for the fact that at a constant distance ratio n the
deviation of $|\Delta V_*|_{3D}$ from $|\Delta V_*|_{2D}$ increases when the range angle tends toward
180° for either the long transfer or the short transfer as shown in Fig. 25a,
since the corresponding two-dimensional velocity-increment tends to decrease
according to Fig. 22.

Second, it is worth to note that in the case of 0° or 180° transfer, the
base triangle defines no plane since it has degenerated into a line segment.
Consequently, the optimum transfer plane is the one defined by the initial
velocity vector and this line segment, and the case is always two-dimensional.
Thus it seems curious that, while the three-dimensional effect tends to become
more significant as ψ approaches 180°, as shown in the preceeding paragraph,
it can be completely eliminated in the limiting case of ψ = 180°.

Third, the reduction of V_0 to $V_0 \cos\omega$ by tilting the initial velocity
vector may effect the region in the hodograph plane where the point Q_0 lies,
and thereby effect the type of the optimum transfer trajectory. Thus it is
quite possible that an initial velocity vector, which calls for an hyperbolic
optimum when it lies in the plane of the base triangle, may call for an elliptic
optimum instead when it is tilted up, though at a greater expense of the initial
impulse. In general, the critical boundary and the unrealistic barrier both
will be effected. In the case of the transfer from a circular orbit, an examina-
tion of the geometry of the hodograph shows that the effect of increasing the
inclination angle ω tends to increase the critical distance ratio n* for a
fixed ψ between 0 and π (see Fig. 25b), and for a fixed n > n* it tends to
shorten the critical range defined by the two critical angles. However, it
is to be noted that such effects are not present in the case of 0° or 180°
transfer, even though the transfer plane is taken to be different from the
optimum one mentioned in the preceeding paragraph, since the critical distance
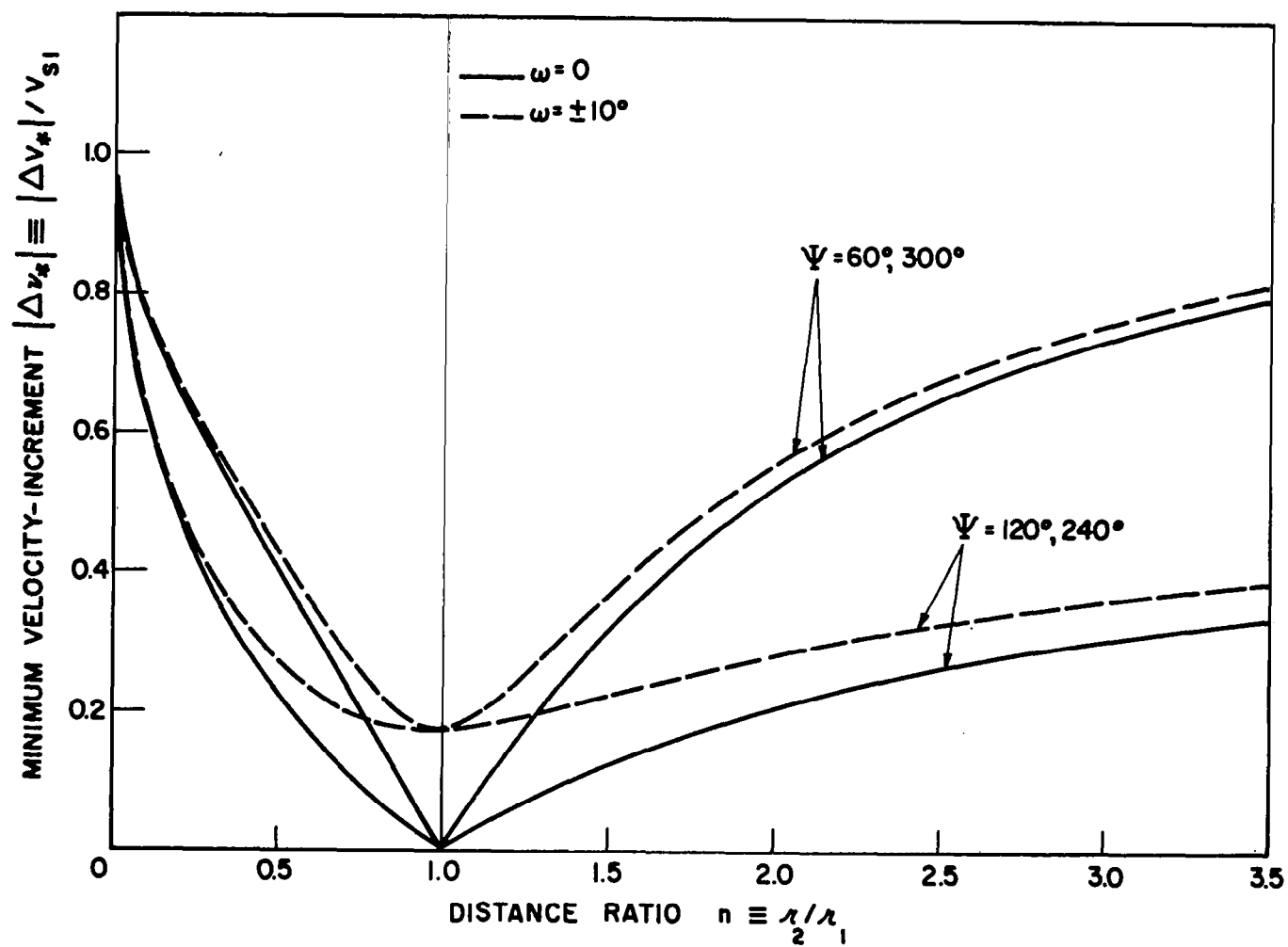ratio n* tends to infinity in both cases.

Fig. 25a Three-dimensional effect on the optimum transfer from a
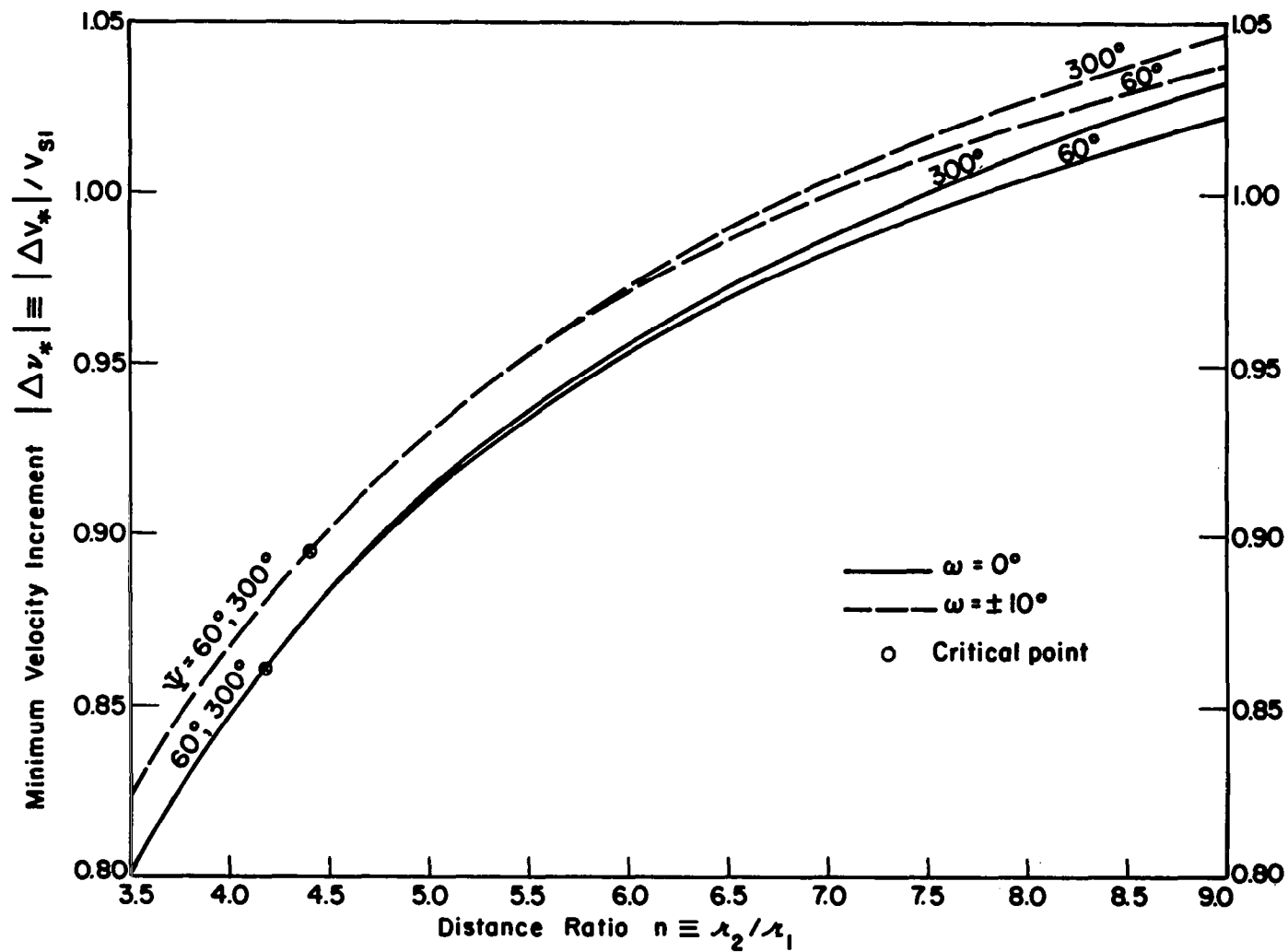circular orbit: Low distance ratio (n < n*).

Fig. 25b Three-dimensional effect on the optimum transfer from a
circular orbit: High distance ratio ($n \geq n*$).

REFERENCES

1. Salmon, G., A Treatise on Conic Sections, 6th Ed., Longmans, Green and Co., 1879, pp. 337-338.

2. Burnside, W. S., and Panton, A. W., The Theory of Equations, Longmans, Green and Co., 7th Ed., 1912, pp. 144-145.

3. Yates, R. C., Curves, Department of Mathematics, U. S. Military Academy, 1946, pp. 84-90, 155-158.

4. Battin, R. H., "The Determination of Round Trip Planetary Reconnaissance Trajectories," J. Aero/Space Sci., Vol. 26, No. 9, September, 1959.

5. Godal, Th., "Conditions of Compatibility of Terminal Positions and Velocities," Proceedings XIth International Astronautical Congress, Stockholm, 1960, Springer Verlag, Vol. I, pp. 40-44.

6. Stark, H. M., "Optimum Trajectories Between Two Terminals in Space," ARS J., February, 1961, pp. 261-263.

7. Sun, F. T., "On the Hodograph Method for Solution of Orbit Problems," XIIth International Astronautical Congress, Washington, D.C., October, 1961, Academic Press, Inc., Vol. II, pp. 879-915.

8. Altman, S. P., and Pistiner, J. S., "Comment on the Correlation of Stark's Two-Terminal Trajectory Optimization with an Orbital Hodograph Analysis," ARS J., 1962, Vol. 31, No. 11, November, 1961.

9. Sun, F. T., "Hodograph Analysis of the Free-Flight Trajectories Between Two Arbitrary Terminal Points," NASA CR-153, Washington, D.C., January, 1965.

APPENDIX A

GLOSSARY OF TERMS FOR TWO-TERMINAL TRAJECTORIES[†]

(see Fig. A-1)

Base Triangle

The triangle formed by the initial terminal (Q_1), the final terminal (Q_2) and the center of the gravity field (O).

Normal and Complementary Groups

A two-terminal trajectory is said to be of the normal group or the complementary group according as its range angle is smaller or larger than 180°, corresponding to the so-called short and long transfers respectively.

High and Low Classes

A two-terminal trajectory is said to be of the high class or the low class according as its direction is inclined above or below the local minimum energy direction at the initial terminal.

Conjugate Trajectories

Two trajectories are said to be conjugate to each other if they have the same initial and final terminals, the same range angle, and the same speed at the initial terminal.

Complementary Trajectories

Two trajectories are said to be complementary to each other if they have the same initial and final terminals, the same initial speed and going in opposite directions around the field center.

Complementary-Conjugate Trajectories

Two trajectories are said to be complementary-conjugate to each other if one is the complementary of the conjugate of the other.

[†]For details see Section II, Ref. (9), in which these terms were introduced and discussed.

Realistic and Unrealistic Trajectories

A two-terminal trajectory is said to be realistic if every point on the trajectory is at a finite distance from the field center; otherwise it is said to be unrealistic.

## Forbidden Region for the Direction of Departure

For a fixed base triangle the forbidden region for the direction of departure is the angular region for such a direction along which no trajectory from the initial terminal Q_1 can reach the final terminal Q_2 whatever the departure speed. There are two such regions for the Keplerian trajectories, according to Ref. (9), as follows:[†]

The Outer Forbidden Region: the angular region included between the two directions of the conjugate pair of parabolic trajectories from Q_1 to Q_2.

The Inner Forbidden Region: the angular region included between the two sides, OQ_1 and Q_1Q_2 of the base triangle.

[†]Similar regions exist for the direction of approach, see Ref. (9), pp. 11-13.
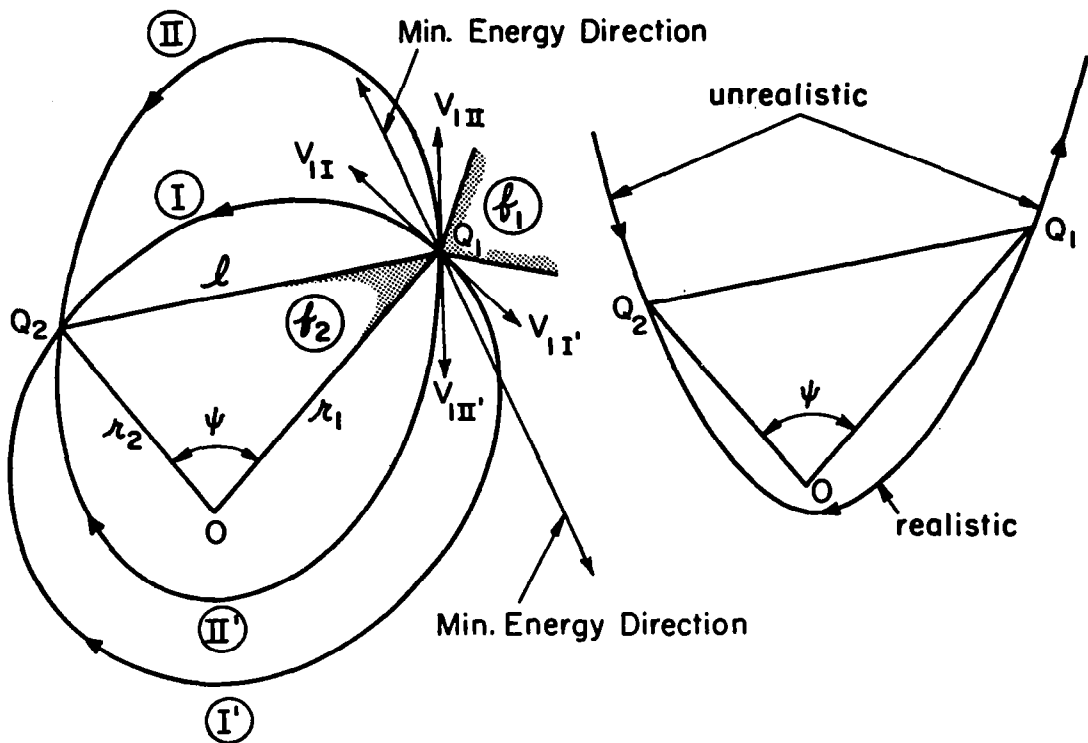
I	Normal, low	I, II (or I', II')	Conjugate pair
II	Normal, high	I, I' (or II, II')	Complementary pair
I'	Complementary, high		
II'	Complementary, low	I, II' (or I', II)	Complementary-Conjugate pair
f_1	Outer forbidden region for departure direction	f_2	Inner forbidden region for departure direction

Fig. A-1 The two-terminal trajectories.

APPENDIX B

THE INTERSECTING PROPERTY OF THE NORMALS OF A HYPERBOLA

Statement of the Property

Two normal lines at two distinct points on a hyperbola in the same quadrant will always intersect in the adjacent quadrant on the opposite side of the transversal axis of the hyperbola.

An Analytical Proof

Let the equation of the hyperbola be given by the parametric equations

$$x = B \tan \omega$$
$$y = A \sec \omega$$
$$(B-1)$$

Consider two normal lines at the points $Q_1(\omega_1)$ and $Q_2(\omega_2)$ on the hyperbola, and let their point of intersection be $P(x_P, y_P)$. For definiteness let us assume

$$0 < \omega_1 < \omega_2 < \frac{\pi}{2} \qquad (B-2)$$

so that Q_1 and Q_2 are distinct and in the same quadrant I. Then we are required to show that the point P is in the quadrant II (see Figure B-1.)

Now the equation of the normal line at any point $Q(\omega)$ on the hyperbola may be written

$$B \, x \sec \omega + A \, y \tan \omega = C^2 \tan \omega \sec \omega \qquad (B-3)$$
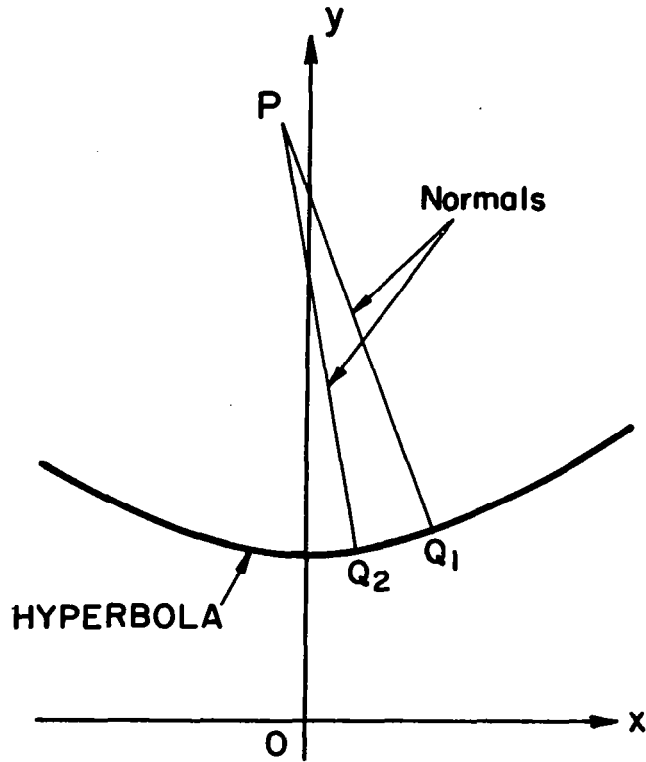
where

$$C^2 = A^2 + B^2 \qquad (B-4)$$

Fig. B-1   Intersection of two normal lines to a hyperbola.

Thus for the point P we have

$$B\, x_p \sec \omega_1 + A\, y_p \tan \omega_1 \;=\; c^2 \tan \omega_1 \sec \omega_1$$

$$B\, x_p \sec \omega_2 + A\, y_p \tan \omega_2 \;=\; c^2 \tan \omega_2 \sec \omega_2$$

(B-5)

Solving for x_p and y_p we find

$$x_p \;=\; \frac{c^2}{B}\, \tan \omega_1 \tan \omega_2 \; \frac{\cos \omega_2 - \cos \omega_1}{\sin \omega_2 - \sin \omega_1}$$

(B-6)

$$y_p \;=\; \frac{c^2}{A}\, \frac{\tan \omega_2 - \tan \omega_1}{\sin \omega_2 - \sin \omega_1}$$

from which we conclude under the assumption (B-2), that

$$x_p < 0 \ , \quad y_p > 0 \tag{B-7}$$

In other words, P is in the quadrant II.